IN THE UNITED STATES PATENT AND TRADEMARK OFFICE

In re patent application of

Shigeo T. Oyama

Serial No. 10/089,515 Group Art Unit 1755

Filed July 3, 2002 Examiner Wood, Elizabeth P.

For NOVEL TRANSITION METAL PHOSPHIDE CATALYSTS

Commissioner for Patents
PO Box 1450
Alexandria, Virginia 22313-1450

DECLARATION OF SHIGEO T. OYAMA ("TED OYAMA")
UNDER 37 C.F.R. §1.132

Shigeo T. Oyama declares as follows:

1. I am the inventor of the above-identified application. I am also an expert in the field of catalysts qualified to provide experimental evidence and opinion evidence directed to such matters at the level of skill of one of ordinary skill in the art and obviousness to one of ordinary skill in the art. I have attached hereto a one page, short form resume, to establish my credentials as an expert. As demonstrated by the resume, I hold the degree of Ph.D. in Chemical Engineering; I have been involved in research in Chemical Engineering, Chemistry, an Catalysts for over two decades; I am a titled professor at Virginia Polytechnic Institute & State University; I am a noted author on over 140 refereed publications; I have edited several books; and I am on the Editorial Board of the *Journal of Natural Gas Chemistry*.

2. I have read and understand the application as originally filed, the amendment to be concurrently submitted with this declaration, the office action mailed July 30, 2004, and each of the references cited by the Examiner. It is my opinion that the

claimed invention, particularly as amended in claims 1 and 7, would not be anticipated by or be obvious to one of ordinary skill in the art over U.S. Patents 4,454,246 and 4,359,406 to Fung, the Journal of Catalysis article (XP009009979), or U.S. Patent 4,367,137 to Antos.

A. Claimed invention

The claimed invention can best be understood with reference to independent claims 1 and 7, as amended, which recite as follows:

1. (Currently Amended) A catalyst comprising:

a metal phosphide complex having the formula MP_x, wherein M is selected from the group consisting of V, Cr, Mn, Fe, Co, Ni, Nb, Mo, Ta, and W, and wherein x ranges from about 0.1 to about 10; and

a high surface area support of at least $50m^2/g$, wherein the metal phosphide complex is dispersed on the high surface area support, wherein said high surface area support is selected from the group consisting of carbon, silica, titania, thoria, magnesia, zirconia, kaolin, bentonite, kieselguhr, zeolites, and combinations thereof.

7. (Currently Amended) A metal phosphide catalyst comprising:

a metal phosphide complex having the formula $A_aB_bP_y$, wherein A and B are each selected from the group consisting of V, Cr, Mn, Fe, Co, Ni, Nb, Mo, Ta, and W, wherein the sum of a and b is 1, the ratio of a and b ranges from about 0.01 to about 100, and y ranges from about 0.1 to about 10; and

a high surface area support of at least $50m^2/g$, wherein the metal phosphide complex is dispersed on the high surface area support, wherein said high surface area support is selected from the group consisting of carbon, silica, titania, thoria, magnesia, zirconia, kaolin, bentonite, kieselguhr, zeolites, and combinations thereof.

It is noted that the claims specify particular metals (V, Cr, Mn, Fe, Co, Ni,

Nb, Mo, Ta, and W) which are "base" metals. In contrast the Fung and Antos patents are directed to "noble" metal phosphides. As will be discussed below in more detail, neither Fung nor Antos describe procedures which would yield metal phosphides from the specified metals (V, Cr, Mn, Fe, Co, Ni, Nb, Mo, Ta, and W). In view of this, these references do not anticipate and would not make obvious to one of ordinary skill in the art that metal phosphide catalysts of the particular metals (V, Cr, Mn, Fe, Co, Ni, Nb, Mo, Ta, and W). A person of ordinary skill in the art to which the present invention pertains would typically hold a Ph.D. and typically with 5-15 years research experience after graduation. He or she would have access to a variety of trade journals and reference books in the fields of chemistry, chemical engineering and catalysis, and would be skilled at reviewing the data presented in those references.

Furthermore, the claims specify particular high surface area supports which include carbon, silica, titania, thoria, magnesia, zirconia, kaolin, bentonite, kieselguhr, zeolites, and combinations thereof. Unlike claims 2 and 8 of the application, which have now been canceled, claims 1 and 7, as amended, do not specify alumina as the support. Alumina is the support used in the Nozaki (Journal of Catalysis 79, 207 (1983)) reference identified as (XP009009979). As will be discussed in more detail below, alumina is a poor support for phosphides because of its strong interaction with phosphorous to form aluminum phosphate ($AlPO_4$) and necessitates the use of higher temperatures for reduction.

B. U.S. Patents 4,454,246 and 4,359,406 to Fung

These patents describe the preparation of metal-phosphorous compounds deposited on a high surface area support. While the patents discuss Group VIII metals generally, and Group VIII noble metals specifically, it is noted that the synthesis method described is inappropriate for the non-noble metals. Specifically, the reduction temperature employed in Fung is low (300-500°C), which is appropriate for noble metals, but not for base metals (e.g., V, Cr, Mn, Fe, Co, Ni, Nb, Mo, Ta, and W).

In Fung, there is described a procedure for impregnation of a support with soluble metal compounds, a phosphorous source, and reduction of the compounds directly in hydrogen, without high temperature calcination. Note particularly Examples 1-2 of the Fung references where there is described low temperature drying at 120°C before reduction. Although, this method works for the preparation of PtP_2 because Pt can be reduced easily. It does not work for non-noble metal phosphides.

In sharp contrast, in the present invention, the metal precursors are first calcined at high temperature to ensure that the components are combined in the form of a phosphate, and then the reducing is performed. If this is not done, the components are not combined, and metal phosphide catalysts will not be produced. To demonstrate this, the following experiments was performed:

Method of Reduction of Samples

Phosphide samples supported on a silica support were prepared by impregnating the support with aqueous metal nitrate and ammonium phosphate solutions by the method of incipient wetness impregnation. Prior to use, the silica was dried at 393 K for 3 h and calcined at 773 K for 6 h. The incipient wetness point of the silica was found to be 2.2 cm^3g^{-1}. After impregnation, the powders were dried at 393 K for 3 h and either used as such or calcined at 773 K for 6 h. The reduction of the samples was carried out using temperature-programmed reduction (TPR). The reduction was carried out in a U-shaped quartz reactor placed in a furnace controlled by a temperature programmer (Omega Model CN 2000). A portion of the exit gas flow was sampled through a leak valve into a mass spectrometer (Ametek/Dycor Model MA 100) for following the progress of the reaction. The temperature was monitored by a local chromel-alumel thermocouple placed in a thermowell near the center of the reactor bed. The H_2 flow rate was set at 1000 mol s^{-1} (1500 cm^3 min^{-1}) per gram sample. The heating rate was 1 K min^{-1}.

Results

Reduction of Components

Compound	Reduction temperature separate components	Result	Reduction temperature combined components	Result
FeP/SiO_2	570-700 K (300-430°C)	Metal	930 K (660°C)	phosphide
CoP/SiO_2	540-590 K (270-320°C)	Metal	830 K (560°C)	phosphide
Ni_2P/SiO_2	530-650 K (250-280°C)	Metal	820 K (550°C)	phosphide

As can be seen from the above table, the precursors employed are metal salts like nitrates, and a phosphorous source like ammonium phosphate. The metal has a positive charge which is balanced by the negative nitrate ion and the phosphate has a negative charge which is balanced by the positive ammonium ion. Because the charges are balanced, there is no need for the metal to combined with the phosphate (so the result is a "metal"). However, in the calcination step, the nitrate ion and the ammonium ion are destroyed, to form gaseous nitrogen oxides and ammonia which are released from the solid. This leaves behind the positive metal ion and the negative phosphate species which combine in order to balance their charges.

The table above demonstrates that direct reduction of components, as contemplated by the Fung references, does not work for the base metals recited in the claims. Because the metal component is not combined with phosphorous, the metal is reduced to a metallic state at a low temperature, and then sinters (grows in particle size) as the temperature is raised, precluding its combination with phosphorous.

One of ordinary skill in the art would recognize that the results in the Fung patents are limited to Pt phosphides (this being the only metal where test results

are presented). Further, one of ordinary skill in the art would recognize that Pt is a noble metal, and is chemically different from the base metals recited in the claims. Thus, one of ordinary skill in the art would recognize that Fung's data could not be extended to all group VIII metals. This is verified by the results in the Table above.

C. U.S. Patent 4,367,137 to Antos et al.

This patent describes an acidic catalytic composite composed of a carrier metal supporting a platinum group metal, cobalt, tin, phosphorous, and halogen. It is noted that nowhere in Antos is it demonstrated that a phosphide is formed. Rather, only a brief statement in the text alludes to this, but acknowledges uncertainty. See particularly column 14 where it is stated:

"Despite the fact the precise form of the chemistry of association of the phosphorous component with the catalytic composite of the present invention is not known, it is believed to be most intimately related with the cobalt component of the catalytic composite, although it may be associated physically and/or chemically with the carrier marerial and/or the platinum group and tin components"... "it is believed that best results are obtained when the phosphorous component exists in the catalytic composite substantially in the form of a phosphide with the cobalt component."

In fact, the procedures used by Antos would not yield a metal phosphide as claimed by the present application. This is because the temperature used in Example II of Antos (reduction of the Co and P containing composite at 975 °F (524°C), is too low for phosphide formation. As evidence of this, attached hereto are the following:

1) Goodenough, *J. Appl. Phys.* Vol. 40, p. 1250 (1969). This document reports that phosphide formation takes place been 850-900°C between metal and phosphorous. See also, Schonbert, *Acta Chemica Scandinavica* 8:226-239 (1954)

2) Wang et al. *J. Catalysis* 208-321-331 (2002). This document, on which I am noted as joint-author, shows that with Co/P, major reduction took place at 820 K

(550°C), but completion required 690°C. (See Figure 4 on page 325). This corresponds to Example 5 of the present application where 690°C was used.

Based on these reported results, as well as the lack of data and analysis in Antos, and Antos' own statements of uncertainty, it should be concluded that Antos does not suggest a methodology which would yield metal phosphide catalysts which fall within the ambit of the claims of the present application. Thus, one of ordinary skill in the art would not find Antos as suggesting the claimed invention.

D. Nozaki et al, *Journal of Catalysis* 79, 207 (1983)

In this paper, the authors report catalysts composed of Ni_2P, Co_2P, and FeP deposited on an alumina support. The catalysts were obtained from phosphate precursors by reduction in hydrogen.

One of ordinary skill in the art will recognize that the use of other supports, as set forth in independent claims 1 and 7, provide certain new and unobvious advantages over alumina supports. In fact, alumina is a poor support for phosphides, as it interacts very strongly with the phosphorus forming an aluminum phosphate ($AlPO_4$) and necessitates that use of high temperatures of reduction. The attached figures, which are taken from referenced publications on which I am noted as a joint author, show reduction provides for the different catalysts obtained by following the production of water as a function of temperature. In all cases, the precursor is a phosphate which undergoes reduction to a phosphide.

Attached Figure 1 shows the reduction profile of pure MoP and MoP/SiO_2 (see, Clark et al., *J. Catal.* 207,256, (2002) attached). Figure 2 shows the reduction provide for MoP/Al_2O_3 (see, Clark et al., *J.Catal.* 218, 78 (2003) attached). As can be seen, the reduction for MoP/SiO_2 requires only 820 K (547°C), while that for MoP/Al_2O_3 necessitates 1170 k (900°C). Published work also shows that this is because of the formation of the $AlPO_4$ phase as a result of the strong interaction between Al and P.

Similar results are found for Ni_2P on other supports claimed in the present

application. Attached Figure 3 compares the synthesis of Ni_2P supported on two zeolites (KUSY, potassium promoted ultra-stable Y) and MCM-41, to Ni_2P supported on silica and Ni_2P supported on Al_2O_3. The reduction temperatures for the KUSY, MCM-41, and SiO_2 supports are between 860-880 K (590–610° C), whereas that for Al_2O_3 support is at 1270 K (1000°C). The presence of Ni_2P has been confirmed on all these supports by x-ray diffraction and x-ray absorption measurements. This work shows that supports other than alumina can produce the phosphide at much lower temperatures. This is a non-obvious, and highly important finding.

Attached Figure 4 shows the results of preparing MoP, WP, and Ni_2P using a carbon support. Again, the reduction temperatures are low, ranging from 810-860 K (540-590°C).

3. I hereby declare that all statements made herein of my own knowledge are true and that all statements made on information and belief are believed to be true; and further that these statements were made with the knowledge that willful false statements and the like so made are punishable by fine or imprisonment, or both, under 18 U.S.C. 1001 and that such willful false statements may jeopardize the validity of the application or any patent issued thereon.

Date: Nov 16, 2004

Shigeo T. Oyama

S. TED OYAMA
Department of Chemical Engineering
Virginia Polytechnic Institute and State University
Blacksburg, Virginia 24061-0211 (tel. 540-231-5309, email oyama@vt.edu)

Current Position Fred W. Bull Professor of Chemical Engineering and
Professor of Chemistry, *by courtesy*, Virginia Polytechnic Institute

Birth February 16, 1955. Tokyo, Japan.

Education

1972-1976 **Yale University**, New Haven, CT
B.S. Chemistry, B.S. Engineering & Applied Science (Double major)
1976-1981 **Stanford University**, Stanford, CA
M.S, Ph.D. Chemical Engineering
Thesis: Ammonia Synthesis and Decomposition on Molybdenum Alloys
Advisor: Professor Michel Boudart

Experience

5/80-9/80 **University of Tokyo**, Visiting Research Student
Advisor: Professor Kenzi Tamaru
6/81-8/86 **Catalytica Associates, Inc.**, Research Engineer/Project Leader
9/86-6/88 **University of California, Berkeley**, Visiting Scholar
Advisor: Professor Gabor Somorjai
5/92-7/92 **MITI Research Institute, Osaka**, Visiting Scholar
7/88-6/93 **Clarkson University**, Associate Professor
7/93-4/96 **Virginia Polytechnic Institute**, Associate Professor
4/96-8/99 **Virginia Polytechnic Institute**, Professor
9/99-Pres **Virginia Polytechnic Institute**, Fred W. Bull Professor

Fields of Research

Reactivity of Surfaces; Catalysis; Surface Science; Kinetics; Solid State Chemistry;
Design, Synthesis and Characterization of Advanced Materials, Oxides and Ceramics.

Professional

Member: American Association for the Advancement of Science
American Chemical Society, Chemical Society of Japan
American Institute of Chemical Engineers, IUPAC, Material Research Society
Sigma Chi, Tau Beta Pi
Editorial Board: Journal of Natural Gas Chemistry
Chairman, ACS Northern New York Section, 1990-1993
Program Committee, ACS Petroleum Division, 1991-present
Coordinator, NSF USA/Brazil University Exchange Program, 1992-present
Visiting Professor, Univ. Rio de Janeiro, 1992, Univ. P. & M. Curie, Paris, 1995, Univ. L. Pasteur, 1996; Univ. Tokyo, 1997, Tokyo Inst. Technol., 1999
Professor of the Year, Omega Chi Epsilon, 1993, 1995
Chairman, Gordon Conference on Hydrocarbon Resources, 1994
Dean's Award for Excellence in Research 1997
Edited Books: 5 Authored Book: 1

Refereed Publications > 140, **Invited Lectures at Universities and Industries** > 230

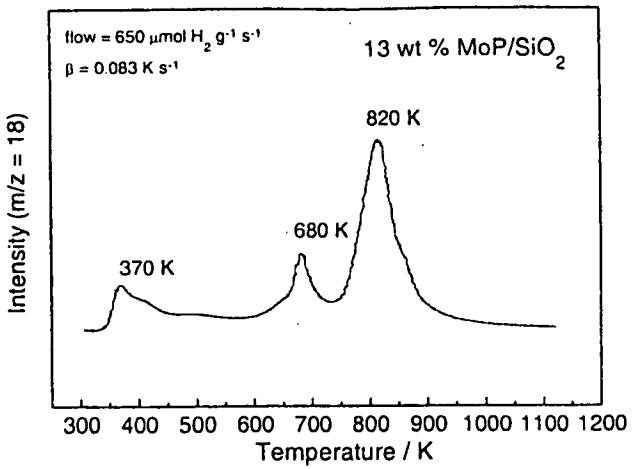

Figure 1 Synthesis of MoP/SiO_2

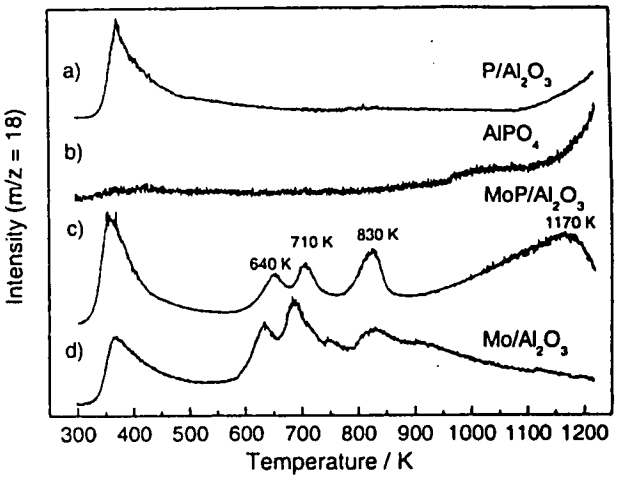

Figure 2. Synthesis of MoP/Al_2O_3

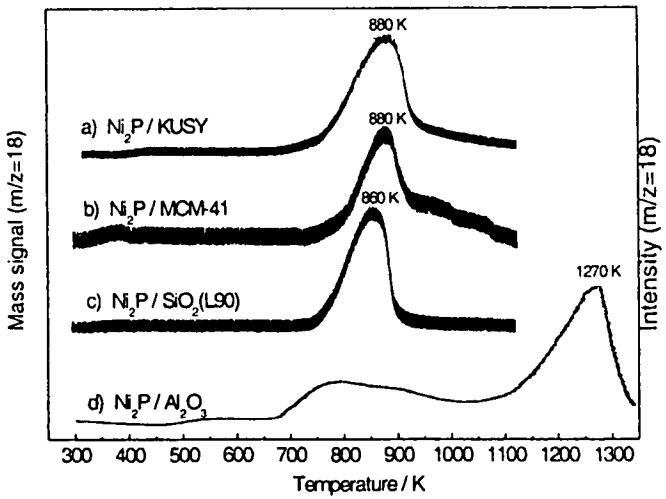

Figure 3. Synthesis of Ni_2P on various supports

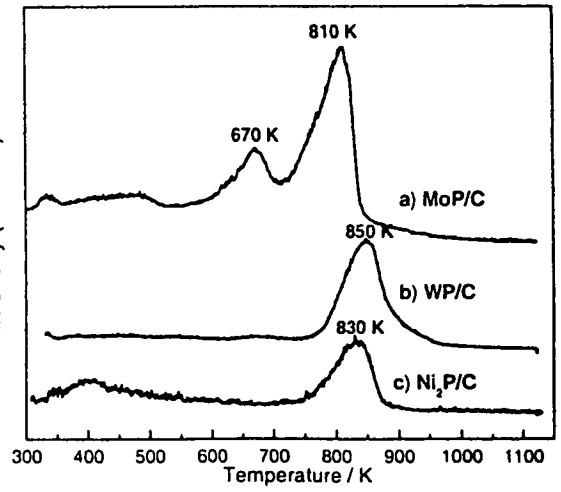

Figure 4. Synthesis of phosphides on carbon

JOURNAL OF APPLIED PHYSICS VOLUME 40, NUMBER 3 1 MARCH 1969

Transition Metal Compounds

J. B. GOODENOUGH, *Chairman*

Crystallographic and Magnetic Properties of Solid Solutions of the Phosphides M_2P, M = Cr, Mn, Fe, Co, and Ni

R. FRUCHART, A. ROGER, AND J. P. SENATEUR
C.E.C.M., 15 Rue G. Urbain, 94 Vitry sur Seine, France

Several phosphides with the chemical formula M_2P crystallize in a hexagonal structure: Mn_2P, Fe_2P, and Ni_2P. The structure of Co_2P is orthorhombic. These two structures are related via an identical elementary subcell consisting of a tetrahedral-site and a pyramidal-site M-atom pair. This investigation shows that solid solutions between two hexagonal end members, such as Fe_2P or Ni_2P with Mn_2P, may exhibit orthorhombic structures at intermediate compositions. Fe_2P shows complete solid solubility with Ni_2P. Curiously, hexagonal and orthorhombic symmetries alternate with decreasing number of 3*d* electrons, Ni_2P(hex)–Co_2P(ortho)–Fe_2P(hex)–FeMnP(ortho)–Mn_2P(hex). Lattice parameter variations with composition and Mössbauer studies reveal atomic ordering in the mixed systems, Mn and Cr substituting for pyramidal-site iron in FeMnP and FeCrP while Ni and Co substitute preferentially for tetrahedral-site iron in FeCoP and FeNiP. While neither Co_2P nor Mn_2P are ferromagnetic, intermediate phases are, the Curie temperature and magnetization reaching the maximum values 310°C and 3.03 μ_B/molecule for MnCoP. Metamagnetism appears for a range of compositions about $(Mn_{0.7}Co_{0.3})_2P$. The Co_2P–Fe_2P system is also ferromagnetic with a maximum Curie temperature near FeCoP. This system shows a sharp discontinuity in magnetization, but only a small discontinuity in Curie temperature, across the phase transition. Sensitivity to stoichiometry in the magnetization of $Fe_{2-x}P$ is attributed to an electron/atom ratio near that for the appearance of metamagnetism.

I. INTRODUCTION

Several phosphides of the first-row transition metals are ferromagnetic: for example, Fe_3P,[1,2] Fe_2P,[1,3,4] and MnP.[5] Near 50°K, MnP exhibits an antiferromagnetic to ferromagnetic transition,[6–11] the antiferromagnetic phase consisting of two parallel helices.[11,12] Other phosphides, such as Mn_3P [13] and Mn_2P,[14] are antiferromagnetic.

Studies of MnP–FeP solid solutions show that FeP is not ferromagnetic even at very low (1.5°K) temperatures.[3,4,15–18] MnP–MnAs solid solutions are magnetically complex, exhibiting several magnetic transitions.[19–23] Substitutions of boron for phosphorous in Fe_3P [24,25] have shown that the metalloid electrons are donors to the 3d bands of iron, whereas substitutions of chromium,[26] nickel or cobalt[13,27] give changes of magnetization with composition similar to those found[28,29] for the borides M_2B and MB.

This work is concerned with the magnetic properties of solid solutions of phosphides of the type M_2P. Nowotny and Henglein[30] have presented a brief structural survey of a few solid solutions among M_2P phosphides. Not all the phosphides M_2P have the same crystal structure[30–33]; some, like Mn_2P and Ni_2P, are

[1] H. Le Chatelier and S. Wologdine, Compt. Rend. 149, 709 (1909).
[2] J. L. Haughton, J. Iron Steel Inst. 115, 417 (1927).
[3] Shu Chiba, J. Phys. Soc. Japan 15, 581 (1960).
[4] A. J. P. Meyer and M. C. Cadeville, J. Phys. Soc. Japan 17, 223 (1962).
[5] K. H. Sweeny and A. B. Scoot, J. Chem. Phys. 22, 917 (1954).
[6] B. F. Stein and R. H. Walmsley, Phys. Rev. 148, 933 (1966).
[7] G. P. Felchert, J. Appl. Phys. 37, 1056 (1966).
[8] J. Komatsubara, K. Kinoshita, and E. Hirahara, J. Phys. Soc. Japan 20, 2036 (1965).
[9] A. Roger and R. Fruchart, Compt. Rend. 264, 508 (1967).
[10] E. E. Hubert Jr. and D. H. Ridgley, Phys. Rev. 135, 1099 (1964).
[11] J. B. Forsyth, S. J. Pickart, and P. J. Brown, Proc. Phys. Soc. 88, 333 (1966).
[12] S. Takeuchi and K. Motizuki, J. Phys. Soc. Japan 24, 742 (1967).
[13] R. J. Gambino, T. P. McGuire, and Y. Nakamura, J. Appl. Phys. 38, 1253 (1967).
[14] M. Yessik, Phil. Mag. 17, 623 (1968).
[15] M. C. Cadeville, thèse, Strasbourg (1965), p. 29.
[16] A. Gerard, Bull. Soc. Belg. Phys. 5, 43 (1966).
[17] J. Bonnerot, R. Fruchart, and A. Roger, Phys. Letters 26A, 536 (1968).
[18] R. E. Bailey and J. F. Duncan, Inorg. Chem. 6, 1444 (1966).
[19] J. B. Goodenough, D. H. Ridgley, and W. A. Newman, in Proc. Intern. Conf. Mag., Nottingham (1964).
[20] D. H. Ridgley and J. H. Geisman, J. Appl. Phys. 39, 592 (1968).
[21] H. Ido and T. Suzuki, J. Phys. Japan 24, 964 (1968).
[22] R. M. Rosenberg, W. H. Cloud, F. J. Darnell, and R. B. Flippen, Phys. Letters 25A, 723 (1967).
[23] A. Roger and R. Fruchart, Mat. Res. Bull. 3, 253 (1968).
[24] E. Fruchart, A. M. Triquet, and R. Fruchart, Ann. Chim. 9, 323 (1964).
[25] R. Fruchart, A. M. Blanc, E. Fruchart, J. P. Bouchaud, and J. P. Senateur, Colloque International No. 157 du C.N.R.S. (1965), p. 95.
[26] A. M. Blanc, E. Fruchart, and R. Fruchart, Ann. Chim. 2, 251 (1967).
[27] A. M. Blanc, E. Fruchart, and R. Fruchart (unpublished).
[28] M. C. Cadeville and A. J. P. Meyer, Compt. Rend. 255, 339 (1962).
[29] M. C. Cadeville, E. Daniel, and A. J. P. Meyer, Colloque International No. 157 du C.N.R.S. (1965), p. 361.
[30] H. Nowotny and E. Henglein, Monats. Chem. 79, 385 (1948).
[31] S. Rundqvist and F. Jellinek, Acta Chem. Scand. 13, 425 (1959).
[32] O. Arstad and H. Nowotny, Z. Physik. Chem. B38, 356 (1937).
[33] H. Nowotny and E. Henglein, Z. Physik. Chem. B40, 28 (1938).

isomorphous with hexagonal Fe_2P,[31,32] and others have the orthorhombic structure[34] of Co_2P. The structure of Cr_2P has not yet been determined. Rundquist[35] has discussed the similarities between the hexagonal and orthorhombic phosphides. In order to relate magnetic properties to crystal structure, we review briefly this similarity here, emphasizing the metalloid environment of the metal atoms and the elementary structural unit common to both structures.

Along the [001] direction of the hexagonal structure or the [010] direction of the orthorhombic structure, phosphorous atoms form, alternately, tetrahedra and square-based pyramids, as shown in Fig. 1(a), making a canal of triangular cross section. Occupation of both tetrahedral and pyramidal sites cannot occur simultaneously along the same canal. Consequently, two

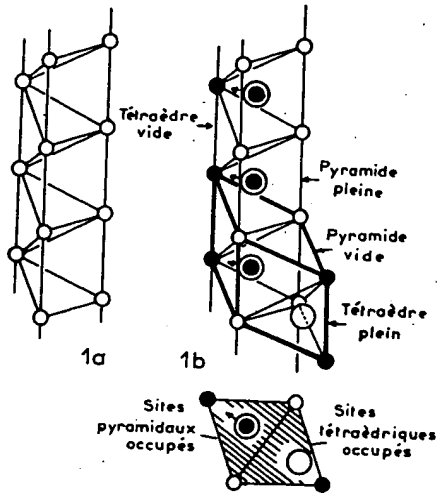

FIG. 1. Building blocks of hexagonal and orthorhombic M_2P structures. (a) Phosphorous canals. (b) Relationship of pyramidal-site and tetrahedral-site atoms forming a rhombohedral subcell.

kinds of canals are possible: one has only tetrahedral sites occupied, the other only pyramidal sites occupied. In both the hexagonal Fe_2P and orthorhombic Co_2P structures, canals of different type share common pyramidal square bases to form canal pairs. This pairing creates a sequence of elementary structural units along the paired canals. As shown in Fig. 1(b), these units are rhombohedral and consist of an occupied tetrahedron-occupied pyramid pair, and an empty-tetrahedron-empty-pyramid pair. The hexagonal Fe_2P structure of Fig. 2 corresponds to an hexagonal assembly of these canal pairs whereas the orthorhombic Co_2P structure of Fig. 3 results from a zig-zag stacking.

II. SAMPLE PREPARATION

Solid solutions were prepared at temperatures between 850° and 900°C in evacuated, sealed silica am-

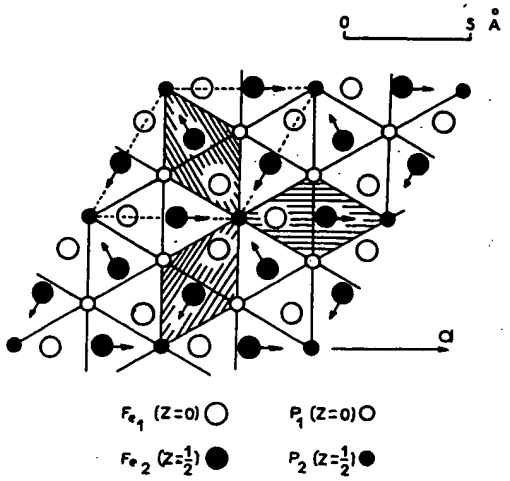

FIG. 2. Arrangement of rhombohedral subcells in hexagonal Fe_2P structure.

pules by solid-phase diffusion of phosphides prepared by a previously described method.[9]

III. EXPERIMENTAL METHODS

1. *X-ray diffraction*: Diffraction patterns were taken with a Seeman–Bohlin camera with monochromatic chromium $K\alpha_1$ radiation. The precision of the measurements is about 10^{-3} Å.

2. *Magnetic analysis*: Curie and magnetic-transition temperatures were determined with a thermomagnetic balance from 77°–1400°K in fields of a few hundred Oersteds. Magnetic moments were obtained in fields up to 26.6 kOe and in temperatures down to 20.4°K.

3. *Mössbauer spectra*: The apparatus includes a Co^{57} source imbedded in palladium and placed in a parabolic-movement vibrator having a parabolic displacement. The spectra, obtained from 90° to 650°K, were recorded in a four-hundred-channel analyzer. Zone-melted iron was used as a standard.

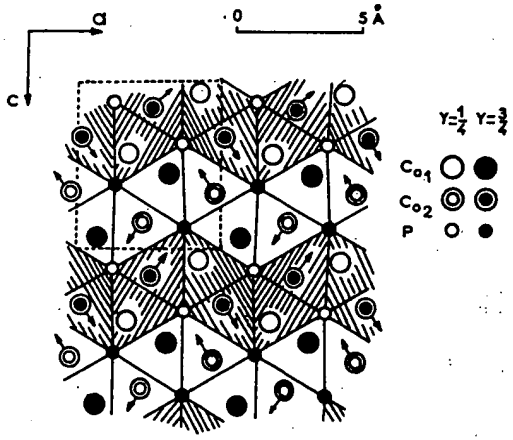

FIG. 3. Arrangement of rhombohedral subcells in orthorhombic Co_2P structure.

[34] H. Nowotny, Z. Anorg. Chem. **254**, 31 (1947).
[35] S. Rundqvist, Arkiv für Kemi **20**, 7 (1962).

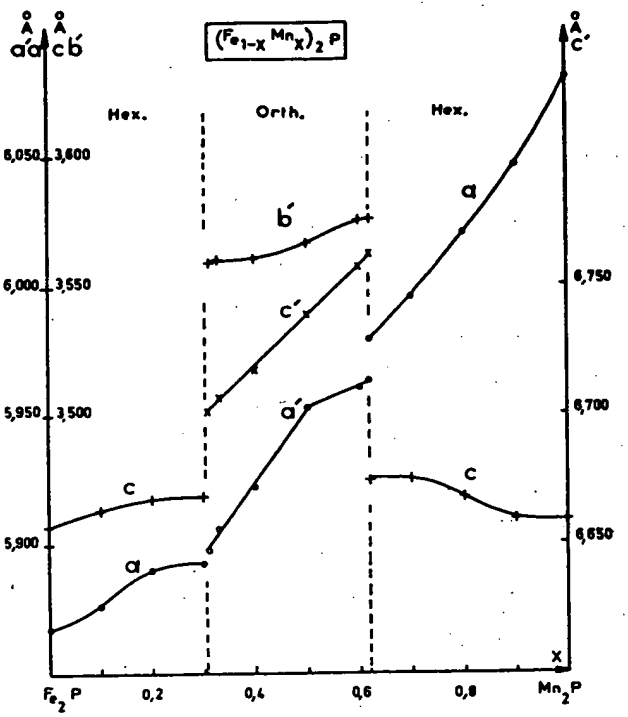

FIG. 4. Lattice-parameters and structural homogeneity ranges for the system $(Fe_{1-x}Mn_x)_2P$.

IV. CRYSTALLOGRAPHIC STUDY

A. Systems with Three Single-Phase Regions

1. $(Fe_{1-x}Mn_x)_2P$: The solid-solution system $(Fe_{1-x}Mn_x)_2P$ has orthorhombic symmetry in the intermediate compositional range $0.31 \leq x \leq 0.62$ (Fig. 4). The orthorhombic and hexagonal phases are separated by very narrow two-phase regions, and the limiting compositions are very slightly dependent on the temperature of sample preparation. Lattice parameters do not obey Vegard's law, and abrupt changes in a' occur at $x=0.5$, or MnFeP. The hexagonal phase is more dense than the orthorhombic phase (107.58 Å^3 vs 108.19 Å for $x=0.62$.)

2. $(Mn_{1-x}Ni_x)_2P$: This system is similarly characterized by orthrhombic structures in the intermediate compositional range $0.20 \leq x \leq 0.50$.

3. $(Fe_{1-x}Cr_x)_2P$: This system has orthorhombic structures in the compositional range $0.15 \leq x \leq 0.55$, and the rate of change with x of all three orthrhombic parameters a', b', c', show anomalous changes at $x=0.50$. However, for $x>0.60$ the system is multiphase.

B. Systems with Two Single-Phase Regions

1. $(Co_{1-x}Fe_x)_2P$: In this system hexagonal structures are restricted to the relatively narrow compositional range $x>0.84$ (Fig. 5). Here the limiting compositions of the very narrow two-phase region, of width Δx, vary with thermal treatment: $\Delta x \approx 0.01$, 0.04 for preparation at 600° and 950°C, respectively. Végard's law is not obeyed, and c' vs x shows an inflection point near $x=0.60$. To obtain a unique phase at 850°C, it was necessary to add an excess of 3 at.% phosphorous throughout the range $x<0.50$.

2. $(Co_{1-x}Mn_x)_2P$: Hexagonal structures in this system are restricted to the compositional range $x>0.80$ (Fig. 6). Particularly marked anomalies in a' and b' occur at the composition MnCoP.

3. $(Mn_{1-x}Cr_x)_2P$: Substitution of 10 at.% chromium into Mn_2P is sufficient to make the hexagonal structure disappear. For $x \geq 0.10$, the system is multiphase.

4. $(Co_{1-x}Ni_x)_2P$: In this system, hexagonal structures are found over most of the compositional range, orthorhombic structures being restricted to the range $x \leq 0.15$. The hexagonal c parameter has a broad minimum at $x=0.65$.

C. Complete Solid Solutions

The hexagonal system $(Fe_{1-x}Ni_x)_2P$ has complete solid solutions. The lattice parameters vary anomalously with x (Fig. 7), the most accentuated changes occurring at the composition $x=0.85$, which has the minimum volume.

V. MAGNETIC STUDY

1. $(Co_{1-x}Mn_x)_2P$: Although the binary compounds Mn_2P and Co_2P are not ferromagnetic, the orthorhombic domain of the system $(Co_{1-x}Mn_x)_2P$ contains a large

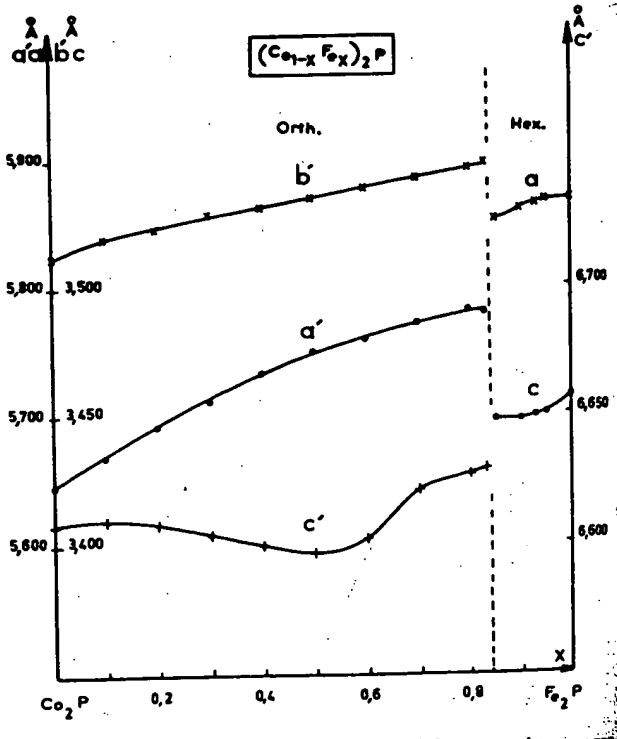

FIG. 5. Lattice parameters and structural homogeneity ranges for the system $(Co_{1-x}Fe_x)_2P$.

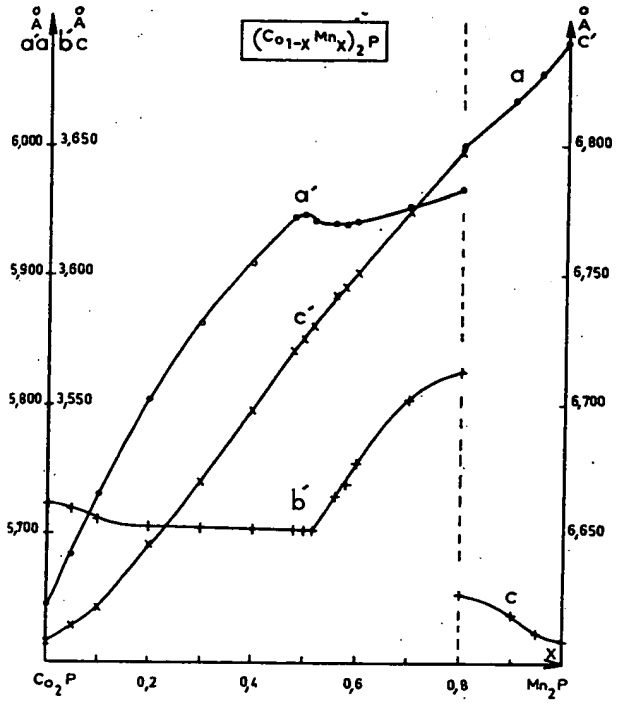

FIG. 6. Lattice parameters and structural homogeneity ranges for the system $(Co_{1-x}Mn_x)_2P$.

ferromagnetic compositional region (Fig. 8). The Curie temperatures T_c vary rapidly with x, exhibiting a sharp maximum of 583°K at $x=0.5$ (CoMnP). In the interval $0.56 \leq x \leq 0.66$, there is a metamagnetic to ferromagnetic transition with increasing temperature.

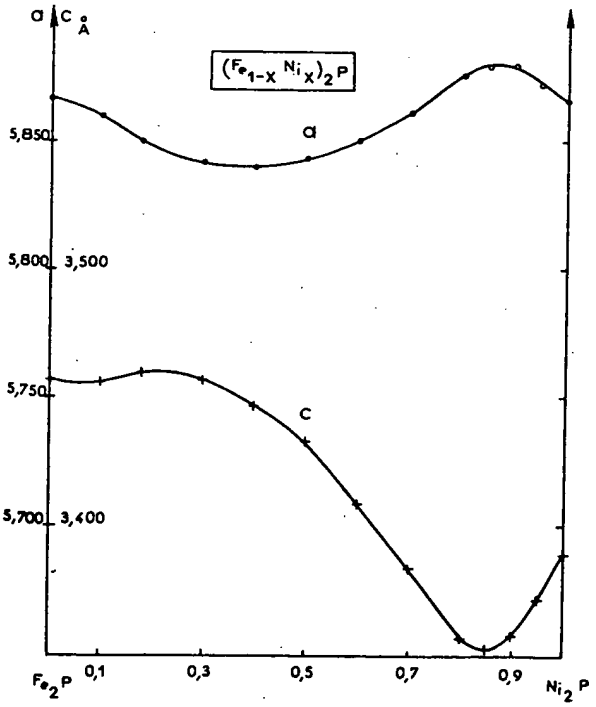

FIG. 7. Lattice parameters for the system $(Fe_{1-x}Ni_x)_2P$.

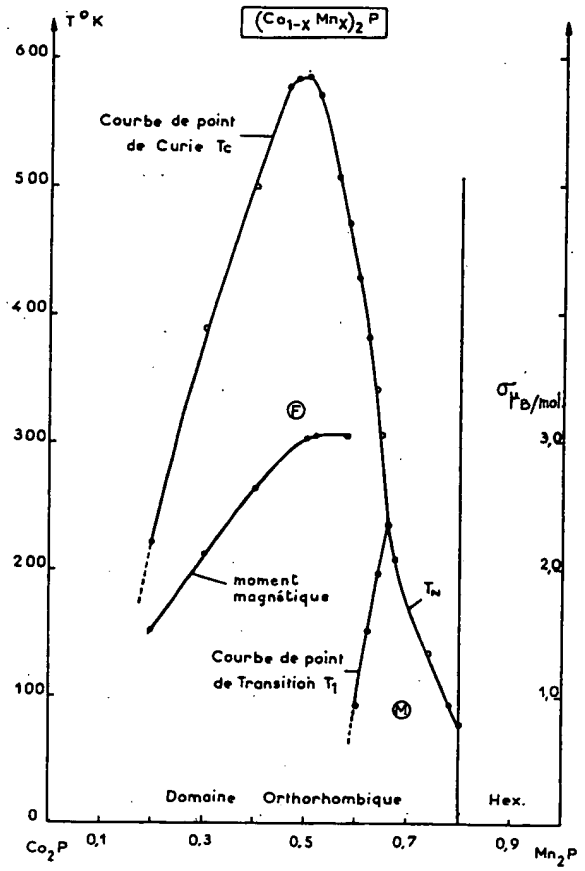

FIG. 8. Magnetic transition temperatures and magnetization at 0°K for the system $(Co_{1-x}Mn_x)_2P$.

The transition temperature T_1 increases rapidly with x while T_c decreases, the domain of ferromagnetism in weak external fields terminating at $x=0.66$. T_1 varies strongly with applied field (Figs. 9–11), and for $x \geq 0.66$ the magnetic order-disorder transition is a Néel temperature T_N (Figs. 8–10). The saturation magnetiza-

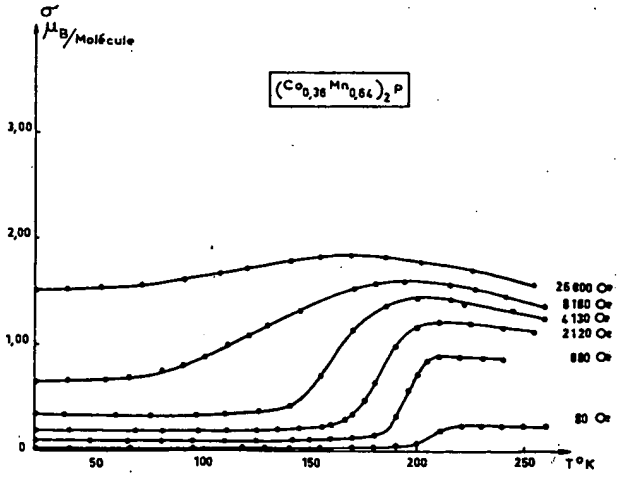

FIG. 9. Thermomagnetic curves at various applied field strengths for $(Co_{0.36}Mn_{0.64})_2P$.

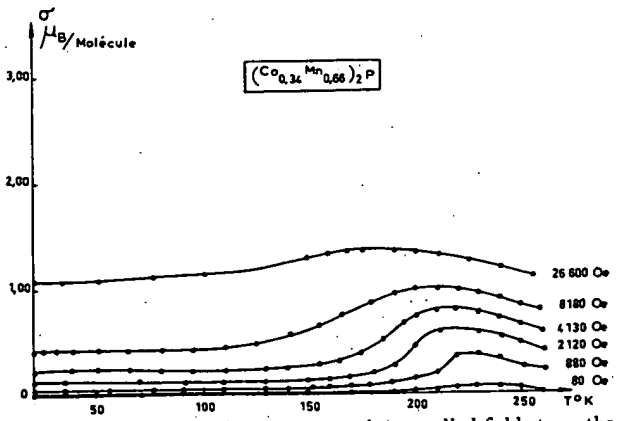

FIG. 10. Thermomagnetic curves at various applied field strengths for $(Co_{0.34}Mn_{0.66})_2P$.

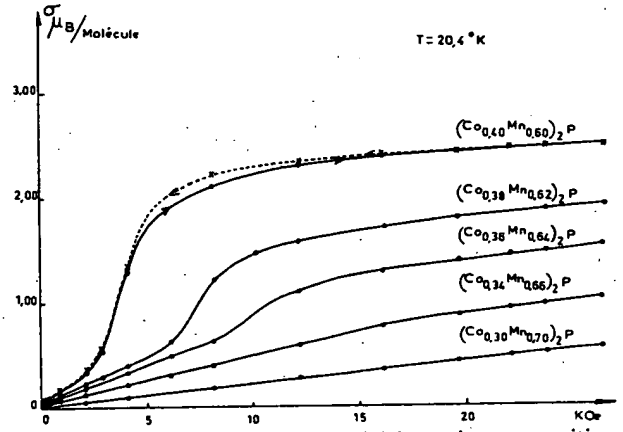

FIG. 11. Magnetization curves at 20.4°K for various compositions $(Co_{1-x}Mn_x)_2P$ that are metamagnetic at low temperatures.

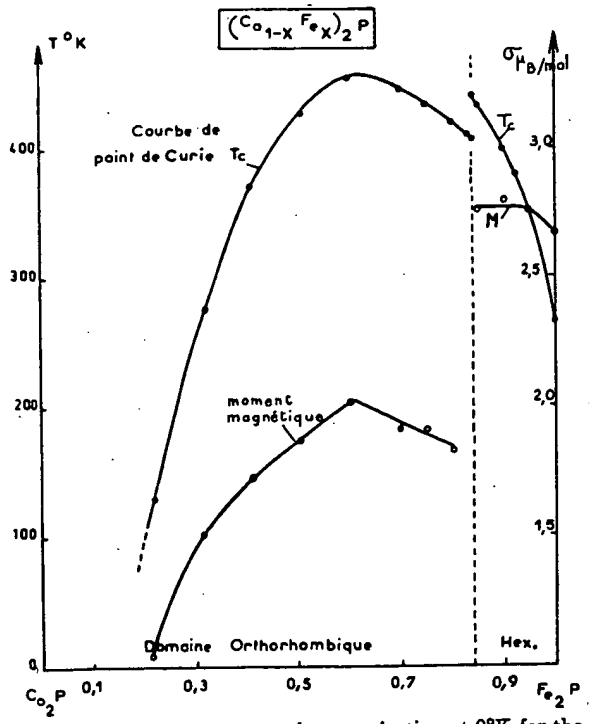

FIG. 12. Curie temperature and magnetization at 0°K for the system $(Co_{1-x}Fe_x)_2P$.

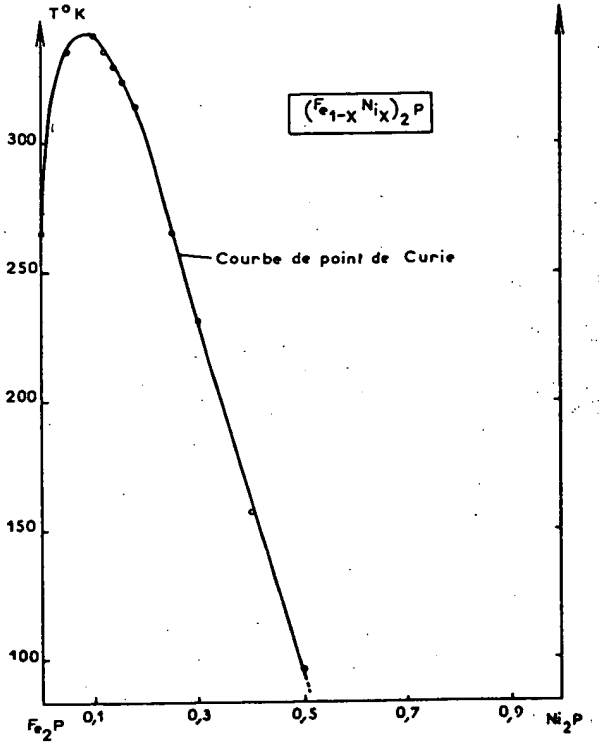

FIG. 13. Curie temperature for the system $(Fe_{1-x}Ni_x)_2P$.

tion, extrapolated to 0°K, is also shown in Fig. 8. It reaches a maximum of 3.06 μ_B/molecule at $x \approx 0.55$.

2. $(Co_{1-x}Fe_x)_2P$: As in the previous system, the Curie temperature T_c rises rapidly with x to a maximum of 459°K at $x=0.62$ (Fig. 12). However, here there is no metamagnetic state, and there is a discontinuity in T_c at $x=0.84$, where the structural change occurs, from 407°–441°K. Since thermomagnetic analysis of samples with $x \leq 0.50$ revealed the presence of a magnetic impurity (the amount increasing with preparation temperature) having a Curie temperature slightly less than that of pure cobalt, for $x \leq 0.50$, the phosphorous content was systematically increased by 3 at.% in these

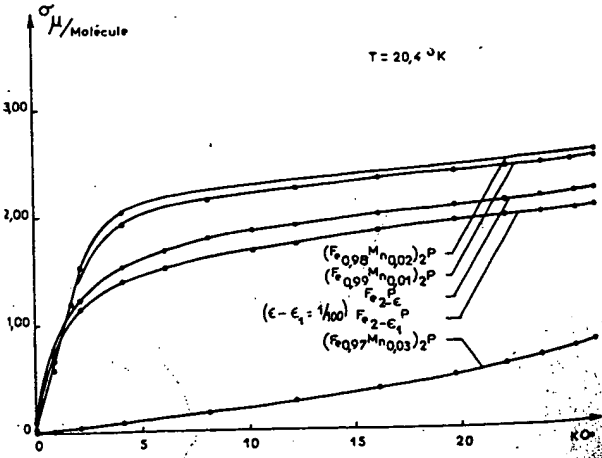

FIG. 14. Magnetization vs applied field at 20.4°K of Fe_2P and Fe_2P:Mn.

compositions in order to obtain single magnetic phases. The magnetization (Fig. 12) decreases abruptly from 2.75 to 1.83 μ_B/molecule on passing from the hexagonal to the orthorhombic phase, and within the orthorhombic phase it reaches a maximum of 2.02 μ_B/molecule at $x=0.60$.

3. $(Fe_{1-x}Ni_x)_2P$: Substitution of Ni into Fe_2P produces a similar sharp increase in T_c (Fig. 13), which reaches a maximum of 342°K at $x=0.08$, decreasing rapidly with larger x to less than 100°K at $x=0.50$. The saturation magnetization has not yet been measured.

4. $(Fe_{1-x}Mn_x)_2P$: Very small substitutions of manganese into Fe_2P induce metamagnetism. By $x=0.03$, the antiferromagnetic state is stable in fields up to 26.6 kOe (see Fig. 14). Similar changes occur with chromium substitutions.

5. $Fe_{2-x}P$: Cadeville and Meyer[15] have reported variations in magnetization with deviations from stoichiometry as large as 2.76 μ_B/molecule for Fe_2P to 2.14 μ_B/molecule for $Fe_{2-x}P$. Similarly, we find that two single-phase samples of nominal compositions (Fe_2P), but differing by one weight percent iron, have magnetizations of 2.67 μ_B and 2.44 μ_B/molecule.

VI. MÖSSBAUER SPECTRA

A. Studies in the Paramagnetic State

The Mössbauer spectrum of Fe_2P has already been studied.[16,18] Pyramidal-site iron atoms are subject to a significant electric-field gradient that splits the resonance line by ≈0.4 mm/sec. The tetrahedral-site iron atoms exhibit a single resonance line of enlarged width, probably reflecting a slight deformation of the tetrahedron. Therefore, Mössbauer studies of $(Fe_{1-x}M_x)_2P$ systems permit a direct determination of the site preferences of the solute M atoms.

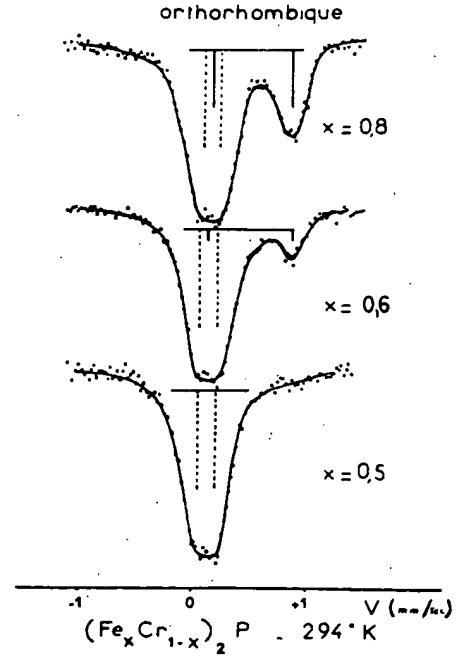

FIG. 15. Mössbauer spectra of $(Fe_xCr_{1-x})_2P$ in the paramagnetic state.

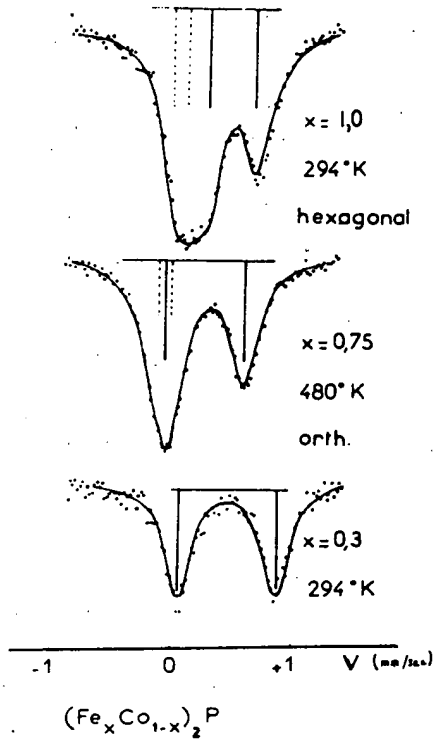

FIG. 16. Mössbauer spectra of $(Fe_xCo_{1-x})_2P$ in the paramagnetic state.

1. M=Mn *or* Cr: Changes with x in the Mössbauer spectra indicate a total substitution of manganese and chromium atoms for pyramidal-site iron. Only the single line with enlarged width remains in the spectra of FeMnP and FeCrP (Fig. 15).

2. M=Co *or* Ni: Cobalt and nickel substitute preferentially for tetrahedral-site iron. About 15% of the cobalt atoms occupy pyramidal sites in FeCoP. For $x>0.70$, only the symmetric doublet, separated by 0.83 mm/sec, appears in the spectrum (Fig. 16). About 25% of the nickel atoms occupy pyramidal sites in FeNiP.

B. Studies in the Ferromagnetic State

The spectra of the system $(Fe_{1-x}Co_x)_2P$ at $T=294°K<T_c$ for a series of compositions in the range $0<x<0.25$ vary regularly with x and show little change on passing from hexagonal to orthorhombic symmetry. They have been interpreted with the method of Wertheim,[36] where the parameters to be determined are the internal fields at the tetrahedral-site and pyramidal-site nuclei H_n^t and H_n^p, the quadrupolar field strengths $\frac{1}{2}eqV_{zz}$ at pyramidal sites (those at tetrahedral sites

[36] G. K. Wertheim, Phys. Rev. 121, 63 (1961).

TABLE I. Mossbauer parameters at 294°K for $(Co_{1-x}Fe_x)_2P$.

x	H_n^I (kOe)	H_n^{II} (kOe)	$\frac{1}{2}eqV_{zz}$	η	θ
0.8	67	132	0.63	0.46	90°
0.75	69	141	0.67	0.56	90°
0.70	69	153	0.67		20°
0.50	69	153	0.74		20°

assumed negligible), an asymmetry parameter η, and the angle θ between the spin direction and the principal axis of the electric-field gradient in the pyramidal sites. The results are summarized in Table I. By symmetry, the principal axis of the electric-field gradient should be perpendicular to the phosphorous canals, so that a $\theta=90°$ means that the spins are parallel to the c axis in the hexagonal structure, to the b' axis in the orthorhombic structure.

In the range $x>0.25$, an increase in the complexity of the spectra (Fig. 17) indicates a spin reorientation. In first approximation and neglecting the asymmetry parameters, a $\theta\approx20°$ is obtained with the aid of Kündig's[37] graphs. Since the axes of the pyramidal sites make an angle of about 30° with the orthorhombic c' axis, it is reasonable to assume that the spins have become oriented parallel to this axis. For $x=0.25$, the spins rotate continuously with temperature in the b'–c' plane: at 90°K they are parallel to c′ and at 294°K to b′ (Fig. 18). These results are confirmed by x-ray diffraction on powder samples oriented in a magnetic field at 294°K. A detailed, complete analysis of the spectra will be published soon.[38]

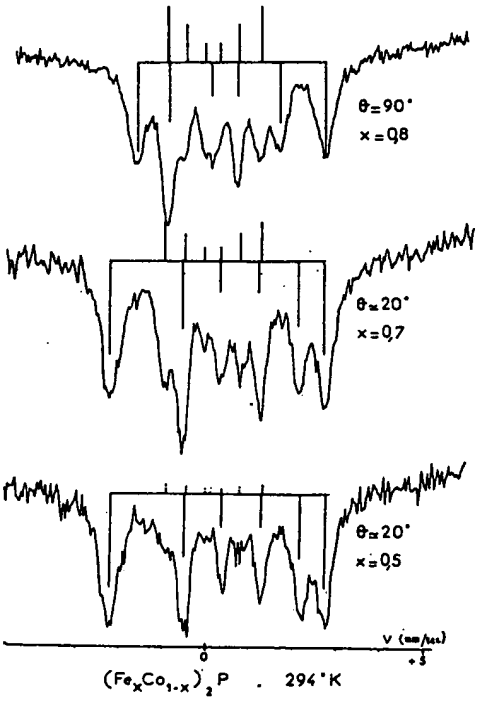

FIG. 17. Rotation of spins as a function of composition in $(Fe_xCo_{1-x})_2P$.

VII. DISCUSSION

Mixed phosphides of formula M_2P have a remarkable alternation of hexagonal and orthorhombic structures with increasing electron/atom ratio,

$$Mn_2P(hex)–MnFeP(ortho)–Fe_2P(hex)$$

$$–Co_2P(ortho)–Ni_2P(hex).$$

Anomalies in the variation with composition of lattice parameters and magnetic properties, which are particularly pronounced in the system $(Co_{1-x}Mn_x)_2P$, can be attributed, as a result of the Mössbauer studies, to the site preferences of the solute atoms. The completely ordered compounds FeMnP, FeCrP, MnCoP, and, without doubt, MnNiP, belong to the important family of orthorhombic E phases represented by ZrFeP [39,40]; a homologous family of ordered hexagonal phases would be represented by NbMnSi.[41,42] For many members of these families, the ordering energy may be so large that the homogeneity range is strictly limited to the ideal compositions, as in ZrFeP and NbMnSi.

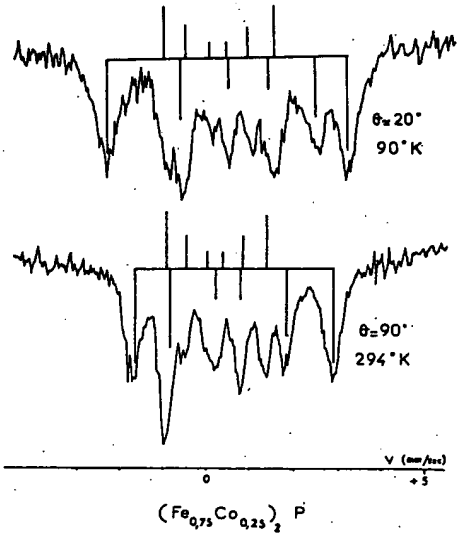

FIG. 18. Rotation of spins as a function of temperature in $(Fe_{0.75}Co_{0.25})_2P$.

[37] W. Kundig, Nuclear Instr. Method 48, 219 (1967).
[38] J. P. Senateur, A. Roger, and R. Fruchart (unpublished).
[39] S. Rundqvist and P. C. Nawapong, Acta Chem. Scand. 20, 2251 (1966).
[40] W. Jeitschko, Acta Cryst. 24, 930 (1968).
[41] B. Deyris, J. Roy-Montreuil, R. Fruchart, and A. Michel, Bull. Soc. Chim. de France 4, 1303 (1968).
[42] J. Roy-Montreuil, B. Deyris, R. Fruchart, and A. Michel, Compt. Rend. 264, 587 (1967).

Not only the substitutional ordering, but also deviations from stoichiometry of the metal and not the metalloid atom,[43] suggest that the two structures Fe_2P and Co_2P should both be viewed as metalloid skeletal arrays having twice as many interstitial metal atoms as metalloid atoms and the common, rhombohedral subcell of Fig. 1(b).

Although incomplete, magnetic studies reveal a fundamental difference between the phosphides M_2P and M_3P: In the systems $(Fe_{1-x}M_x)_3P$, where $M=Co$ or Ni, the linear change with x in magnetization[13,26,27] agrees with the hypothesis of filling of incomplete $3d$ half-bands, cobalt contributing one and nickel two extra electrons. The magnetization changes by 0.94 μ_B/cobalt atom and by 1.92 μ_B/nickel atom.[27] Likewise, the abrupt decrease with x of the magnetization if $M=Cr$ shows that the scheme proposed[29] for the borides M_2B and MB applies equally to the M_3P phosphides. This scheme uses the virtual-state concept of Friedel,[44,45] which was introduced to account for the magnetic properties of the alloys of the first-row transition metals. Thus the behavior of the compounds M_3P, like M_2B and MB, is essentially the same as for the constituent metals, except for the contribution of the metalloid electrons to the $3d$ bands. Here the metal-atom array forms the skeletal net. On the other hand, the phosphides M_2P, although poor in metalloid atoms, exhibit a behavior reminescent of boron- or phosphorous-rich compounds and compounds having a pronounced ionic character, such as oxides and sulfides, for which the anionic array provides the structural skeleton. This curious contrast is supported by two additional observations:

1. Although maximum Curie temperatures are high (583°K), nevertheless ferromagnetism is confined to a relatively narrow range of electron/atom ratios in both the $(Co_{1-x}Mn_x)_2P$ system, which is completely ordered, and the $(Co_{1-x}Fe_x)_2P$ system, which is partially ordered. (The maximum T_c would probably occur for CoFeP were the atomic ordering complete.)

2. Ferromagnetism is replaced by metamagnetism for electron/atom ratios a little smaller than that of CoMnP in the system $(Co_{1-x}Mn_x)_2P$. Therefore, it is reasonable to anticipate that Fe_2P, which should have a similar $3d$ electron/atom ratio, exhibits a magnetization that is extremely sensitive to any reduction in this ratio (whether by substitution of Mn or Cr or by deviation from stoichiometry, $Fe_{2-x}P$) because it is at the critical ratio at which ferromagnetism gives place to metamagnetism. Although not well established by experiment, it appears from the Mössbauer spectra,[38] that small reductions in the electron/atom ratio induce progressively a partial canting of the spins in Fe_2P.

ACKNOWLEDGMENTS

This work has been made possible through the aid of the D.R.M.E.

The authors gratefully wish to thank J. B. Goodenough for the help he provided for correcting and presenting the paper at the conference.

[43] S. Rundqvist, Acta Chem. Scand. **14**, 1961 (1960).
[44] J. Friedel, Nuevo Cimento Sup. VII **2**, 287 (1958).
[45] J. Friedel, J. Phys. Radium **23**, 692 (1962).

Journal of Catalysis 209, 321–331 (2002)
doi:10.1006/jcat.2002.3604

Synthesis, Characterization, and Hydrotreating Activity of Several Iron Group Transition Metal Phosphides

Xianqin Wang, Paul Clark,[1] and S. Ted Oyama[2]

Environmental Catalysis and Materials Laboratory, Department of Chemical Engineering (0211), Virginia Polytechnic Institute and State University, Blacksburg, Virginia 24061

Received September 20, 2001; revised March 9, 2002; accepted March 9, 2002

A series of iron, cobalt, and nickel metal phosphides of chemical formula Fe_2P, CoP, and Ni_2P with specific surface areas of around 3 $m^2 g^{-1}$ were synthesized by means of temperature-programmed reduction (TPR) of the corresponding phosphates. These phosphides were also successfully prepared in dispersed form on a silica support (90 $m^2 g^{-1}$) for use as catalysts. The phase purity of these materials was established by X-ray diffraction (XRD), and surface properties were determined by N_2 BET specific surface area (S_g) measurements and CO uptake determinations. The activity of the silica-supported catalysts in hydrodenitrogenation (HDN) and hydrodesulfurization (HDS) was evaluated in a three-phase trickle-bed reactor using a model liquid feed containing 2000 ppm nitrogen as quinoline, 3000 ppm sulfur as dibenzothiophene, 500 ppm oxygen as benzofuran, 20 wt% aromatics as tetralin, and balance aliphatics as tetradecane. The reactivity study showed that the HDS activity sequence for the three samples was $Ni_2P/SiO_2 > CoP/SiO_2 > Fe_2P/SiO_2$, while the HDN activity followed the sequence $CoP/SiO_2 > Ni_2P/SiO_2 > Fe_2P/SiO_2$. Compared with a commercial Ni–Mo–S/γ-Al_2O_3 catalyst, Ni_2P/SiO_2 had a higher HDS activity (90 vs 76%), but a lower HDN activity (14 vs 38%), based on equal sites loaded in the reactor. The sites were determined by CO chemisorption for the phosphide and low-temperature O_2 chemisorption for the sulfide. XRD and X-ray photoelectron spectroscopy characterizations of the spent catalysts indicated that the Ni_2P/SiO_2 catalyst was tolerant of sulfur.

Key Words: hydrodesulfurization; hydrodenitrogenation; transition metal phosphides; Fe_2P; CoP; Ni_2P.

INTRODUCTION

Demands for a cleaner environment have led to a global tightening in the allowed sulfur content in fuels and increased restrictions on the release of nitrogen oxides. For example, in the case of sulfur the U.S. Environmental Protection Agency (EPA) has issued regulations that would lower its allowed content in diesel fuel from the current 500 to 15 ppmw in 2006, and in gasoline from 300 to 30 ppmw by 2004 (1, 2). For this reason there are considerable efforts being expended to develop new technologies for the production of clean fuels, like adsorption, extraction, oxidation, alkylation, and bioprocessing (3). Currently, however, hydroprocessing appears to be the technologically prefered solution (3). Hydroprocessing refers to a variety of catalytic hydrogenation processes that saturate heteroatomatic rings and remove S, N, O, and metals from different petroleum streams in a refinery (4). Because of the tighter environmental regulations new types of catalysts, which are economic, have long life, and possess high activity, are highly desired. In this work we present results on a new type of hydroprocessing catalyst: transition metal phosphides.

Transition metal phosphides have attracted considerable interest for some time because these materials are technologically important as semiconductors, luminescent devices, and electronic components (5). A brief thermodynamic analysis of the potential stability in H_2S was carried out early in 1975 (6), and it was revealed that this group of materials is potentially stable and sulfur resistant. However, the transition metal phosphides as a class of materials have received little attention in the field of catalysis. This is probably because the development of synthetic methods of producing materials with high surface areas was not achieved.

The combination of the iron group metals Co and Ni with Mo and W in commercial hydroprocessing catalysts (7–9) and the use of phosphorus as a promoter (10–12) is well-known. Many workers have studied the effect of phosphorus in sulfide catalysts (13–16), and the topic has been reviewed by Iwamoto and Grimblot (17). It was concluded that in these materials, the phosphorus was found as a phosphate and primarily modified the properties of the support, and only indirectly the active phase. For example, phosphorus altered the acid–base character of alumina and improved dispersion of molybdenum on the support. It also enhanced the solubility of the precursor metals in the preparation stages and allowed the synthesis of high-loading catalysts (18). The effect of phosphorus strongly depended on its content, with an effect that was usually negative at high

[1] Present address: Luna Innovations, 2851 Commerce St., Blacksburg, VA 24073.

[2] To whom correspondence should be addressed. E-mail: oyama@vt.edu.

0021-9517/02 $35.00

loadings. Phosphorus showed no effect or a small positive effect on the hydrodesulfurization (HDS) of thiophene, and a positive effect on the hydrodenitrogenation (HDN) of quinoline (19), pyridine (20), and piperidine (11). Notwithstanding the considerable studies on promoter effects, until recently phosphorus compounds in the form of phosphides had not been examined in the hydroprocessing field. The first report of the use of the iron group metal phosphides as hydrodenitrogenation catalysts was by Robinson *et al.* (21), who prepared Co_2P and Ni_2P on silica, alumina, and carbon. They reported that carbon and silica were the best supports and that Ni_2P, in particular, was very effective in HDN. These studies were carried out at high conversion, and an assessment of the intrinsic activity is not possible. The first studies on Mo and W phosphides were carried out by Li *et al.* (22), Oyama *et al.* (23), and Clark *et al.* (24), who reported good activity for HDS and HDN. Studies in the Prins group (25) confirmed the activity in HDN, and in a recent comparison of Co_2P, Ni_2P, MoP, CoMoP, and NiMoP (26) it was concluded that the areal activity of MoP was the highest. Earlier, the olefin hydrogenation activity of Ni_2P supported on alumina and other phosphides was explored by Nozaki and coworkers (27–29). It was found that the hydrogenation activity for butadiene drastically decreased, in the order $Ni_2P > Co_2P >$ FeP. They also reported that a trace of oxygen could increase the activity of Ni_2P while lowering the activity of Ni for the butadiene hydrogenation reaction. Nickel–phosphorus alloys have been reported also in amorphous form and their activities for hydrogenation have also been studied (30, 31). The amorphous alloy was prepared by an electroless plating technique from mixtures of sodium citrate, nickel sulfate, sodium hypophosphite, sodium acetate, and a silica gel support, or by the chemical reduction of nickel acetate and sodium phosphate with sodium borohydride. The supported material was subjected to various treatments, including oxidation at 403 K and reduction in H_2 at 553 K. The catalyst was found to be active for the hydrogenation of nitrobenzene (32) and benzaldehyde (33), with a turnover rate similar to that of Ni (1×10^{-3} s^{-1}). In summary, although there are some reports concerning the catalytic behavior of these phosphides, few studies have concentrated on the subject of hydrodesulfurization and hydrodenitrogenation for application in petroleum refining.

The present work presents an in-depth study of the preparation of transition metal phosphides of the iron group (Fe, Co, Ni) and their evaluation in the hydroprocessing of a model feed mixture. Initially unsupported bulk materials were prepared to provide a reference for the synthesis of supported materials. Several metal-to-phosphorus (M/P) ratios were explored to ascertain which stable phases could be prepared and to determine the conditions for temperature-programmed reduction. Subsequently, the preparation was extended to the supported system to obtain materials of high surface area suitable for catalytic testing. Silica was chosen as the carrier to minimize support effects and make possible the elucidation of the intrinsic catalytic activity of the phosphides.

EXPERIMENTAL

Materials

The support used in this study was a fumed silica (Cabosil, L90). The precursors for iron, cobalt, and nickel were $Fe(NO_3)_3 \cdot 9H_2O$ (Aldrich, 99.99%), $Co(NO_3)_2 \cdot 6H_2O$ (Aldrich, 99.99%), and $Ni(NO_3)_2 \cdot 6H_2O$ (Aesar, 99%), respectively, while the precursor for P was ammonium orthophosphate $(NH_4)_2HPO_4$ (Aldrich, 99%). The chemicals utilized in the reactivity study were dibenzothiophene (Aldrich, 99.5%), quinoline (Aldrich, 99.9%), benzofuran (Aldrich, 99.9%), tetralin (Aldrich, 99.5%), and tetradecane (Jansen Chimica, 99%). The gases employed were He (Airco, Grade 5), CO (Linde Research Grade, 99.97%), 0.5% O_2/He (Airco, UHP Grade), H_2 (Airco, Grade 5), N_2 (Airco, 99.99%), and 30% N_2/He (Airco, UHP Grade).

Synthesis

Unsupported bulk transition metal phosphides were prepared in two steps. In the first step, phosphate precursors were synthesized by reacting metal nitrates with ammonium phosphate, and in the second step, these phosphates were reduced to phosphides by the method of temperature-programmed reduction. Because the procedures for preparing unsupported bulk iron, cobalt, and nickel phosphates were similar, the preparation of iron phosphate ($FePO_4$) is used here to illustrate the process. First, 4.9 g (37.13 mmol) of ammonium phosphate $(NH_4)_2HPO_4$ was dissolved in 300 cm^3 of distilled water to form a transparent colorless solution, and 15 g (37.13 mmol) of iron nitrate ($Fe(NO_3)_3 \cdot 9H_2O$) was then added. The clear solution immediately turned into a light color mixture with some precipitate, but stirring resulted in the formation of a transparent solution. In the case of nickel and cobalt, several drops of nitric acid were needed to give rise to a homogenous solution. The water was then vaporized from the solution on a hot plate and the resulting paste was dried at 393 K for 3 h and calcined at 773 K for 6 h in an oven. The amount collected (with some minor losses) was 5.54 g, which corresponds to 36 mmol of iron phosphate of formula $FePO_4 \cdot H_2O$. The phosphate was then ground with a mortar and pestle and sieved to 16/20 mesh (0.65- to 1.2-mm-diameter particles). In the second step of preparation, temperature-programmed reduction (TPR) was utilized to convert the phosphate into phosphide. The reduction was carried out in a U-shaped quartz reactor placed in a furnace controlled by a temperature programmer (Omega Model CN 2000). The temperature was raised at $\beta = 0.0167$ K s^{-1} (1 K min^{-1}) and was monitored by a local chromel–alumel

TABLE 1

Quantities Used in the Preparation of Supported Samples

	Materials used			Catalyst properties	
Sample	Silica (g)	Metal nitrate (mol)	$(NH_4)_2HPO_4$ (mol)	Phosphide loading (wt% M_xP)	Metal loading (mol% M)
Fe_2P/SiO_2	20	0.0462	0.0231	14	11
CoP/SiO_2	20	0.0231	0.0231	9.4	6.2
Ni_2P/SiO_2	20	0.0231	0.0231	9.4	6.1

thermocouple placed in a thermowell near the center of the reactor bed. The H_2 flow rate was set at 1000 μmol s^{-1} (1500 cm^3 min^{-1}) per g of sample. A portion of the exit gas flow was sampled through a leak valve into a mass spectrometer (Ametek/Dycor Model MA 100) and the masses 2(H_2), 4(He), 18(H_2O), 28(N_2), 32(O_2), 34(PH_3), 15(NH), 44(CO_2), 31(P), and 62(P_2) were monitored during the experiment, and these were recorded together with the temperature by an online computer. At the end of the temperature program, the sample was cooled in helium to room temperature and was passivated in a 0.5% O_2/He flow for 2 h.

Phosphide samples supported on a silica support were prepared by modifying the two-step procedure used in the synthesis of the unsupported samples. Aqueous phosphate solutions were obtained as before and were used to impregnate silica by the incipient wetness impregnation method. The quantities used for the three supported samples are listed in Table 1. Prior to use, the silica was dried at 393 K for 3 h and calcined at 773 K for 6 h and was found to have an incipient wetness point of 2.2 cm^3 g^{-1}. After impregnation, the powders were dried at 393 K for 3 h and calcined at 773 K for 6 h. The calcined samples were ground with a mortar and pestle, pelletized with a press (Carver, Model C), and sieved to 16/20 mesh size. The TPR process was similar to that used for the bulk samples using the same heating rate, $\beta = 0.0167$ K s^{-1} (1 K min^{-1}).

Characterization

The synthesized materials were characterized by CO chemisorption, N_2 physisorption, and X-ray diffraction (XRD) measurements. Irreversible CO uptake measurements were used to titrate the surface metal atoms and to provide an estimate of the number of active sites on the catalysts. Uptakes were obtained after passivated samples were rereduced and are denoted *ex situ* in this paper. Usually, 0.2 g of sample was loaded into a quartz reactor and treated in H_2 at 723 K for 2 h. After cooling to room temperature in He, pulses of CO in a He carrier flowing at 27 μmol s^{-1} (40 cm^3 NTP min^{-1}) were injected through a sampling valve and the 28 (CO) signal was monitored with a mass spectrometer. Uptakes of CO were also measured for the spent samples. The procedures were the same as those used for the fresh samples. Prior to the measurement, the spent samples removed from the hydrotreating reactors were washed in hexane and dried.

BET surface area measurements were carried out right after the CO uptake determinations, using a similar technique. Adsorption at liquid nitrogen temperature was performed using a 30% N_2/He stream, and the desorption area obtained after rapid heating was compared to the area of a calibrated volume (35.4 μmol). The surface area was calculated from the one-point BET equation, which is reasonable for nonmicroporous materials such as those used here. X-ray diffraction (XRD) patterns of the samples were determined with a Scintag XDS-2000 powder diffractometer operated at 45 kV and 40 mA, using Cu $K\alpha$ monochromatized radiation (λ = 0.154178 nm). The crystallite size of the supported sample was calculated using the Scherrer equation, $D_c = K\lambda/\beta\cos(\theta)$, where K is a constant taken as 0.9, λ is the wavelength of the X-ray radiation, β is the width of the peak at half-maximum, corrected for instrumental broadening (0.1°), and 2θ is the Bragg angle (34–36). The near-surface composition of the nickel samples was obtained by X-ray photoelectron spectroscopy (XPS) (Perkin–Elmer, Model 5300 with a Mg source) operated at 15 kV and 30 mA. The 285.0-eV binding energy peak of adventious carbon was used as reference. In the case of the spent catalysts, samples were removed from the reactor, washed in hexane, heated in H_2 to 673 K, and then passivated. Since the samples were exposed to the atmosphere and not sputtered, contamination by carbon from the atmosphere was present.

Reactivity Studies

Hydrotreating activities of the samples were obtained in a three-phase trickle-bed reactor for hydrodenitrogenation (HDN) and hydrodesulfurization (HDS) with a model petroleum liquid containing 2000 ppm nitrogen (quinoline), 3000 ppm sulfur (dibenzothiophene), 500 ppm oxygen (benzofuran), 20 wt% aromatics (tetralin), and balance aliphatics (tetradecane). The operating conditions were close to industrial conditions, 3.1 MPa and 643 K, with a liquid flow rate of 5 cm^3/h and a hydrogen flow rate of 100 μmol s^{-1}(150 cm^3 min^{-1}) corresponding to a gas–liquid ratio of 9800 SCF H_2/barrel. The detailed description of the testing system is reported elsewhere (37). Quantities of catalysts loaded in the reactor correspond to the same amount of *ex situ* CO uptake (35 μmol). Prior to reactivity measurements, the catalyst samples were pretreated in exactly the same manner as before the *ex situ* CO uptake determinations. Hydrotreating samples were collected every 2 or 3 h in sealed septum vials and were analyzed off-line with a gas chromatograph (Hewlett Packard, 5890A) equipped with a 0.32 mm i.d. × 50 m fused silica capillary column (CPSIL-5CB, Chrompack, Inc.) and a flame ionization detector.

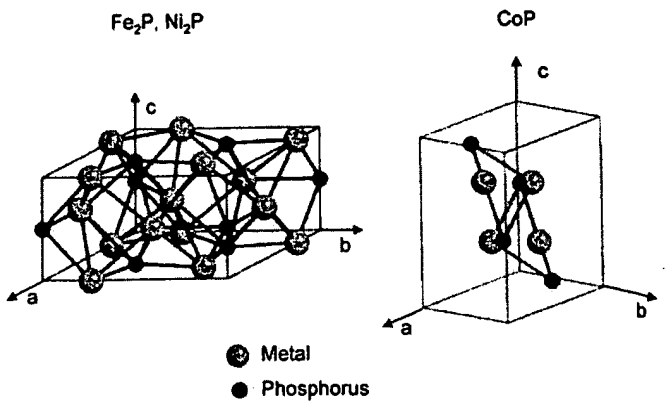

FIG. 1. Crystal structures of Fe_2P, CoP, and Ni_2P.

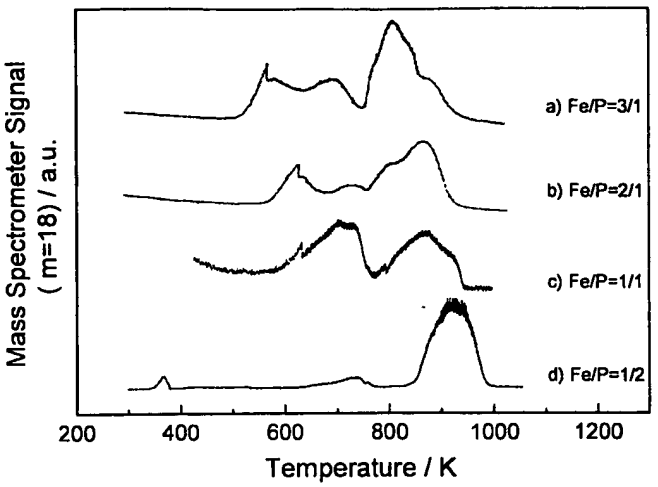

FIG. 2. Temperature-programmed reduction of bulk iron phosphates at $\beta = 1$ K/min (0.01667 K s^{-1}) (Fe-to-P ratios used in the preparation are indicated).

RESULTS AND DISCUSSION

Properties and Preparation of Bulk Phosphides

The crystal structures of the Fe, Co, and Ni phosphides are shown in Fig. 1 and their lattice parameters are summarized in Table 2. Both Fe_2P (38) and Ni_2P (39) adopt the same hexagonal structure (space group: $P_{\bar{6}2m}$), while CoP (40) takes on an orthorhombic structure (space group: P_{nma}). The crystal structures (Fig. 1) and lattice parameters can be used to calculate the bulk density (ρ) and the surface metal atom density ($\bar{n}$) of the solids (Table 2). For the Fe_2P and Ni_2P samples there are two, three, and two atoms on the *ac*, *ab*, and *bc* unit cell faces, respectively. For CoP, every unit cell face has two atoms.

The investigation of the phosphide materials in this study was begun by a study of the synthesis of bulk materials of various metal-to-phosphorus ratios (M/P) by the temperature-programmed method. This was carried out to prepare suitable references for the supported materials, and to evaluate the conditions of preparation needed when a support was employed.

The synthesis of the bulk phosphides involved two stages, preparation of phosphate precursors and reduction of the precursors in a temperature-programmed manner. The results for iron are discussed first. The precursors prepared in the first stage had different Fe/P ratios, set at the time of preparation by adjusting the mole ratio of the constituents. The precursors were formed by the thermal decomposition of mixtures of the metal nitrate and ammonium phosphate in air. Because the nitrate and ammonium ions are unstable at high temperature, it was expected that the mixture would decompose to a metal phosphate or metal oxide–phosphate. At high metal ratios some metal oxide was also likely. X-ray diffraction patterns of the precursors showed that they were amorphous.

Temperature-programmed reduction (TPR) of the precursors was carried out in the second stage (Fig. 2). Only the results for mass 18(H_2O) are shown, as the other monitored masses were featureless or provided little additional information. The TPR traces show two systematic trends for the samples with different Fe/P ratios. First, for higher Fe contents (Figs. 2a–2c), the TPR traces show more peaks and a more complicated overall reduction pattern. Second, for higher Fe contents, all the reduction peaks including the initial and final features are shifted to lower temperatures. These trends are reasonable. For higher Fe contents, the precursor is probably a mixture of iron oxide, iron phosphate, and possibly other components, and their separate reduction results in different peaks. Also for these higher Fe contents, the proportion of iron oxide should increase, and since this oxide is easily reducible, its TPR peaks appear at lower temperatures. In fact, it is likely that some metallic

TABLE 2

Surface Metal Density and Bulk Density of Fe_2P, CoP, and Ni_2P

Sample	Lattice parameter (nm)			Surface metal density (10^{15} atoms cm^{-2})				Compound density (ρ) (g cm^{-3})
	a	*b*	*c*	*ab* plane	*bc* plane	*ac* plane	Average ($\bar{n}$)	
Fe_2P	0.5867	0.5867	0.3458	1.01	0.986	0.986	0.994	6.67
CoP	0.5077	0.3281	0.5587	1.20	1.09	0.706	0.999	6.20
Ni_2P	0.5859	0.5859	0.3382	1.01	1.01	1.01	1.01	7.09

Fe is formed and that it assists in the reduction of the other components. For low Fe contents (Fig. 2d), there is no iron oxide and reaction occurs at the intrinsic reduction temperature of the main phosphate phase (~920 K). Because this temperature is high, even if a mixture of components other than phosphates existed, individual reduction steps cannot be resolved and the whole process appears to occur in one stage.

Analysis of the products of TPR was carried out by XRD (Fig. 3). The diffraction patterns all show a high background because of fluorescence by the iron. However, the presence of distinct iron phosphides can be seen easily. For the samples with Fe/P ratios of 3/1 and 2/1, the XRD results show the expected phases of Fe_3P (Fig. 2a) and Fe_2P (Fig. 3b). Comparison is made with standards from the powder diffraction file (PDF) (41), as indicated in the figure. For the sample with Fe/P ratio of 1/1, the obtained phase was still Fe_2P (Fig. 3c), and there was a deficiency in phosphorus. Similarly, for the sample with an Fe/P ratio of 1/2, the observed phase was FeP. Thus, although the preparations were carried out with stoichiometric quantities of metal and phosphorus, the final products tended to be metal-rich.

There are probably several processes which contributed to the loss of phosphorus in these samples. Some of the loss may have occurred during the TPR process, as traces of PH_3 were detected in the mass spectrometer signal and some volatile products were observed to condense at the exit of the reactor. Some of the loss probably also occurred in the calcination step at 773 K to form the phosphate precursor. A small amount of a white solid was found to have sublimed onto the lid of the ceramic calcination vessel. This was likely to be P_2O_5, with a melting point of 563 K and a sublimation temperature of 787 K. The loss of P was observed in all

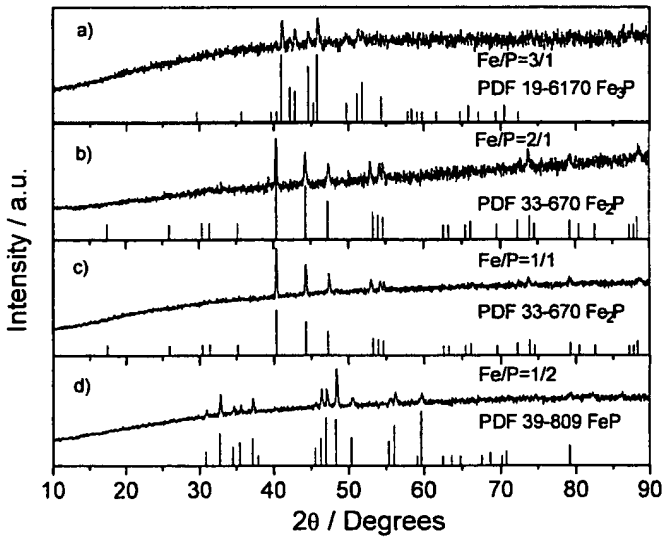

FIG. 3. X-ray diffraction patterns of iron phosphides (PDF file references are also included).

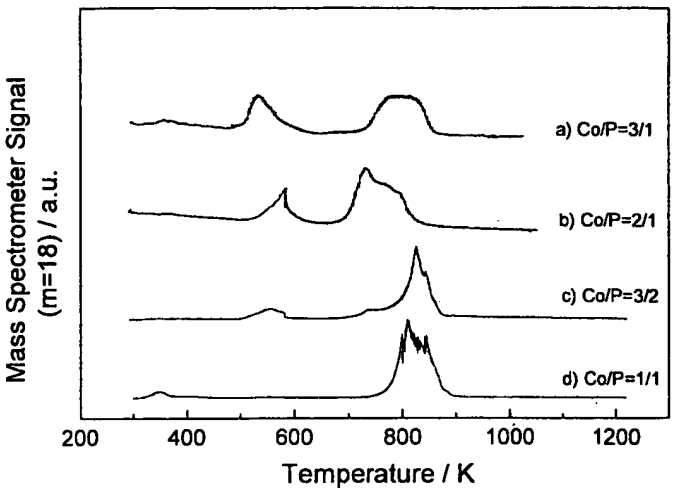

FIG. 4. Temperature-programmed reduction of bulk cobalt phosphates at $\beta = 1$ K/min (0.01667 K s^{-1}) (Co-to-P ratios used in the preparation are indicated).

samples with high P levels. There is also a possibility that some extra phosphorus in amorphous form remained mixed in the samples, and that the observed phases were simply the stable ones under the preparation conditions.

The trends in the TPR results for the cobalt samples (Fig. 4) are similar to those of the iron samples. The reaction traces consist of two main features, a low-temperature peak and a more complicated high-temperature signal. (The sample with Co/P = 1/1 has a small feature at ~350 K, probably due to dehydration). The low-temperature peak appears between 500 and 600 K and is more intense for higher Co contents (Figs. 4a–4c). It also shifts to lower temperature with increasing Co content. This behavior is consistent with the reduction of a cobalt oxide species. The higher temperature signal appears between 700 and 900 K and probably corresponds to the reduction of cobalt phosphate, which is expected to be more difficult to reduce. It is the main feature for the Co/P = 1/1 sample (Fig. 4d). The XRD patterns of the reduced cobalt samples (Fig. 5) show that Co_2P was obtained from the samples with Co/P ratios of 3/1, 2/1, and 3/2 (Figs. 5a–5c), and CoP was obtained as expected from the sample with a Co/P ratio of 1/1 (Fig. 5d). It appears that Co_2P is a particularly stable phase at these conditions.

The same trends in the TPR traces were also observed with the nickel samples (Fig. 6). The reduction features were a composite of different peaks, occurring at a low-temperature range of 500–700 K, and at a high-temperature range of 700–850 K. These various features are attributed again to the reduction of different compounds, likely nickel oxides and nickel oxide phosphate at the low temperatures and nickel phosphate at the high temperatures. As expected, Ni_3P was observed in the sample with a Ni/P ratio of 3/1 (Fig. 7a). But for the Ni/P ratios of 2/1, 3/2, and 1/1 (Figs. 7b–7d), the phase obtained was Ni_2P. Probably, this is

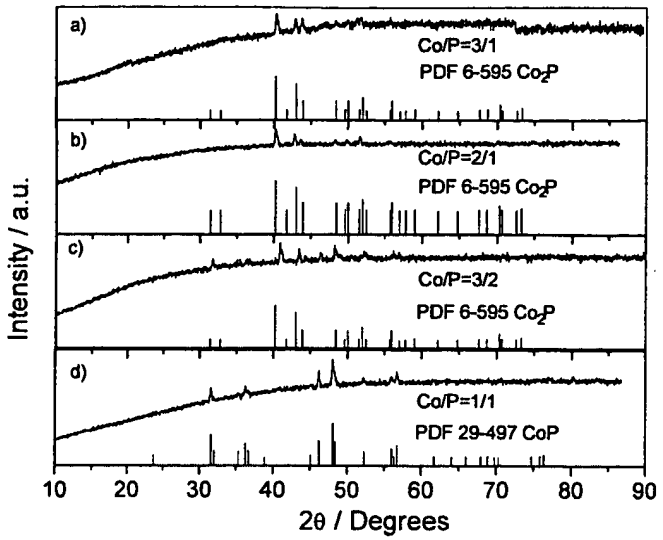

FIG. 5. X-ray diffraction patterns of reduced cobalt phosphates (PDF file references are also included).

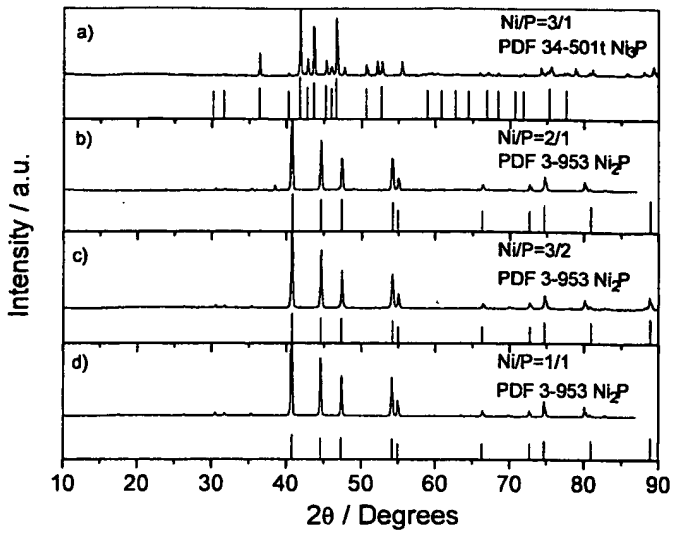

FIG. 7. X-ray diffraction patterns of reduced nickel phosphates (PDF file references are also included).

the stable phase at the conditions of the preparation, since not all the phosphorus in the precursor phosphate mixtures is likely to have sublimed. Different from the other samples, the TPR trace of the sample with the Ni/P ratio of 1/1 did show some P and PH_3 during the reduction process. This accounts for the loss of P in this sample.

To summarize these TPR and XRD results, the reduction of phosphate precursors occurs readily in the Fe, Co, and Ni systems, with maximum temperatures of about 900 K. A number of bulk phosphide compounds can be produced, depending on the stoichiometric proportions of M/P used, but the Fe_2P, CoP, and Ni_2P products are the preferred phases under the experimental conditions used in this study.

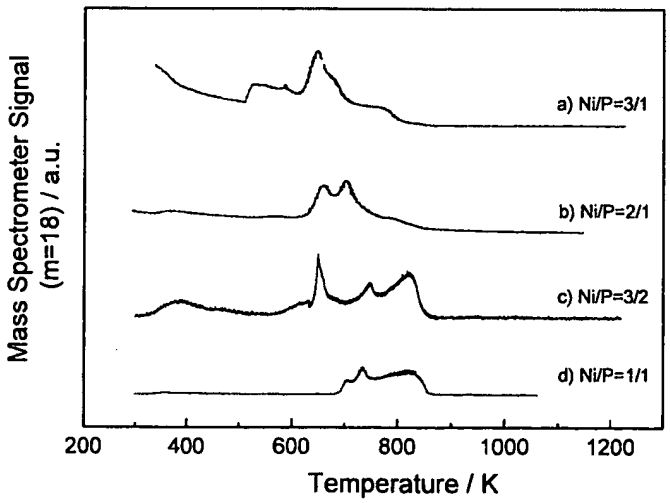

FIG. 6. Temperature-programmed reduction of bulk nickel phosphates at β = 1 K/min (0.01667 K s^{-1}) (Ni-to-P ratios used in the preparation are indicated).

Properties and Preparation of Supported Phosphides

In order to study the catalytic properties of the Fe, Co, and Ni samples high-surface-area materials were desired, and therefore, the phosphides were prepared in supported form using silica as the carrier. The preparation involved the same steps used in the synthesis of the bulk compounds. First, phosphates were prepared on the support and then were reduced by TPR. The final temperatures for preparing hydrotreating catalysts were determined by noting the point where the intensity of the water signal returned to baseline in preliminary TPR test measurements on small samples. The final temperature for supported iron, cobalt, and nickel samples were 1000, 900, and 850 K, respectively (Fig. 8). Silica was selected as the carrier because in dehydrated form it has few acid and base sites and is likely to

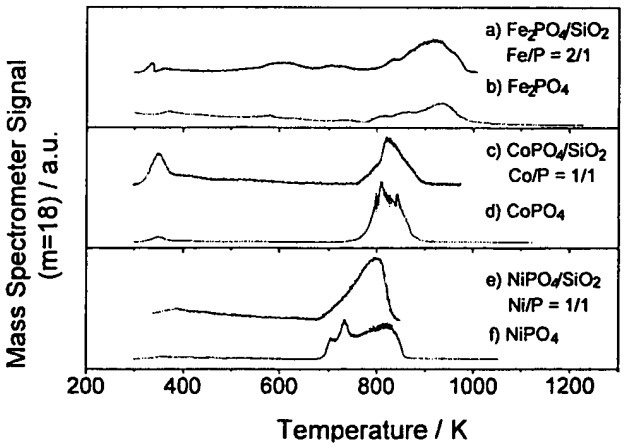

FIG. 8. TPR comparison of supported and unsupported catalysts at β = 1 K/min (0.01667 K s^{-1}).

TABLE 3

Characterization Results of Samples

Samples	BET surface area (S_g/m^2 g^{-1})	CO uptake (μmol g^{-1})	D_p (nm)	D_c (nm)	Metal site concentration (μmol g^{-1})
Fe_2P	2.7	3	330	38	45
Fresh Fe_2P/silica	97	16		23	90
Spent Fe_2P/silica	83	0		23	90
CoP	3.1	3	310	40	51
Fresh CoP/silica	87	16		21	72
Spent CoP/silica	90	4		21	72
Ni_2P	3.3	4	260	36	55
Fresh Ni_2P/silica	98	15		20	67
Spent Ni_2P/silica	100	13		20	67

offer minimal support interaction to affect the properties of the phosphides. Thus, the intrinsic activity of the phosphides could be determined.

Comparison of the TPR results obtained for the bulk samples and the corresponding supported samples (Fig. 8) provides strong evidence that the transformation of the phosphates to phosphides proceeded in the same manner for both bulk and supported samples. Aside from a slightly more pronounced low-temperature dehydration feature for the supported samples, the TPR traces for the samples of iron and cobalt were very similar to those of the unsupported forms. The reduction trace of the supported nickel sample was somewhat simpler than that of the bulk sample, but occurred at essentially the same temperature range.

The characterization results for the bulk and supported samples are reported in Table 3. The specific surface areas (S_g) of the bulk materials were low, approximately 3 m^2 g^{-1}, while those of the supported materials were close to that of the support (90 m^2 g^{-1}). The experimental CO uptakes of the samples are reported in the third column of Table 3. They were low for the bulk materials but increased for the supported samples.

The particle diameter of the bulk materials was calculated by the equation $D_P = 6/\rho S_g$ using their surface area and the bulk density (Table 2). The particle sizes for the bulk Fe_2P, CoP, and Ni_2P samples were similar, about 260–330 nm (Table 3). The crystallite sizes (D_c) were obtained from the Scherrer equation presented in the experimental section. The crystallite sizes for the bulk phosphides were again similar, about 36–40 nm. For all the bulk samples, $D_p > D_c$, and this could be due to strain and disorder in the crystallites or crystallite agglomeration. The latter is probably the larger contributor, as no support was used to stabilize the samples.

The last column in Table 3 reports the theoretical metal site concentration assuming that the samples were composed of uniform spherical particles. It was calculated from the equation

$$\text{Metal site concentration} = S_g \cdot \bar{n} \cdot f,$$

where S_g is specific surface area, $\bar{n}$ is the surface metal atom density, and f is the fractional weight loading (e.g., grams of Fe_2P/gram of catalyst) of the sample (Table 1). For the bulk samples the actual S_g was employed, while for the supported samples it was calculated from the crystallite size using the equation $S_g = 6/\rho D_c$. The last factor, f, accounts for the loading of the active phase on the supported samples.

In all cases the experimental CO uptake was considerably smaller (average 6.6% for the bulk samples; average 20.5% for the fresh supported samples) than the theoretically expected metal site concentration (Table 3) for a clean surface. This indicates that possibly the surface is blocked by some species that prevents adsorption, such as phosphorus or unreduced oxygen. In the case of transition metal carbides it is found that oxygen uptakes are considerably higher than CO uptakes (42, 43), and this suggests that oxygen should be tried as a chemisorption probe.

The effect of the heating rate on the peak temperature (T_p) associated with the reduction of supported catalysts (Fig. 9) was briefly examined in this work. The peak positions for water formation shifted to a temperature about 40–60 K higher as the heating rate (β) was increased from 0.0167 (1 K min^{-1}) to 0.0833 K s^{-1} (5 K min^{-1}). According to temperature-programmed reaction theory (44), the peak temperature (T_p) is related to the heating rate (β) and the apparent activation energy (E_a) (Table 4) by the Redhead equation ($2 \ln T_p - \ln \beta = E_a/RT_p + \text{Constant}$) (44). The activation energies found for Fe_2P/silica, CoP/silica, and Ni_2P/silica were 200, 220, and 150 kJ mol^{-1}, respectively. The results here are comparable with the activation energy

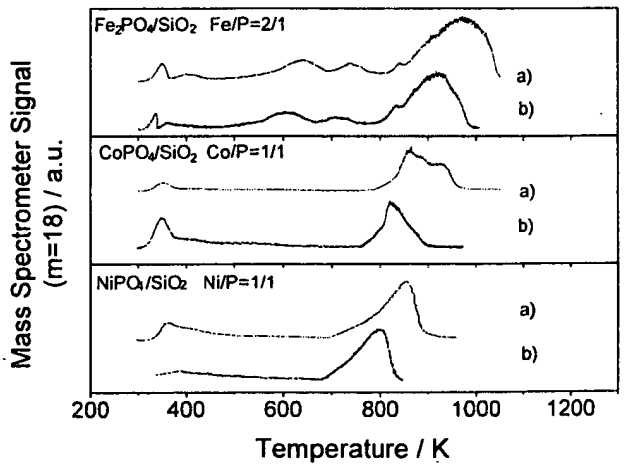

FIG. 9. TPR profiles of supported catalysts at different heating rates (β). (a) β = 5 K/min (0.08333 K s^{-1}); (b) β = 1 K/min (0.01667 K s^{-1}).

TABLE 4

Apparent Activation Energy (E_a) of Synthesis of the Supported Catalysts

Samples	E_a (kJ mol^{-1})
Fresh 14 wt% Fe_2P/silica	200
Fresh 9.4 wt% CoP/silica	220
Fresh 9.4 wt% Ni_2P/silica	150

of oxygen diffusion in the corresponding metal oxides, FeO, CoO, and NiO, which are 126, 144, and 166 kJ mol^{-1}, respectively, with preexponential factors of 1.4×10^{-2}, 2.15×10^{-3}, and 2×10^{-4} cm^2 s^{-1} (45). The correspondence is reasonable, as many solid state transformations are governed by diffusion processes (46).

Catalytic Activity in Hydroprocessing

Figures 10 and 11 present the HDS and HDN activities for the reactions of dibenzothiophene and quinoline, respectively. All three samples have high initial activities for HDS and HDN. However, except for the nickel sample in HDS, all catalysts undergo deactivation. The Fe_2P/SiO_2 lost all HDS and HDN activity by 60 h, while the CoP/SiO_2 appeared to reach a baseline of about 32% HDS and 31% HDN at around 100 h. Only the Ni_2P/SiO_2 had good, stable activity in HDS. The HDS sequence for the three samples was $Ni_2P/SiO_2 > CoP/SiO_2 > Fe_2P/SiO_2$, while the HDN sequence was $CoP/SiO_2 > Ni_2P/SiO_2 > Fe_2P/SiO_2$. Compared with a commercial Ni–Mo–S/γ-Al_2O_3 catalyst at the same conditions (24), Ni_2P/SiO_2 had a higher HDS activity, with 90 versus 76% conversion, but a lower HDN activity, with 14 versus 38% conversion. The measurements were made on the basis of equal chemisorption sites loaded in the reactor (35 μmol for the phosphides, 33 μmol for the sulfide). For the phosphides CO at room temperature was used for the chemisorption and for the sulfide O_2 at dry ice/acetone temperature was used. It may be that the CO chemisorption underestimates sites on the phosphide, so the conversions should be taken just as an approximation of intrinsic activity.

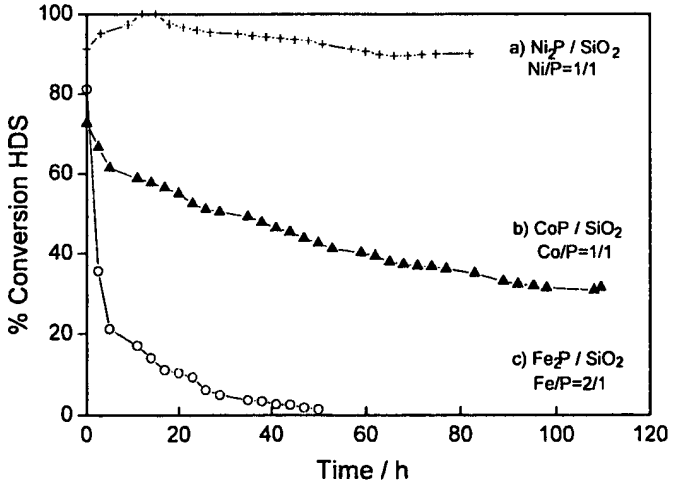

FIG. 10. Hydrodesulfurization performance of supported catalysts. (Basis: 35 μmol of chemisorption sites).

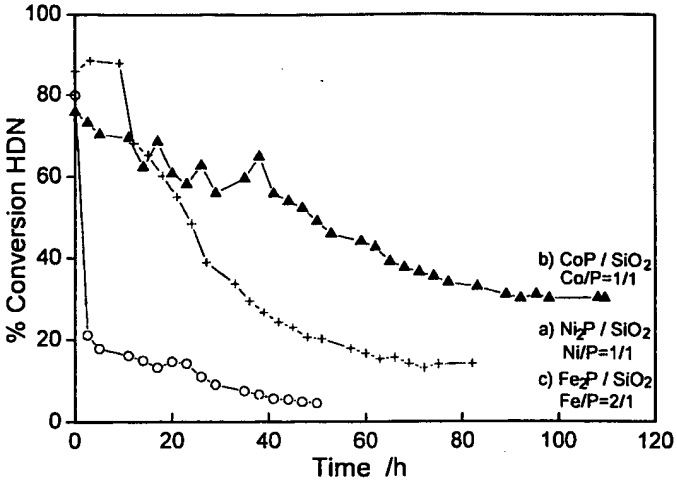

FIG. 11. Hydrodenitrogenation performance of supported catalysts. (Basis: 35 μmol of chemisorption sites).

A listing of conversions and selectivities for all the reactions is provided in Table 5. For dibenzothiophene the only product observed was biphenyl. However, for quinoline a number of species were obtained, and these were categorized as HDN products and hydrogenation (HYD) products. For benzofuran, again only one product was obtained, ethylbenzene. The amount of benzofuran used was small (500 ppm) and the reaction is facile so is unlikely to interfere with the HDS and HDN reactions, as known from other studies with carbides, nitrides, and sulfides (47, 48). In the case of tetralin, at the reaction conditions the major species obtained was the dehydrogenation product naphthalene, although small amounts of *cis*- and *trans*-decalin were also observed.

Turnover rates and areal rates measured at the baseline levels are listed in Table 6. The basis of comparison is now 70 μmol of sites, to make the numbers directly comparable to others published elsewhere (49). The procedure for conversion assumes a first-order reaction and is given in the footnotes of the table. The turnover rates are based on the experimentally determined CO uptakes on the fresh catalysts, while the areal rates are based on the calculated surface area of the phosphide crystallites using $S_g = 6/\rho D_c$ and the weight loading factor f. The Fe_2P catalyst deactivated completely and its rate is reported as zero. The CoP/SiO_2 had areal rates of 1.4×10^{15} mol m^{-2} s^{-1} in HDS and 2.1×10^{15} mol m^{-2} s^{-1} in HDN, while the Ni_2P/SiO_2 had rates of 3.4×10^{15} mol m^{-2} s^{-1} in HDS and 1.4×10^{15} mol

TABLE 5

Product Distribution in Hydroprocessing[a]

Reactants	Conversion (%)			Selectivity (%)		
	Type	Ni_2P/SiO_2	CoP/SiO_2	Product	Ni_2P/SiO_2	CoP/SiO_2
Dibenzothiophene	HDS	90	32	Biphenyl	100	100
Quinoline	HDN	14	31	Propylcyclohexane	4	16
	HYD	44	49	Propylbenzene	9	9
				5,6,7,8-Tetrahydroquinoline	33	30
				Orthopropylaniline	31	23
				1,2,3,4-Tetrahydroquinoline	24	22
Benzofuran	HDO	35	11	Ethylbenzene	100	100
Tetralin	deHYD	31	6.5	Naphthalene	98.2	91.5
	HYD	0.6	0.6	*trans*-Decalin	0.6	3.6
				cis-Decalin	1.2	4.9

[a] Catalyst loaded was equivalent to 35 μmol of CO uptake sites.

TABLE 6

Rates of HDS and HDN of the Supported Catalysts

Sample	Turnover rate[a] (10^{-3} s^{-1})		Areal rate[b] (10^{15} mol m^{-2} s^{-1})		Specific rate[c] (10^{8} mol g^{-1} s^{-1})		Volumetric rate[d] (10^{9} mol cm^{-3} s^{-1})	
	HDS	HDN	HDS	HDN	HDS	HDN	HDS	HDN
Fe_2P/SiO_2	0	0	0	0	0	0	0	0
CoP/SiO_2	0.81	1.2	1.4	2.1	1.3	1.9	4.8	7.0
Ni_2P/SiO_2	1.5	0.60	3.4	1.4	2.2	0.9	8.1	0.33

[a] Calculated from $r_t = QX/S$, where Q is the molar rate of reactant, X is the conversion, and S is the mole of sites loaded. The basis used was 70 μmol. Conversions were adjusted using the first-order formula $X_2 = 1-(1-X_1)^{S_2/S_1}$, where $S_2/S_1 = 70$ μmol/35 μmol = 2, and gave higher X than reported in Table 5 (CoP: HDS, 54%, HDN, 52%; Ni_2P: HDS, 99%, HDN, 26%).

[b] Calculated from $r_A = QXN_A/WS_gf$, where N_A is Avogadro's number, W is the weight of catalyst, S_g is the metal phosphide surface area, and f is the fractional loading of phosphide.

[c] Calculated from $r_S = r_t$(CO uptake).

[d] Calculated from $r_V = r_S\rho$, where ρ is the apparent density of the catalysts, ~0.37 g cm^{-3}.

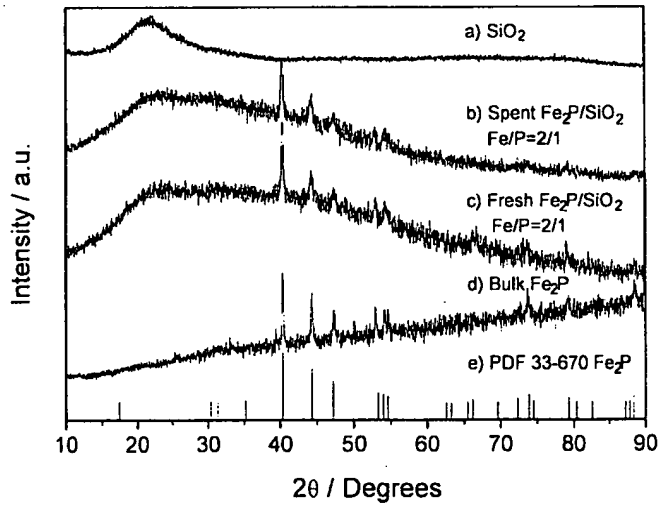

FIG. 12. X-ray diffraction patterns of iron phosphides and references. (a) Blank sample, SiO_2; (b) spent sample, Fe_2P/SiO_2; (c) fresh sample, Fe_2P/SiO_2; (d) bulk sample, Fe_2P; and (e) PDF 33-670 Fe_2P (Ref. 41).

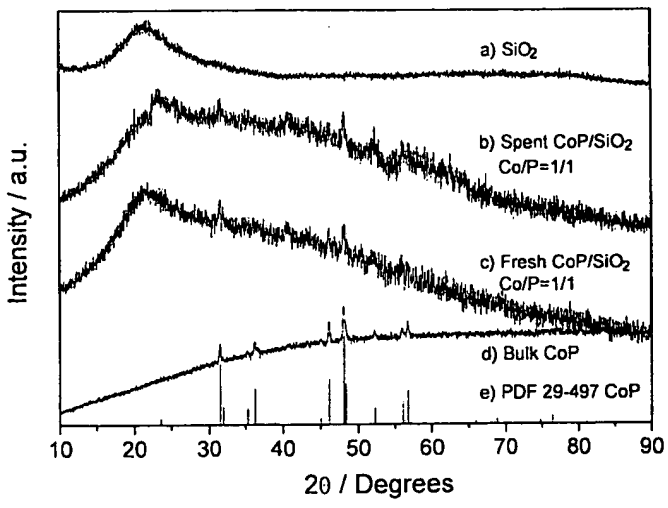

FIG. 13. X-ray diffraction patterns of cobalt phosphides and references. (a) Blank sample, SiO_2; (b) spent sample, CoP/SiO_2; (c) fresh sample, CoP/SiO_2; (d) bulk sample, CoP; and (e) PDF 29-497 CoP (Ref. 41).

m^{-2} s^{-1} in HDN. In a recent study of the HDN on unsupported samples Stinner *et al.* report areal rates of 4.8×10^{16} mol m^{-2} s^{-1} on Co_2P and 5.8×10^{16} mol m^{-2} s^{-1} on Ni_2P (26). The higher HDN rates on those samples can be attributed to several factors. First, Stinner *et al.* studied only HDN and employed a more reactive substrate (*o*-propylaniline rather than quinoline), which probably led to higher rates. They also carried out their tests without using sulfur compounds in the feed. Sulfur compounds can lead to competitive adsorption and lower rates. Finally, Stinner *et al.* used low-surface-area (1–3 m^2 g^{-1}) unsupported materials in a low-conversion regime, which would tend to result in higher rates. Nevertheless, despite the differences in experimental conditions the rates are of similar orders of magnitude.

The XRD patterns of the silica support, fresh phosphide samples, spent samples, and PDF references are compared in Figs. 12–14. These results show that silica did not influence the phases of the phosphides formed, which were the same as those obtained in the bulk materials Fe_2P, CoP, and Ni_2P. The XRD patterns for the spent iron and cobalt samples were unchanged from the corresponding fresh samples, which shows that the Fe_2P phase (Fig. 12) and CoP phase (Fig. 13) are stable during the hydrotreating reaction. For the spent nickel sample, one more peak was observed (Fig. 14). Comparing this pattern with those of other nickel phosphide compounds, it was found that the peak (*) matched one due to $Ni_{12}P_5$. This indicated that possibly a part of the Ni_2P phase transformed to a $Ni_{12}P_5$-like phase during hydrotreating. XPS measurement for this sample (Table 7) showed a P/Ni ratio close to 1 for the fresh sample, which decreased to 0.77 for the spent catalyst. This decrease may be related to the drop in HDN activity for this sample. The XPS analysis surprisingly also indicated a lack of S or N on the spent sample. The measurements were repeated on samples treated in He (just to remove volatile compounds), but the results were the same. This is likely due to lack of sensitivity by XPS at the levels expected for surface sulfur species in these supported samples. Already the signals for Ni and P were very low.

The results of posthydrotreating characterization are also presented in Table 3. For the iron sample, the CO uptake decreased to zero after the hydrotreating. The loss of the CO uptake is likely associated with the dramatic deactivation of the iron sample (Figs. 10c and 11c). As to the spent cobalt sample, the CO uptake also decreased substantially, but not to zero, as in the case of the iron sample. This was in line with the less complete deactivation of the catalyst. In the case of nickel, again a decrease in CO uptake was observed, but the decrease was much smaller than those of the iron and cobalt samples. Overall, the trend appears to indicate that the decrease in catalytic performance is related to the loss of active sites.

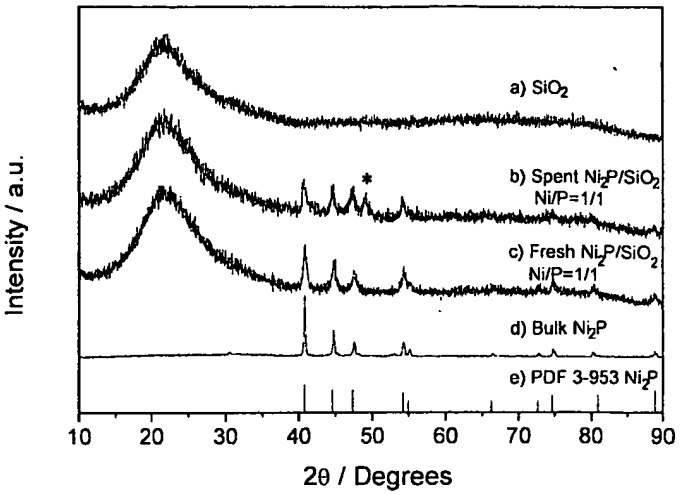

FIG. 14. X-ray diffraction patterns of nickel phosphides and references (a) Blank sample-SiO_2; (b) spent sample Ni_2P/SiO_2; (c) fresh sample Ni_2P/SiO_2; (d) bulk sample Ni_2P; and (e) PDF 3-953 Ni_2P (Ref. 41).

The reduction in the number of active sites is apparently caused by sulfidation of the catalysts. This is currently being investigated by extended X-ray absorption spectroscopy (EXAFS) of the fresh and spent samples (49). The results indicate that the catalysts are phase pure and sulfidation is restricted to the surface of the phosphide crystallites, as X-ray diffraction analysis shows that the phosphide phase is retained. The surface sulfidation process appears to be more pronounced in iron and cobalt phosphide, which show considerable deactivation in HDS and HDN. The nickel phosphide appears to be more tolerant to sulfur and thus retains high HDS activity. This is entirely reproducible. Its HDN activity is lowered, probably because the latter reaction is structure sensitive (49), and the site requirements for nitrogen removal are disrupted.

TABLE 7

XPS Results for Supported Nickel Samples

Fresh 9.4 wt% Ni_2P/silica	Element	C 1s	O 1s	N 1s	S 2p	P 2p	Ni 2p	Si 2p
	Concentration (%)	16.73	55.42	0	0	0.80	0.83	26.22
Spent 9.4 wt% Ni_2P/silica	Element	C 1s	O 1s	N 1s	S 2p	P 2p	Ni 2p	Si 2p
	Concentration (%)	19.24	53.16	0	0	0.36	0.47	26.77

CONCLUSIONS

Pure Fe_2P, CoP, and Ni_2P phases were successfully synthesized by means of temperature-programmed reduction of the corresponding phosphates. The silica-supported forms of these samples were also successfully prepared, with retention of the active phase and increased CO uptake and BET surface area. It was found that Fe_2P/SiO_2 had good initial activity for HDS of dibenzothiophene and HDN of quinoline, but that this activity fell to zero in about 60 h. The CoP/SiO_2 catalyst also deactivated but appeared to reach a stable baseline of 32% HDS and 31% HDN conversion. Only the Ni_2P/SiO_2 had a stable and high conversion in HDS of 90%, although its HDN was low at 14%. The deactivation in all cases was associated with a decrease in the number of surface metal sites as titrated by the chemisorption of CO. For the most promising catalyst, Ni_2P/SiO_2, HDS was higher than that of a commercial catalyst, Ni–Mo–S/γ-Al_2O_3, based on equal sites loaded in the reactor, as measured by CO uptake for the phosphide and low-temperature O_2 chemisorption for the sulfide. The development and improvement of this group of phosphides in the hydroprocessing field is a promising area of research.

ACKNOWLEDGMENTS

The authors are indebted to the Department of Energy (DOE) Office of Basic Energy Science, Grant DE-FG02-96ER14669, for financial support and to the NEDO International Joint Research Grant Program.

REFERENCES

1. U.S. Environmental Protection Agency, Press Release, May 1, 1999; December 21, 2000.
2. "Federal Register," Vol. 65, No. 28. U.S. Govt. Printing Office, Washington, DC, 2000.
3. O'Connor, P., and Mayo, S., *ACS Prep. Div. Fuel Chem.* **46**, 381 (2001).
4. Topsøe, H., Clausen, B. S., and Massoth, F. E., *in* "Hydrotreating Catalysis, Science and Technology" (J. R. Anderson and M. Boudart, Eds.), Vol. 11. Springer-Verlag, Berlin/Heidelberg/New York, 1991.
5. Aronsson, B., Lundström, T., and Rundqvist, S., "Borides, Silicides and Phosphides." Wiley, New York, 1965.
6. Boudart, M., Cusumano, J. A., and Levy, R. B., "New Catalytic Materials for the Liquefaction of Coal, Research Project 415, Final Report," p. 184. Catalytica Associates, Inc., 5 Palo Alto Square, Palo Alto, CA, 1975.
7. Damyanova, S., Spojakina, A., and Vit, Z., *Collect. Czech. Chem. Commun.* **57**, 1033 (1992).
8. Ozkan, U. S., Zhang, L. P., Ni, S. Y., and Moctezuma, E., *J. Catal.* **148**, 181 (1994).
9. Gulková, D., and Zdražil, M., *Collect. Czech. Chem. Commun.* **64**, 735 (1999).
10. Poulet, O., Hubaut, R., Kasztelan, S., and Grimblot, J., *Bull. Soc. Chim. Belg. Eur. Sec.* **100** (11–12), 857 (1991).
11. Fitz, C. W., Jr., and Rase, H. F., *Ind. Eng. Chem. Prod. Res. Dev.* **22**, 40 (1983).
12. Lewis, J. M., Kydd, R. A., Boorman, P. M., and Van Rhyn, P. H., *Appl. Catal. A* **84**, 103 (1992).
13. Jian, M., Rico Cerda, J. L., and Prins, R., *in* "Vth Workshop on Hydrotreating Catalysis, European Section, Lille-Villeneuve d'Ascq," p. 225. 1995.
14. Jian, M., and Prins, R., *Catal. Lett.* **35**, 193 (1995).
15. Atasanova, P., Tabakova, T., Vladov, Ch., Halachov, T., and Lopez Agudo, A., *Appl. Catal. A* **161**, 105 (1997).
16. Mangnus, P. J., van Veen, J. A. R., Eijsbouts, S., De Beer, V. H. J., and Moulijn, J. A., *Appl. Catal.* **61**, 99 (1990).
17. Iwamoto, R., and Grimblot, J., *Adv. Catal.* **44**, 417 (1999).
18. Chadwick, D., Aitchison, D. W., Badilla-Ohlbaum, R., and Josefsson, L., *Stud. Surf. Sci. Catal.* **16**, 323 (1982).
19. Eijsbouts, S., van Gestel, J. N. M., van Veen, J. A. R., de Beer, V. H. J., and Prins, R., *J. Catal.* **131**, 412 (1991).
20. López Agudo, A., López Cordero, R., Palacios, J. M., and Fierro, J. L., *in* "Vth Workshop on Hydrotreating Catalysis, European Section, Lille-Villeneuve d'Ascq," p. 237. 1995.
21. Robinson, W. R. A. M., van Gestel, J. N. M., Korányi, T. I., Eijsbouts, S., van der Kraan, A. M., van Veen, J. A. R., and de Beer, V. H. J., *J. Catal.* **161**, 539 (1996).
22. Li, W., Dhandapani, B., and Oyama, S. T., *Chem. Lett.* 207 (1998).
23. Oyama, S. T., Clark, P., Teixeira da Silva, V. L. S., Lede, E. J., and Requejo, F. G., *J. Phys. Chem. B* **105**, 4961 (2001).
24. Clark, P., Li, W., and Oyama, S. T., *J. Catal.* **200**, 140 (2001).
25. Stinner, C., Prins, R., and Weber, Th., *J. Catal.* **191**, 438 (2000).
26. Stinner, C., Prins, R., and Weber, Th., *J. Catal.* **202**, 187 (2001).
27. Nozaki, F., Kitoh, T., and Sodesawa, T., *J. Catal.* **62**, 286 (1980).
28. Nozaki, F., and Tokumi, M., *J. Catal.* **79**, 207 (1983).
29. Nozaki, F., and Adachi, R., *J. Catal.* **40**, 166 (1975).
30. Wang, W., Qiao, M., Li, H., and Deng, J., *Appl. Catal. A* **166**, L243 (1998).
31. Robinson, W. R. A. M., van Gestel, J. N., Korányi, M., Eijsbouts, T. I. S., van der Kraan, A. M., van Veen, J. A. R., and de Beer, V. H. J., *J. Catal.* **161**, 539 (1996).
32. Lee, S.-P., and Chen, Y.-W., *J. Mol. Catal. A* **152**, 213 (2000).
33. Li, H., Wang, W., Li, H., and Deng, J.-F., *J. Catal.* **194**, 211 (2000).
34. Guinier, A., *in* "X-Ray Diffraction in Crystals, Imperfect Crystals, and Amorphous Bodies," p. 121. Freeman, San Francisco, 1963.
35. Warren, B. E., *in* "X-Ray Diffraction," p. 254. Addison-Wesley, Menlo Park, CA, 1969.
36. Cullity, B. D., *in* "Elements of X-Ray Diffraction," 2nd ed., p. 102. Addison-Wesley, Menlo Park, CA, 1978.
37. Ramanathan, S., and Oyama, S. T., *J. Phys. Chem.* **99**(44), 16365 (1995).
38. Carlsson, B., Gölin, M., and Rundqvist, S., *J. Sol. St. Chem.* **8**, 57 (1973).
39. Rundqvist, S., *Acta Chem. Scand.* **16**, 992 (1962).
40. Rundqvist, S., *Acta Chem. Scand.* **16**, 287 (1962).
41. "Powder Diffraction Data Files." JCPDS International Center for Diffraction Data, Swathmore, PA, 1992.
42. St. Clair, T. P., Dhandapani, B., and Oyama, S. T., *Catal. Lett.* **58**, 169 (1999).
43. St. Clair, T. P., Oyama, S. T., and Cox, D. F., *Surf. Sci.* **468**, 62 (2000).
44. Boudart, M., and Djéga-Mariadassou, G., *in* "Kinetics of Heterogeneous Catalytic Reactions, Physical Chemistry: Science and Engineering," p. 57. Princeton University Press, Princeton, NJ, 1984.
45. O'Keeffe, M., *in* "Diffusion in Oxide and Sulfides, Sintering and Related Phenomena, Proc. Intl. Conf." (G. C. Kuczynski, N. A. Hooton, and C. F. Gibbon, Eds.). Gordon and Breach, New York, 1967.
46. Bruke, J., "The Kinetics of Phase Transformations in Metals," Pergamon, Oxford, 1965.
47. Dhandapani, B., St. Clair, T., and Oyama, S. T., *Appl. Catal. A* **168**, 219 (1998).
48. Ramanathan, S., Yu, C. C., and Oyama, S. T., *J. Catal.* **173**, 10 (1998).
49. Wang, X., Lee, Y.-K., Oyama, S. T., Bando, K., and Requejo, F. G., submitted for publication.

ACTA CHEMICA SCANDINAVICA 8 (1954) 226—239

An X-Ray Investigation of Transition Metal Phosphides

NILS SCHÖNBERG

Institute of Chemistry, University of Uppsala, Uppsala, Sweden

The investigation reported in the following paper treats phosphides of transition metals with a low phosphorus content. The metals belong to the groups IV—VI of the periodic system, *viz.* Ti, Zr, V, Nb, Ta, Cr, Mo, W. The ratio phosphorus/metal is ≤ 1 ("subphosphides" and "monophosphides").

EXPERIMENTAL

Powdered metals of fairly high purities (about 99.5 %) and red phosphorus (Kahlbaum *pro analysi*) were used as starting materials. The phosphides were prepared by the following two methods (*A* and *B*):

A. The metal powder and red phosphorus, to a total amount of about 1 g, were mixed in various proportions, and heated in evacuated and sealed silica tubes. The heating time was varied between 1 hour and 1 month, and the temperature between 550° C and 1 100° C. The best results seemed to be reached under the following reaction conditions: uniform temperature rise from room temperature up to about 800° C over a period of 2 days, heating at a constant temperature of about 800° C for about 2 days, and cooling to room temperature over a period of 1 day. Below about 650° C the rate of reaction is very slow. Above about 850° C there is a certain tendency towards reactions between the silica tube and the materials used. On account of the high vapour pressure of phosphorus at elevated temperatures, explosions are liable to take place if the silica tubes have too thin walls or are improperly sealed.

B. PH_3, obtained from white phosphorus and potassium hydroxide solution, was dried over P_2O_5 and passed together with dry oxygen-free hydrogen over the metal powders placed in alumina boats in a porcelain-tube heated in an electric furnace. The temperatures were varied between 700° and 900° C, and the times between 2 and 10 hours. The air in the apparatus was first driven out by means of carbon dioxide, whereupon a steady stream of hydrogen was passed through. Since it proved very difficult to obtain the mono- and subphosphides in a pure state by this method, it was used for the preparation of diphosphides (800° C, 6 hours). A mixture of metal powder and diphosphides was then heated in evacuated and sealed silica tubes (method A) for the preparation of specimens with the desired compositions.

In order to homogenize the product and to detect the possible presence of high-temperature modifications of the phosphides, some samples were heated in sealed evacuated silica tubes at temperatures between 600° C and 1 100° C, and then quenched in cold water.

The phase analysis and structure determinations were made from powder photographs taken with Cu-$K\alpha$ and Cr-$K\alpha$ radiation in Guinier-type cameras. The monochromator was either a curved quartz monochromator or an aluminium monochromator with double curvature [1]. For measurements of the high-angle reflections additional photographs were taken with Hägg-Phragmén type focusing cameras.

THE STRUCTURES OF THE PHASES

The existence of the diphosphides of all the actual metals (Ti, Zr, V, Nb, Ta, Cr, Mo, W) was confirmed, but no attempt was made to determine the structures.

The structures and approximate compositions of all phases with the phosphorus/metal ratio close to unity were determined.

A synopsis of the phosphides' structure types, unit cell dimensions and densities, both calculated and observed, are given in Table 5. The interatomic distances are listed in Table 6.

1. The Ti—P System

According to Biltz, Rink and Wiechmann [2], two titanium phosphides exist, one of them being homogeneous in the interval $TiP_{0.92-0.96}$ and the other having the approximate composition Ti_2P.

The existence of a "subphosphide" was confirmed in the present work, although its structure and composition is unknown.

TiP

The powder photograph reflections of a phase which was homogeneous at the composition TiP indicated hexagonal symmetry. The observed density value, 4.08, corresponds to four formula units TiP in the unit cell. There were no reflections with $h-k = 3n$ and $l \neq 2n$ simultaneously. The space-group with the highest symmetry fulfilling these conditions is D_{6h}^4—$P6_3/mmc$ with the atoms in combinations of the positions 2(*a*) 0, 0, 0; 0, 0, $\frac{1}{2}$, 2(*b*) 0, 0, $\frac{1}{4}$; 0, 0, $\frac{3}{4}$; 2(*c*) 1/3, 2/3, $\frac{1}{4}$; 2/3, 1/3, $\frac{3}{4}$, 2(*d*) 1/3, 2/3, $\frac{3}{4}$; 2/3, 1/3, $\frac{1}{4}$, and 4(*f*) 1/3, 2/3, z; 2/3, 1/3, $\bar{z}$; 2/3, 1/3, $\frac{1}{2}+z$; 1/3, 2/3, $\frac{1}{2}-z$ with $z = 1/8$. As is evident from Table 1 good agreement between calculated and observed intensities is obtained for the following atomic grouping:

4 Ti in 4 (*g*) 1/3, 2/3, z with $z = 1/8$,
2 P in 2 (*a*) 0, 0, 0; 0, 0, $\frac{1}{2}$,
2 P in 2 (*d*) 1/3, 2/3, $\frac{3}{4}$; 2/3, 1/3, $\frac{1}{4}$

If the projections of the positions on the basal plane are designated by A, B, and C, the titanium lattice can be symbolized by the sequence AABBAABB . . . The corresponding phosphorus atom sequence is ACBCACBC . . ., a mixture of cubic and hexagonal close-packing. The resulting stacking of atoms is $A_{Ti}B_PA_{Ti}C_PB_{Ti}A_PB_{Ti}C_P$. . .

The phosphorus atoms are thus placed at the centres of metal atom octahedra. The lattice can be considered as a superstructure of the NiAs (B 8) lattice. The same arrangement of metal atoms occurs in MoC (γ'-phase) [3], NbN (I)[4], W_2B_5[5] and Ti_2B_5[6]. In the boride phases the parameter z is slightly differed from 1/8. From space considerations, the nonmetal atoms in MoC (γ') and NbN (I) ought to be placed in the same positions as the phosphorus atoms in TiP. These three compounds are therefore probably isomorphous. The atomic arrangement gives an explanation of the fact that the parameter z does not differ from the value 1/8. The "anti-form" of the TiP structure has recently been found for the ternary nitride Ta_3MnN_4[7].

Table 1. Calculated and observed intensities for the TiP phase.

hkl	I_{calc}	I_{obs}
0,0,2	0	0
1,0,0	41	35
1,0,1	83	75
0,0,4	8	10
1,0,2	108	115
1,0,3	231	250
1,0,4	96	80
0,0,6	0	0
1,0,5	127	115
1,1,0	176	175
1,1,2	0	0
1,0,6	28	25
2,0,0	6	5
2,0,1	14	35
1,1,4	19	
2,0,2	21	25
1,0,7	14	50
0,0,8	46	
2,0,3	81	80
2,0,4	40	25
1,0,8	11	10
1,1,6	0	0
2,0,5	62	50
2,0,6	17	15
1,0,9	74	75
0,0,10	0	0
2,1,0	71	75
2,1,1	14	10
2,1,2	23	25
2,0,7	71	75
1,1,8	147	175
2,1,3	83	80
1,0,10	21	10
2,1,4	49	50
2,0,8	71	80
2,1,5	83	80
3,0,0	15	10
1,0,11	37	35
3,0,2	0	0
2,1,6	23	25
2,0,9	5	0
0,0,12	1	0
1,1,10	0	0
3,0,4	5	0
2,1,7	11	10
1,0,12	16	10
2,0,10	7	0
2,1,8	10	10
3,0,6	0	0
2,2,0	43	35
2,0,11	25	25
2,2,2	0	0
1,0,13	27	25
2,1,9	7	0
1,1,12	5	0
3,1,0	5	0
3,1,1	8	10
2,2,4	5	
0,0,14	0	0
3,1,2	18	15
3,0,8	111	115
3,1,3	71	80
2,0,12	21	15
2,1,10	22	15
3,1,4	51	50
1,0,14	14	15
2,2,6	0	0

2. The Zr—P system

Strotzer, Biltz, and Meisel[8] reported three intermediate phases, *viz.* Zr_3P, ZrP, and ZrP_2.

The present work confirmed the existence of a phosphide of unknown composition and structure within the interval $ZrP_{0.3-0.5}$.

α-ZrP

In the vicinity of the composition $ZrP_{0.9}$, a phosphide occurred which had a comparatively small homogeneity range. The phase is of NaCl type, and the length of the cube edge was found to vary between 5.261 Å and 5.278 Å. The zinc blende structure (B 3 type) could be rejected, both because of disagreement between calculated and observed intensities and from space considerations.

Table 2. Calculated and observed intensities for the VP phase assuming, I: "Anti-NiAs" structure, or II: NiAs structure.

hkl	I_{calc} I	I_{calc} II	I_{obs}
0,0,2	6	6	5
1,0,0	1	35	35
1,0,1	84	29	25
1,0,2	74	101	100
1,0,3	28	8	10
1,1,0	44	44	50

The NaCl structure gives ZrP as the ideal formula for this phase. A small fraction of the P positions is evidently empty. It therefore seems practical to call the phase ZrP and to denote it by α-ZrP in order to distinguish it from the following phase.

β-ZrP

This phase appeared to be homogeneous at the composition ZrP, and is isomorphous with the TiP phase.

3. The V—P system

The vanadium-phosphorus system was examined by Zumbusch and Biltz[9]. Their investigation indicated the existence of the compounds V_3P, VP and VP_2. The formula V_3P was given for the subphosphide by Chêne[10,11] and Andrieux[12].

Powder photographs of samples with the compositions $VP_{0.3}$, $VP_{0.4}$, $VP_{0.6}$, $VP_{0.8}$, $VP_{1.0}$, and $VP_{1.3}$ showed that the only compound existing in the V—VP interval is the VP phase.

From Table 2 is evident that VP has the NiAs structure (B 8 type). The space-group is thus D_{6h}^4—$P6_3/mmc$ with 2 V in 2(*a*) 0, 0, 0; 0, 0, ½ and 2 P in 2(*c*) 1/3, 2/3, ¼; 2/3, 1/3, ¾. The homogeneity range is small. The *c*/*a* value is remarkably high: 1.96. For other crystals with well established NiAs structure *c*/*a* has been found to range between 1.2 and 1.7. The VP phase seems to be the only existing phosphide of B 8 type.

4. The Nb—P and Ta—P systems

According to Zumbusch and Biltz[13,14], the niobium and tantalum phosphides are probably isomorphous. They point out that the monophosphides occur in two modifications, none of them related to the vanadium monophosphide, and that the diphosphides give a diffraction pattern similar to that of the vanadium diphosphide.

The present work confirmed the results given by these authors.

α-NbP

A homogeneous phase was obtained at the approximate composition $NbP_{0.95}$. The powder pattern of this phase corresponds to a body-centered tetragonal cell containing one unit $NbP_{0.95}$. In order to facilitate the comparison

with the following phase the corresponding face-centered cell containing two units $NbP_{0.85}$ has been chosen here.

Consequently, the atoms are distributed over the positions 0, 0, 0; 0, $\frac{1}{2}$, $\frac{1}{2}$; $\frac{1}{2}$, 0, $\frac{1}{2}$; $\frac{1}{2}$, $\frac{1}{2}$, 0. As compared with the cubic close-packing ($c/a = 1$), the tetragonal deformation is very strong, $c/a = 1.71$. The lattice can be considered to be built up of two-dimensional layers parallel to (0, 0, 1). The strong bonds exist within each NbP layer and only comparatively weak bonds between the layers. Since the interatomic distance in a layer reaches the remarkably low value of 2.35 Å (4-coordination), the only possible atomic arrangement is a partly ordered grouping. Within a layer each Nb atom is always surrounded by four P atoms. For it is most unlikely that the Nb—Nb distances are less than 2.6 Å, and the observed P—P distances of all the examined phosphides exceed the value of 3.1 Å. But it is evident from the diffraction pattern (no lines with mixed indices are visible) that the NbP layers are irregularly displaced in relation to each other. The atomic distribution in the unit cell can therefore be written as: 1 Nb + 1 P in 0, 0, 0; $\frac{1}{2}$, $\frac{1}{2}$, 0 and 1 Nb + 1 P in 0, $\frac{1}{2}$, $\frac{1}{2}$; $\frac{1}{2}$, 0, $\frac{1}{2}$, with ordered positions of the atoms within each 001-plane.

β-NbP

This phase was found to be homogeneous at the composition 1 : 1. Besides the strong diffraction lines characteristic for the face-centered arrangement of atoms, the powder photograph showed a series of extra reflections from a tetragonal lattice having the value of the c-axis twice that of the α-NbP phase. Reflections with $h + k + l = 2n$, $h00$ with $h = 2n$, 0, 0, l with $l = 4n$, $2h + l = 2n + 1$ or $4n$ appeared in the photographs. This is characteristic for the space-group C_4^6—$I4$ and D_4^{10}—$I4_12$. According to the density determinations, the unit cell contains 4 Nb and 4 P atoms. The only possible atomic position in the space-group C_4^6—$I4$ is 4(a) (0, 0, 0; $\frac{1}{2}$, $\frac{1}{2}$, $\frac{1}{2}$) + 0,0,z; 0, $\frac{1}{2}$, $\frac{1}{4}$ + z. Both the metal and nonmetal atoms have to be placed in this position. From $p|F|^2$ calculations it was found that $|z_{Nb}—z_P| = \frac{1}{2}$, meaning a fourfold screw-axis 4_1 (or 4_3) in the |0, 0, 1|-direction. The space group is thus D_4^{10}—$I4_12$ with 4 Nb in 4(a) (0, 0, 0; $\frac{1}{2}$, $\frac{1}{2}$, $\frac{1}{2}$) + 0, 0, 0; 0, $\frac{1}{2}$, $\frac{1}{4}$ and 4 P in 4(b) (0, 0, 0; $\frac{1}{2}$, $\frac{1}{2}$, $\frac{1}{2}$) + 0, 0, $\frac{1}{2}$; 0, $\frac{1}{2}$, $\frac{3}{4}$.

While the NbP layers of the α-NbP phase occupy disordered positions in relation to each other, the β-NbP lattice has an ordered atomic arrangement.

Intensities for the β-NbP phase, both calculated and observed, are compared in Table 3.

α-TaP

α-TaP is isomorphous with α-NbP, and probably has the corresponding approximate composition $TaP_{0.95}$. It was not possible to obtain this phase in a pure state.

β-TaP

The β-TaP phase is isomorphous with β-NbP, and was found to be homogeneous at the composition 1 : 1.

Table 3. Calculated and observed intensities for the β-NbP phase.

hkl	I_{calc}	I_{obs}	*hkl*	I_{calc}	I_{obs}
1,0,1	51	40	1,1,10	28	25
0,0,4	65	85	2,0,9	4	0
1,0,3	26	25	3,0,5	4	0
1,1,2	117	125	1,0,11	3	0
1,0,5	12	10	2,1,9	6	0
2,0,0	31	40	0,0,12	5	5
1,1,6	52	60	3,1,6	39	40
2,1,1	17		3,2,1	6	
1,0,7	8	5	3,0,7	3	0
2,0,4	52	60	2,2,8	18	15
0,0,8	13	15	3,2,3	6	0
2,1,3	6	5	3,2,5	6	0
2,1,5	12	10	2,1,11	5	0
1,0,9	5	5	1,0,13	3	0
2,2,0	16	25	3,0,9	3	0
3,0,1	6	5	4,0,0	10	10
2,1,7	9	5	4,1,1	9	10
2,2,4	28	25	3,2,7	9	10
2,0,8	28	25	4,0,4	34	40
3,0,3	4	0	4,1,3	10	10
3,1,2	56	60			

5. The Cr—P system

The existence of the Cr_3P and CrP phases was proved by Nowotny and Henglein [15] by X-ray methods. Cr_3P is isomorphous with Mn_3P [16], Fe_3P[17,18], Ni_3P[13] and $(Fe, Ni)_3P$[20] with the atoms in the probable space-group S_4^2—$I\bar{4}$[18,21]. CrP is of the B 31 type [22], isomorphous with MnP, FeP, and CoP[23].

CrP

The CrP phase has 4 Cr and 4 P atoms in the positions 4(c) ± (x, y, $\frac{1}{4}$; $\frac{1}{2}$—x, $\frac{1}{2}$ + y, $\frac{1}{4}$) in the space-group D_{2h}^{16}—$Pbnm$. Nowotny and Henglein reported the same parameter values for CrP as was earlier given for MnP[23], *i.e.* $x_{Cr} = 0.20$; $y_{Cr} = 0.005$; $x_P = 0.57$; $y_P = 0.19$. The present author, however, found the best agreement between calculated and observed intensities for the following values: $x_{Cr} = 0.16$; $y_{Cr} = 0.00$; $x_P = 0.63$; $y_P = 0.20$.

The B 31 type (MnP structure) can be regarded as an orthorhombic deformed B 8 type (NiAs structure). Though the NiAs structure is hexagonal, it may be described as an arrangement with the symmetry of D_{2h}^{16} in the special case of the axial ratio $\sqrt{3} : b/c : 1$ and the atoms located in two four-fold positions 4(c) x, y, $\frac{1}{4}$, with the parameters for the metal atoms $x = 0.25$; $y = 0$ and for the phosphorus atoms $x = 0.58$; $y = 0.25$. As is evident from the parameter values given above, those obtained in the present investigation signify a comparatively large deviation from the "ideal" atomic positions.

But on the other hand, the resulting interatomic distances are in good agreement with analogous distances observed for the monophosphides of the other transition metals studied here (Table 6).

6. The Mo—P system

The phases Mo_2P and MoP were reported by Andrieux and Chêne[12,24] and according to Faller and Biltz [25] Mo_3P is isomorphous with Cr_3P [18].

MoP

The MoP phase was found to have the WC structure. Very small variations of the lattice constants were measured, and the formula was found to correspond to the composition 1 : 1. No extra reflections appeared in the powder photographs. This excludes an arrangement of the P atoms corresponding to the NiAs type.

7. The W—P system

Whereas the formula W_4P and W_2P were given for the tungsten subphosphides by Hartmann and Orban [26], Faller and Biltz [27] showed that W_2P is a mixture of W and WP of MnP type. But the latter authors did not publish any parameter values. They further pointed out that WP_2 is isomorphous with MoP_2, but not with CrP_2.

The present author found that powder photographs of samples with the compositions $WP_{0.2}$, $WP_{0.4}$, $WP_{0.6}$, and $WP_{0.8}$, only showed diffraction lines of the W and WP phases, confirming the results obtained by Faller and Biltz [27].

WP — space group 62 (same as CoP)

As I pointed out above, no unit cell dimensions or parameter values for the atomic positions have hitherto been given for the WP phase. In the diffraction pattern there appeared $0kl$ reflections with $k = 2n$ and $h0l$ reflections with $h + l = 2n$, characteristic for the space-group D_{2h}^{16}—$Pbnm$ (compare the isomorphous CrP phase). The lines, which did not fulfill the conditions: $h + k + l = 2n$, $0kl$ with $k = 2n$ and $l = 2n$, were found to be very weak and only appeared at relatively small diffraction angles. It was therefore assumed that the phosphorus gave rise to these weak reflections. This gives $y_w = 0$. A systematic variation of x_w within the limits of closest approach between the tungsten atoms (about 2.6 Å) resulted in a value of $x_w = 0.175$ for the best agreement between calculated and observed intensities. Because of the great difference between the atomic factors of tungsten and phosphorus, it is very difficult to determine the position of the nonmetal atoms by means of X-ray data. The parameters x and y for the phosphorus atoms have thus been determined with a view to the best space distributions $x_P = 0.62$ and $y_P = 0.20$.

WP thus has 4 W and 4 P atoms located in two four-fold positions 4(c) $\pm (x, y, \frac{1}{4}; \frac{1}{2}-x, \frac{1}{2}+y, \frac{1}{4})$ in the space-group D_{2h}^{16}—$Pbnm$, with the following parameter values: $x_w = 0.175$; $y_w = 0$; $x_P = 0.62$; $y_P = 0.20$.

Calculated and observed intensities are compared in Table 4.

W = ± (.175, 0, .25) (0.325, .5, .25)

P = ± (.62, .20, .25) (-0.12, 0.70, .25)

Table 4. Calculated and observed intensities for the WP phase.

hkl	I_{calc}	I_{obs}	*hkl*	I_{calc}	I_{obs}
1,0,1	125	75	0,2,4	7	5
0,0,2	56	75	4,1,3	2	0
0,1,1	182	175	1,2,4	0	0
2,0,0	103	110	2,1,5	36	35
1,0,2	4	5	5,0,2	0	0
2,0,1	1	5	4,2,0	36	35
1,1,1	6	5	0,3,1	28	35
2,1,0	1	5	5,1,1	0	0
2,0,2	39	40	3,2,3	67	70
1,1,2	175	175	4,2,1	0	0
2,1,1	211	175	4,0,4	4	0
1,0,3	94	110	1,3,1	0	0
3,0,1	25	25	2,2,4	7	5
2,1,2	0	0	3,0,5	17	15
0,1,3	7	10	0,0,6	16	15
2,0,3	0	0	1,0,6	0	0
1,1,3	1	0	5,1,2	43	35
3,0,2	0	0	4,2,2	22	25
0,2,0	46	50	2,3,0	0	0
3,1,1	1	0	1,3,2	43	35
0,0,4	6	5	5,0,3	31	35
1,2,1	22	25	4,1,4	0	0
1,0,4	0	0	2,3,1	50	50
2,1,3	0	0	3,1,5	0	0
3,1,2	61	50	2,0,6	28	
0,2,2	21	25	1,1,6	58	110
4,0,0	35	35	1,2,5	30	
2,2,0	48	50	3,2,4	0	0
3,0,3	67	75	2,3,2	0	0
1,2,2	2	5	0,3,3	1	0
4,0,1	0		5,1,3	0	0
2,2,1	0	0	6,0,0	13	10
2,0,4	3	0	4,2,3	0	0
1,1,4	102	110	1,3,3	0	0
4,1,0	1	0	6,0,1	0	0
4,0,2	19	15	4,0,5	0	0
3,1,3	0	0	2,1,6	0	0
2,2,2	36	35	2,2,5	0	0
4,1,1	73	75	3,3,1	0	0
2,1,4	1	0	5,2,1	11	10
1,2,3	90	110	5,0,4	0	0
1,0,5	27	25	6,1,0	0	0
3,2,1	28	25	6,0,2	8	10
4,1,2	0	0	3,0,6	0	0
3,0,4	0	0	2,3,3	2	0
4,0,3	1	0	6,1,1	45	50
2,2,3	0	0	4,1,5	25	25
0,1,5	17	15	3,3,2	34	25
3,2,2	0	0	5,2,2	0	0
2,0,5	0	0	5,1,4	44	35
1,1,5	1	0	4,2,4	4	0
3,1,4	74	75	1,0,7	1	0
5,0,1	5	0	6,1,2	0	0

Table 4. Cont.

hkl	I_{calc}	I_{obs}	*hkl*	I_{calc}	I_{obs}
3,1,6	4	0	6,2,0	33	75
1,3,4	46	75	2,1,7	66	
3,2,5	26		0,3,5	18	10
0,2,6	23	25	5,1,5	0	0
6,0,3	0	0	6,1,2	0	0
1,2,6	0	0	6,0,4	3	0
4,3,0	0	0	4,1,6	0	0
0,1,7	28	25	4,2,5	0	0
3,3,3	0	0	7,0,1	7	0
4,3,1	41	50	0,4,0	20	15
5,2,3	53	50	1,3,5	0	0
2,0,7	0	0	3,0,7	2	0
1,1,7	0	0	3,3,4	80	75
2,3,4	0	0	5,2,4	0	0
5,0,5	13	10	4,3,3	5	0
4,0,6	26	25	1,4,1	19	50
6,1,3	5	0	6,2,2	35	
2,2,6	52	50	3,2,6	0	0
4,3,2	0	0	7,0,2	0	0
			6,1,4	0	0

GENERAL DISCUSSION

All the phosphides listed in Table 5 have a greyish black metallic lustre, and are not attacked by water or dilute acid at room temperature. Samples of TiP, ZrP, and VP were not oxidized or decomposed when heated in air at 1 000° C for one hour.

The highest nonmetal content of carbides and nitrides of all transition metals, with the exception of the lanthanides and actinides, is about 50 atom-%. The nonmetals are interstitially situated at the centres of octahedra or trigonal prisms of metal atoms. The metal lattice commonly forms a hexagonal or cubic close-packing, in a few cases a simple hexagonal arrangement of atoms. The interatomic metal-metal distances are up to about 10 % larger than those of the pure metals, and the corresponding coordination numbers are high, varying between 8 and 12.

Hägg [28,29] has found empirically that the radius ratio nonmetal/metal is a determining factor for the structure of the phases and has an upper critical value of about 0.59. When the radius ratio exceeds 0.59 the structure is complicated, but the compounds are still metallic in character. This is characteristic of most borides and silicides. Space considerations account for the decrease in the coordination number of the metal atoms, but the coordination number for metal atom — nonmetal atom is still high. Furthermore, there exist "contact" bonds of non-ionic type between boron-boron and silicon-silicon atoms. Such nonmetal "contacts" have *not* been found to exist among the carbides and nitrides. For this reason, boron and silicon occurring in compounds with transition metals can be characterized as metals.

The radius value for the phosphorus atom has been found to be about 1.06 Å (Table 6). For the metals used here the radius ratio P/Me (Me = transition metal) exceeds the value 0.59 by between 10 and 30 %. From the structure determinations it is further evident that no P—P bonds of non-ionic type exist in the phosphides investigated in the present study. It is therefore of interest, that many of the monophosphides have structures analogous to those of the carbides and nitrides.

Table 5. Structures and unit cell dimensions of the phosphides of Ti, Zr, V, Nb, Ta, Cr, Mo, W and the phosphorus metal ratio ≤ 1.

Phase	Structure type	Space-group	Z	Cell dimensions in Å (Error: < ± 1 ‰)	Vol/metal-atom Å³	Density calc	Density obs
TiP		$P6_3/mmc$	4	$c = 11.65$, $a = 3.487$; $c/a = 3.34$	30.67	4.27	4.08
α-ZrP	NaCl	$Fm3m$	4	$a = 5.27$	36.62	5.43	5.10
β-ZrP	TiP	$P6_3/mmc$	4	$c = 12.52$, $a = 3.677$; $c/a = 3.40$	36.65	5.57	5.35
VP	NiAs	$P6_3/mmc$	2	$c = 6.22$, $a = 3.18$; $c/a = 1.96$	27.20	5.00	4.72
α-NbP		$F4/mmm$	4	$c = 5.69$, $a = 3.32$; $c/a = 1.71$	31.35	6.40	
β-NbP		$I4_12$	8	$c = 11.38$, $a = 3.325$; $c/2a = 1.71$	31.46	6.54	6.15
α-TaP	α-NbP	$F4/mmm$	4	$c = 5.69$, $a = 3.320$; $c/a = 1.71$	31.35	11.04	
β-TaP	β-NbP	$I4_12$	8	$c = 11.39$, $a = 3.330$; $c/2a = 1.71$	31.57	11.15	10.3
Cr_3P	Fe_3P	$(I\bar{4})$	8	$c = 4.567$, $a = 9.144$; $c/a = 0.50$	15.91	6.51	6.25
CrP	MnP	$Pbnm$	4	$a = 6.108$, $b = 5.362$, $c = 3.113$	25.11	5.49	5.25
Mo_3P	Fe_3P	$(I\bar{4})$	8	$c = 4.923$, $a = 9.729$; $c/a = 0.51$	19.42	9.09	8.60
MoP	WC	$P\bar{6}m2$	1	$c = 3.20$, $a = 3.23$; $c/a = 0.99$	28.64	7.50	7.20
WP	MnP	$Pbnm$	4	$a = 6.219$, $b = 5.717$, $c = 3.238$	28.78	12.40	11.7

The metal atoms of the MoP phase form a simple hexagonal lattice. If we assume radii corresponding to neutral atoms, the available space permits another nonmetal atom to be placed in the metal lattice of the carbides and nitrides with the stacking AA . . . In this case both centres of the two trigonal metal atom prisms of the unit cell would be occupied. But as the observed phase composition is always close to the ratio 1 : 1, this case never occurs. This can be explained by an electron displacement from the metal towards the nonmetal atoms causing an increase in the radius of the latter. The corresponding bonds would then not have a pure metallic character but would be partially ionic.

The radius values for the carbon and nitrogen atoms are 0.77 Å and 0.71 Å respectively. Because of the comparatively large value for the phosphorus atoms, about 1.06 Å, the metal lattice in a phosphide of "interstitial" structure must be considerably expanded compared with that of analogous carbides and nitrides. The intermetallic distances in VP are 21 % and in MoP 18 % greater than in the corresponding metals, indicating a weakening of the metal bonds. The stability of the compound must be largely due to strong metal/phosphorus bonds (6-coordination) — probably of a partial ionic nature. The interatomic P—P distances follow the variation of the atomic radii of the metals. As a consequence, the nonmetal atoms are partially or entirely isolated from each other in the lattice, both in a geometrical and in a chemical (no covalent bonds) sense. This is also the case for the metallic carbides, nitrides, and oxides.

If the simple hexagonal metal lattice is "filled" with nonmetal atoms, the so-called AlB_2 structure (C 32 type) is formed, common for several diborides [30]: TiB_2, ZrB_2, HfB_2, VB_2, NbB_2, TaB_2, CrB_2, and MoB_2. As $r_B = 0.87$ Å

Table 6. Interatomic distances (in Å) of closest approach in the phosphides. The atomic radii of phosphorus have been calculated on the assumption of non-ionic bonds and metal coordination numbers = 8.

Phase			r_{Me}[31]/ 8-coord.	r_P(calc.)
TiP	Ti – 1Ti 2.91 6P 2.48	P – 6Ti 2.48 6P 3.49 6P 3.54 } 3.51	1.42	1.06
α-ZrP	Zr – 6P 2.64	P – 6Zr 2.64 12P 3.73	1.54	1.10
β-ZrP	Zr – 1Zr 3.13 6P 2.64	P – 6Zr 2.64 6P 3.68 6P 3.78 } 3.73	1.54	1.10
VP	V – 6P 2.41	P – 6V 2.41 6P 3.18 6P 3.61 } 3.39	1.31	1.10
α-NbP	Nb – 4P 2.35 (4Nb+4P) 3.29	P – 4Nb 2.35 4P 3.32 (4P+4Nb) 3.29	(1.43) * 1.28	1.07
β-NbP	Nb – 4P 2.35	P – 4Nb 2.35 4P 3.32 4P 3.30 } 3.31	(1.43) * 1.28	1.07
α-TaP	Ta – 4P 2.35 (4Ta+4P) 3.30	P – 4Ta 2.35 4P 3.32 (4Ta+4P) 3.30	(1.44) * 1.30	1.05
β-TaP	Ta – 4P 2.36	P – 4Ta 2.36 4P 3.33 4P 3.30 } 3.31	(1.44) * 1.30	1.06
CrP	Cr – 2Cr 2.48 2P 2.25 2P 2.27 1P 2.37	P – 2Cr 2.25 2Cr 2.27 } 2.28 1Cr 2.37 2P 3.08 2P 3.11 } 3.10	1.26	1.02
MoP	Mo – 6P 2.46	P – 6Mo 2.46 2P 3.20 6P 3.23 } 3.22	1.36	1.10
WP	W – 2W 2.71 2P 2.38 2P 2.43 1P 2.55	P – 2W 2.38 2W 2.43 } 2.43 1W 2.55 2P 3.18 2P 3.24 } 3.21	1.37	1.06

* As the niobium and the tantalum atoms have 4-coordination in the MoP planes, the radii values for this coordination number have been calculated from Pauling's correction factors [34], taking the Born exponent $n \sim 9$.

and $r_P = 1.06$ Å the metal-metal distances in the phases VB_2[31] and MoB_2[32] are shorter than in VP and MoP, but still essentially greater than in the corresponding pure metals — for the diborides VB_2 and MoB_2 the increase is 15 % and 13 % respectively. A corresponding comparison between inter-

metallic distances in MoC [8] and Mo, VC [33] and V results in the values 6 % and 8 % respectively.

As has been pointed out above, TiP and β-ZrP phases are isomorphous with MoC (γ'-phase) [8] and NbN (I)[4]. The stacking of the metal atoms can be symbolized by the sequence AABBAABB ... The phosphorus atoms are situated in the lattice holes so that the highest possible P—P distances are attained. A calculation of the mean intermetallic distances (10-coordination) in these two compounds gives values 17 % and 14 % greater than those observed for the corresponding pure metals. The Nb—Nb distances in NbN (I) are 6 % greater than those found in niobium metal.

Two borides with the same arrangement of metal atoms as in the TiP phase have been found to exist, *viz.* W_2B_5[5] and Ti_2B_5[6]. But in these compounds the boron atoms occupy ten lattice "holes" in the unit cell instead of four [TiP, β-ZrP, NbN (I), MoC (γ')], giving rise to hexagonal two-dimensional boron nets and slightly puckered boron nets, both with boron-boron bonds.

The structure of the NbP and TaP modifications seem to be unique, with two-dimensional metal-phosphorus layers. As metal-nonmetal bonds exist only within such layers and not between them, the separate layers must be bonded together by metallic forces. The interatomic P—P distances are so great as to isolate the phosphorus atoms from each other. The metal-metal distances both within the metal-phosphorus layers (4-coordination) and between them (4-coordination) are 15 % greater than in the pure metals.

The metal atoms in CrP, WP and isomorphous phases of the MnP structure (B 31 type)[28] are surrounded by two metal atoms at "contact" distances and six metal atoms at considerably larger distances. The structure can be regarded as a strongly deformed NiAs type, with the phosphorus atoms located at the centres of deformed metal atom octahedra. The calculated mean values of the intermetallic distances are between 15 and 20 % greater than in the corresponding pure metals.

The structures of the subphosphides of the metals Ti, Zr, Cr, and W are not known, but the symmetry, unit dimensions and cell contents are known for the Cr_3P and W_3P phases. An approximate calculation of the intermetallic distances in these compounds by means of the values obtained for unit cell values or densities of the pure metals, the subphosphides and the monophosphides, indicates a linear expansion of about 5 % (8-coordination) compared with the corresponding metals Cr and W. This corresponds to the observed value of the increase in the intermetallic distance for many metallic carbides, nitrides, and oxides. This agrees with the view that a decrease of the nonmetal content in a compound results in an increase of metallic properties. When the number of nonmetal atoms of a fixed kind is increased, or when the nonmetal atoms in a fixed composition are replaced by other nonmetal atoms with a greater atomic radius, the intermetallic distances will be enlarged and/or the metal-metal coordination number will decrease.

A continuous nonmetal-metal transition takes place in group Vb of the periodic system (N, P, As, Sb, and Bi), N being a nonmetal. As having the properties characteristic for a nonmetal as well as a metal, and Bi being a metal. Intermediate phases MeX_x of corresponding composition, containing a transition metal (Me) and any of the group Vb elements (X), must have a

minimum of metallic character when X = phosphorus. The strong metallic properties of the nitrides are explained by the favourable geometrical conditions for the formation of common "interstitial" compounds.

The increase in the radius of X on going from N to P results in an increase in the Me—Me distances. And thus in a weakening of the metal-metal bond in the metallic lattices. And thus in a weakening of the metal-metal bond in lattices of analogous types, i.e. with as high coordination numbers as in the pure metals. With further increase of the radius value of X(As→Sb →Bi), it is highly probable that intermediate phases will occur with the Me—Me coordination number smaller than 8. But on the other hand, the Me—X bonds will show a continuous increase in metallic strength. The antimonides and bismuthides can be characterized as intermetallic compounds.

SUMMARY

The Ti—P, Zr—P, V—P, Nb—P, Ta—P, Cr—P, Mo—P, and W—P systems have been investigated by X-ray methods for phosphorus contents up to about 50 atom-%. The structures of all monophosphides have been determined and — with the exception of NbP and TaP — have been found to be of types analogous to those of metallic carbides and nitrides.

TiP and β—ZrP are isomorphous with MoC (γ'-phase) and NbN (I), the metal atoms being arranged in the stacking sequence AABBAABB . . .

α—ZrP ($ZrP_{0.9}$), VP, and MoP possess NaCl, NiAs, and WC structures respectively.

The phases $NbP_{\sim 0.95}$ (α—NbP) and NbP (β—NbP) have analogous tetragonal lattices, both built up of two-dimensional NbP layers, but in the first phase these are disordered relative to each other and in the latter they occupy ordered positions. The ordering leads to a doubling of the c-axis of the unit cell.

The two TaP modifications are isomorphous with the corresponding NbP phases.

The existence of the compounds Cr_3P and Mo_3P of the Fe_3P structure type has been confirmed.

The positions of the atoms in the CrP and WP phases of the MnP structure type have been redetermined.

All the phosphides have greyish black metallic lustre and are markedly resistant to chemical reagents.

The phosphides are compared with the metallic carbides, nitrides, borides, and silicides of the transition elements in a general discussion. They can be characterized as a peripheric group of these metallic compounds, having similar valency configurations but weaker metal-metal bonds. The metal-phosphorus bonds are strong, probably of a partial ionic nature.

The radius of the phosphorus atom has been found to have a mean value of about 1.06 Å.

The author wishes to express his gratitude to Professor G. Hägg for his encouraging interest in the present investigation. This work has been supported by a grant, which is gratefully acknowledged, from *Statens Tekniska Forskningsråd*. I also wish to thank Mrs. U. Schönberg and Mr. S. Hedling for their valuable assistance in the preparation of the samples.

REFERENCES

1. Hägg, G., and Karlsson, N. *Acta Cryst.* 5 (1952) 728.
2. Biltz, W., Rink, A., and Wiechmann, F. *Z. anorg. Chem.* 238 (1938) 395.
3. Kuo, K., and Hägg, G. *Nature* 170 (1952) 245.
4. Brauer, G., and Jander, J. *Z. anorg. Chem.* 270 (1952) 160.
5. Kiessling, R. *Acta Chem. Scand.* 1 (1947) 893.
6. Post, B., and Glaser, F. W. *J. Chem. Phys.* 20 (1952) 1050.
7. Schönberg, N. *Acta Chem. Scand.* 8 (1954) 213.
8. Strotzer, E. F., Biltz, W., and Meisel, K. *Z. anorg. Chem.* 238 (1938) 395.
9. Zumbusch, M., and Biltz, W. *Ibid.* 249 (1942) 1.
10. Chêne, M. *Compt. rend.* 208 (1939) 1144.
11. Chêne, M. *Ann. Chim.* |11| 15 (1941) 272.
12. Andrieux, J. L. *Rev. Mét.* 45 (1948) 49.
13. Zumbusch, M., and Biltz, W. *Z. anorg. Chem.* 249 (1942) 20.
14. Zumbusch, M., and Biltz, W. *Ibid.* 246 (1941) 33.
15. Nowotny, H., and Henglein, E. *Ibid.* 239 (1938) 14.
16. Årstad, O., and Nowotny, H. *Z. physik. Chem.* |B| 38 (1937) 356.
17. Hägg, G. *Nova Acta Regiae Soc. Sci. Upsaliensis* [4] 7 (1929) No. 1.
18. Hägg, G. *Z. Krist.* 68 (1928) 470.
19. Nowotny, H., and Henglein, E. *Z. physik. Chem.* |B| 40 (1938) 281.
20. Heide, F., Herschkowitz, E., and Preuss, E. *Chem. Erde.* 7 (1932) 483.
21. Nowotny, H. *Naturwiss.* 29 (1938) 631.
22. *Strukturbericht* Band III (Leipzig 1937) p. 17.
23. Fylking, K. E. *Arkiv Kemi. Mineral. Geol.* B 11 (1934) No. 48.
24. Andrieux, J. L., and Chêne, M. *Compt. rend.* 209 (1939) 672.
25. Faller, J. F., Biltz, W., Meisel, K., and Zumbusch, M. *Z. anorg. Chem.* 248 (1941) 216.
26. Hartmann, H., and Orban, J. *Z. anorg. Chem.* 226 (1936) 257.
27. Faller, J. F., Biltz, W., Meisel, K., and Zumbusch, M. *Z. anorg. Chem.* 248 (1941) 209.
28. Hägg, G. *Z. physik. Chem.* |B| 6 (1930) 221.
29. Hägg, G. *Ibid.* |B| 12 (1931) 33.
30. Schwarzkopf, P., and Kieffer, R. *Refractory Hard Metals*, New York 1953, p. 20.
31. Norton, J. T., Blumenthal, H., and Sindeband, S. J. *Trans. AIME* 185 (1949) 749.
32. Bertaut, F., and Blum, P. *Acta Cryst.* 4 (1951) 72.
33. Becker, K., and Ebert, F. *Z. Physik* 31 (1925) 268.
34. Pauling, L. *The Nature of the Chemical Bond*, London 1948, Chapter X.

Received November 27, 1953.

Journ. of Catalysis 207, 256–265 (2002)
doi:10.1006/jcat.2002.3520, available online at http://www.idealibrary.com on IDEAL®

Characterization of Silica-Supported Molybdenum and Tungsten Phosphide Hydroprocessing Catalysts by ^{31}P Nuclear Magnetic Resonance Spectroscopy

P. Clark, X. Wang, and S. T. Oyama[1]

Environmental Catalysis and Materials Laboratory, Department of Chemical Engineering (0211), Virginia Polytechnic Institute and State University, Blacksburg, Virginia 24061

Received July 17, 2001; revised January 4, 2002; accepted January 4, 2002

Silica-supported molybdenum phosphide, MoP/SiO_2, and tungsten phosphide, WP/SiO_2, were prepared and characterized for their catalytic activity in hydrodenitrogenation (HDN) and hydrodesulfurization (HDS). The silica-supported phosphides were tested in the simultaneous hydroprocessing of quinoline and dibenzothiophene at 3.1 MPa and 643 K and were compared to a MoS_2/SiO_2 sample. The supported phosphides had superior HDN and lower HDS activity compared to the sulfide under these conditions. The conversion levels of MoP/SiO_2 were similar to those of bulk MoP, while the WP/SiO_2 was somewhat less active than its bulk WP counterpart. However, when compared on a CO uptake basis, the bulk materials had a clear performance advantage. Solid state nuclear magnetic resonance measurements indicated ^{31}P shifts from 85% H_3PO_4 of 255 ppm for WP and 214 ppm for MoP. Comparison of freshly prepared and passivated samples indicated that the supported phosphides were susceptible to surface oxidation on exposure to the atmosphere as a result of their small particle size.

Key Words: hydrodenitrogenation; hydrodesulfurization; silica; tungsten phosphide; molybdenum phosphide; quinoline; dibenzothiophene; ^{31}P NMR.

INTRODUCTION

Transition metal phosphides like MoP (1–3), WP (4), Ni_2P, and Co_2P (5, 6) constitute a new class of catalysts that have recently been reported to be active for hydroprocessing reactions. This is currently an important area, as there is a need to develop better catalysts to meet severe environmental restrictions on the content of sulfur in transportation fuels. Fundamental understanding of the differences between compounds like MoP and MoS_2 is needed in order to design improved materials. The objectives of the present investigation are to study the preparation of MoP and WP deposited on a silica support and to compare their performance to the unsupported catalysts. A further objective is to determine the applicability of ^{31}P magic-angle spinning–nuclear magnetic resonance (MAS–NMR) spectroscopy for the study of the bulk and supported phosphide samples. Except for one study in our group on WP (7), this technique has not been applied to transition metal phosphides and the spectra presented here are the first to be reported in the literature. The NMR measurements indicate that the silica-supported MoP and WP samples are susceptible to oxidation on exposure to the atmosphere. However, complementary X-ray diffraction measurements show that at reaction conditions the principal supported phases remain phosphides.

The use of silica for hydroprocessing catalysts has not been widely studied because weak interactions with the active phase generally lead to low dispersions (8). It is generally thought that the surface of the silica support contains coordinatively saturated bridging oxide species and surface hydroxyls but is essentially neutral in character (9). This is in contrast to the alumina surface which contains hydroxyl groups with amphoteric character (10) and which interacts strongly with metal (11, 12), sulfide (13), phosphate (14), and phosphide (15) adsorbents. It has been reported that silica-supported CoMo catalysts prepared by impregnation exhibit low hydrotreating activity compared to Al_2O_3-supported catalysts (16), and this has been attributed to the low dispersion of Co and Mo after calcination. However, it has been found that low loading (2–4 wt%) samples of MoS_2/SiO_2 can perform better than their Al_2O_3 counterparts (17, 18). In fact, silica-supported Co sulfide having 7.4% loading has been recently proposed as an inexpensive alternative to conventional catalysts (19). We have undertaken this study to investigate the suitability of SiO_2 as a support for MoP and WP.

EXPERIMENTAL

Catalyst Preparation and Characterization

Catalysts were prepared by incipient wetness impregnation of a silica support with aqueous metal phosphate

[1] To whom correspondence should be addressed. E-mail: oyama@vt.edu.

0021-9517/02 $35.00

precursors, followed by temperature-programmed reduction (TPR) in flowing hydrogen. The silica support (Cabot, Cabosil L90, 99.8%) consisted of 0.2- to 0.3-μm aggregates of spherical particles ~30 nm in diameter prepared by vapor-phase hydrolysis of $SiCl_4$ in a H_2–O_2 flame (20). Stoichiometric amounts of ammonium paramolybdate, $(NH_4)_6Mo_7O_{24} \cdot 4H_2O$ (Aldrich, 99%), or ammonium metatungstate $(NH_4)_6W_{12}O_{39} \cdot xH_2O$ (Aldrich, 90%) were combined with ammonium phosphate $(NH_4)_2HPO_4$ (Aldrich, 99%) in distilled water, and the solution was used to impregnate the silica support by the incipient wetness technique. The concentration of Mo, W, and P in the solution was 0.73 mol/dm^3. The moist paste was calcined in air at 773 K for 6 h, ground and mixed, then pressed, broken, and sieved between 650- and 1180-μm screens to form pelletized supported phosphate materials. The molar loadings of molybdenum and tungsten monophosphide were held constant at 1.16 mmol each of Mo, W, and P per g of silica, leading to 13 wt% MoP/SiO_2 and 20 wt% WP/SiO_2. Sulfidation of samples containing 5.0 wt% MoO_3 and 13 wt% MoO_3 (0.37 and 1.16 mmol of MoO_3 per g of silica) led to 5.6 and 17 wt% MoS_2/SiO_2, respectively.

The precursor phosphates were loaded in quartz u-tube reactors and were reduced to phosphides using linear temperature ramps (0.0833 K s^{-1}, 5.0 K min^{-1}) in flowing hydrogen. Hydrogen flow was set at 650 μmol s^{-1} g^{-1} of starting material (e.g. 300 cm^3(NTP) min^{-1} H_2 flow for a 0.300-g sample) for all syntheses. The final temperature was 850 K for the MoP/SiO_2 and 1000 K for the WP/SiO_2, with this temperature held for 2 h to ensure completion of reaction. Species in the effluent were identified periodically (2–5 s) by a mass spectrometer (Dycor/Ametek MA100) to follow the progress of the reaction. Water was the only gaseous reaction product observed; no P_2 ($m/z = 62$) or PH_3 ($m/z = 34$) were detected. Occasionally, though, traces of a yellow insoluble deposit were formed downstream in the reactor following the higher temperature preparation of WP/SiO_2. After reduction, the phosphide was cooled to room temperature under 65 μmol s^{-1} of helium, and typically was passivated progressively by flowing 78 μmol s^{-1} of 0.1 mol% O_2/He overnight, followed by 13 μmol s^{-1} of 0.5 mol% O_2/He for 2 h. The reactor was then disconnected from the flow system, and ambient air was allowed to diffuse in for 24 h before collecting the sample from the tube.

Unsupported MoP and WP reference samples were also synthesized from phosphate precursors as reported earlier (1, 4). The bulk MoP was prepared by TPR to 913 K at 0.0833 K s^{-1} (5 K min^{-1}), and the bulk WP by TPR to 973 K at the same heating rate.

MoS_2/SiO_2 samples were prepared by sulfiding 5 wt% MoO_3/SiO_2 and 13 wt% MoO_3/SiO_2 for 2 h in a stream of 10 mol% H_2S/H_2 at 678 K, following a temperature ramp of 0.0833 K s^{-1} (5 K min^{-1}). The sulfide sample used for hydroprocessing was sulfided directly from the oxide within the catalytic reactor at a flow rate of 98 μmol s^{-1} (150 cm^3 of NTP min^{-1}) of 10% H_2S/H_2 at atmospheric pressure. The characterization of the sulfide samples by O_2 chemisorption also directly followed sulfidation of the oxide. For the chemisorption measurements on MoS_2/SiO_2, 0.3 g of oxide was sulfided in 195 μmol s^{-1} of 10% H_2S/H_2 employing the same temperature program used for the catalyst samples.

All gases were supplied by Air Products. Hydrogen, helium, and carbon monoxide were all 99.999% pure and were passed through a water trap (Alltech) before coming into contact with the sample. Specialty mixtures, including 0.5% O_2/He, 30% N_2/He, and 10% H_2S/H_2, were used as received.

The total dynamic CO uptakes of the phosphides were measured by passing pulses of CO (5.6 μmol) in a stream of 40 μmol s^{-1} of helium over 0.3-g samples at room temperature. Passivated samples were characterized after rereduction at 723 K in H_2. The phosphides used in all our studies were used within a month of preparation, as it was found that longer term storage in closed vials resulted in a slow degradation, probably due to oxidation. Uptakes of O_2 for the sulfides were measured in an identical manner at dry ice/acetone temperature (195 K). The O_2 uptakes were multiplied by a factor of 2 to account for dissociative adsorption on the surface. Surface area measurements were performed on air-exposed samples by N_2 adsorption using a Micromeritics 2000 sorption unit.

X-ray diffraction (XRD) spectra were collected with a Scintag XDS-2000 X-ray diffractometer using Ni-filtered Cu$K\alpha$ ($\lambda = 0.1541$ nm) radiation. Scans were collected at a rate of 0.035° 2θ s^{-1} and increments of 0.03° 2θ. Crystallite sizes were estimated from the diffraction patterns using the Scherrer equation, $D_{hkl} = K\lambda/\beta \cos\theta$. The constant K was taken here to be 0.9, and the average of the strongest two reflections was used to determine the reported values (21).

Nuclear Magnetic Resonance

Characterization of the samples by ^{31}P MAS-NMR was carried out using a Bruker (MSL 300) instrument operating at 300 MHz. A single-pulse method was used with a pulse delay of 3 μs, an acquisition delay of 3 ms, a recycle delay of 1 s, and approximately 14,500 acquisitions. Measurements were taken at different sample rotation (SR) speeds. Chemical shifts are referenced to 85% H_3PO_4. Samples were loaded into Kel-F capped zirconia rotors without exposure to the atmosphere in a glove box (*in situ*), or were passivated with 0.5% O_2/He and exposed to the atmosphere (*ex situ*).

Reactivity Testing

Hydroprocessing activity was measured by hydrotreatment of a model liquid containing quinoline and dibenzothiophene at 643 K (370°C) and 3.1 MPa (450 psig) in

TABLE 1

Composition of Model Oil

Component	mol%	wt%	N, S, O (wppm)	Delivery rate (μmol h^{-1})
Quinoline	2.6	1.9	2000	580
Dibenzothiophene	1.7	1.7	3000	380
Benzofuran	0.6	0.4	500	130
Tetralin	27	20	0	6,100
Tetradecane	68	76	0	15,500

TABLE 2

Compositional Characteristics of Silica-Supported Catalysts

Sample[a]	mmol of metal g^{-1} of SiO_2	Metal atom nm^{-2} of SiO_2
5.6% MoS_2/SiO_2	0.37	2.44
13% MoP/SiO_2	1.16	7.67
20% WP/SiO_2	1.16	7.67

[a] Weight percent MoP, WP, or MoS_2.

an upward-flow, fixed-bed reactor as described earlier (22). Compositional characteristics and delivery rates of the feed liquid are summarized in Table 1. With the exception of tetradecane of purity 99 mol% , which was purchased from Fisher, chemicals were obtained from Aldrich and had a purity level of 97+%.

To start a reaction, samples were placed in the catalytic reactor and pretreated before starting the oil delivery. The phosphide catalysts were pretreated in 100 μmol s^{-1} of hydrogen at 723 K and 1-atm pressure for 2 h. The sulfide catalyst was pretreated by sulfiding the oxide directly in the catalytic reactor, with a 10 mol% H_2S/H_2 mixture at 678 K and 1-atm pressure for 2 h. After the pretreatment, the reactor conditions were set to 3.1 MPa (450 psig), a hydrogen flow rate of 100 μmol s^{-1} (150 cm^3 NTP min^{-1}), a liquid feed rate of 0.0833 cm^3 s^{-1} (5 cm^3 min^{-1}), and 643 K. The amounts of catalysts used in this study were 2.6 g of MoS_2/SiO_2, 1.4 g of MoP/SiO_2, and 3.1 g of WP/SiO_2. These amounts corresponded to roughly similar quantities (70, 70, and 58 μmol, respectively) of chemisorption sites. For the SiO_2 blank, an arbitrary amount of 3 g was employed, as the material had negligible chemisorption of CO. The compositions of hydroprocessed liquid samples were identified with a Hewlett Packard 5890A gas chromatograph (equipped with a CP Sil 5B column) on samples collected at 2- to 3-h intervals. Reaction products were identified through matching of retention times with commercially available chemicals. Characterization of catalysts after reaction by XRD was made after washing the collected samples in *n*-hexane, drying in air, and mounting ~1-mm-thick powder films on top of a glass slide.

RESULTS

Preparation and Characterization

Silica-supported molybdenum phosphide, tungsten phosphide, and molybdenum sulfide catalysts were prepared by incipient wetness impregnation of a silica support with ammonium salts of Mo, W, and P dissolved in distilled water. Compositional characteristics of each sample are summarized in Table 2.

Oxidic catalyst precursors were reduced to phosphide form by temperature-programmed reduction in hydrogen and were subsequently passivated. Prior to the reactivity measurements and *ex situ* CO uptake characterization, passivated phosphides were pretreated in hydrogen at 723 K for 2 h to remove the surface oxide layer.

The temperature-programmed reduction (TPR) trace at 5 K min^{-1} of MoP/SiO_2 is compared to that of bulk MoP in Fig. 1. The predominant reduction features appeared at 680 and 820 K for the supported sample and 770 and 920 K for the unsupported reference. X-ray diffraction (XRD) patterns of the fresh and spent MoP/SiO_2 samples are shown in Fig. 2 along with that of a bulk MoP reference. An insert depicts the crystal structure of MoP. The diffraction patterns of the supported catalysts showed only features of bulk MoP and amorphous silica (the broad peak near 22° 2θ) both before and after reaction.

The TPR traces of WP/SiO_2 and WP are shown in Fig. 3. Here, the predominant reduction peaks occurred at 890 and 970 K for the supported material and 1010 K for the unsupported reference. XRD patterns of the fresh and spent WP/SiO_2 samples are shown in Fig. 4 along with that of a bulk WP reference. Again the insert depicts the crystal structure. The diffraction patterns of the supported catalyst showed features only of WP and amorphous silica both before and after reaction in hydrotreating.

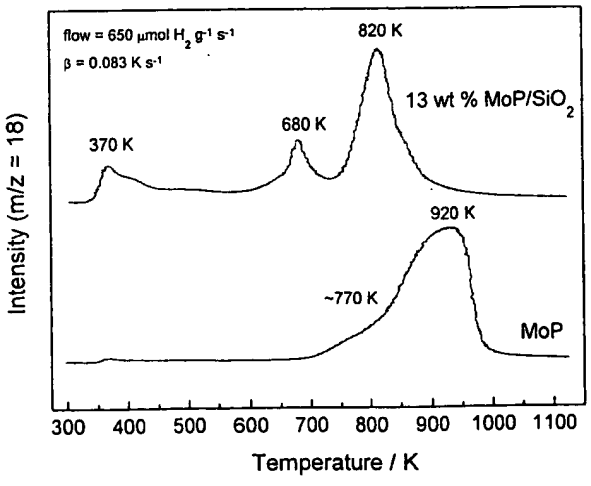

FIG. 1. Temperature-programmed reduction profiles in the preparation of MoP/SiO_2 and MoP at 0.0833 K s^{-1} (5 K min^{-1}).

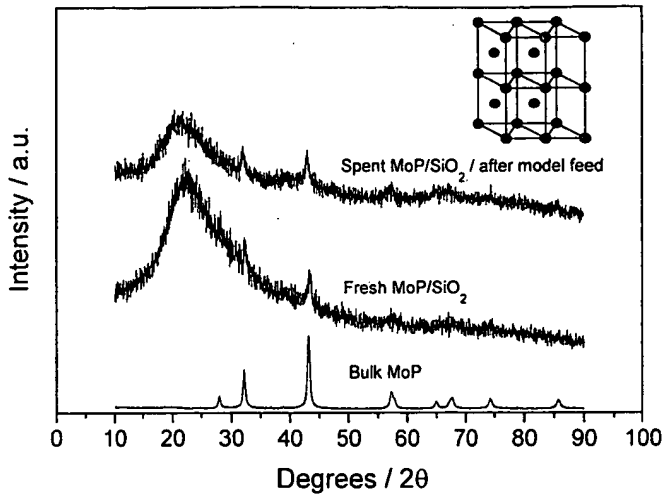

FIG. 2. X-ray diffraction spectra for fresh and spent MoP/SiO_2 samples.

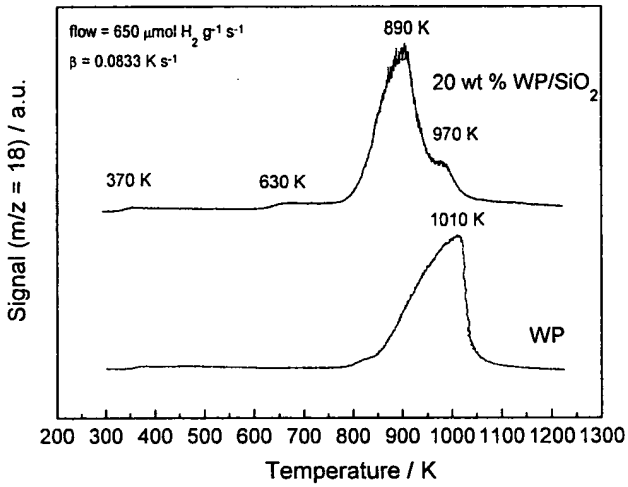

FIG. 3. Temperature-programmed reduction profiles in the preparation of WP/SiO_2 and WP at 0.0833 K s^{-1} (5 K min^{-1}).

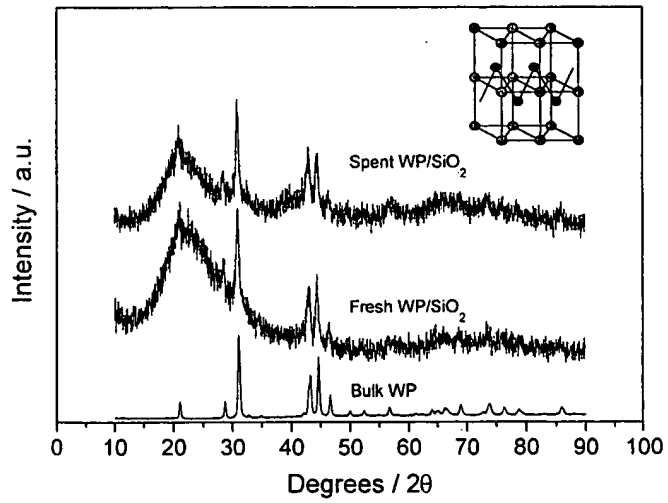

FIG. 4. X-ray diffraction spectra for fresh and spent WP/SiO_2 samples.

TABLE 3

Physical Characteristics of Silica-Supported Catalysts

Sample	Surface area[a] ($m^2\ g^{-1}$)	Crystallite size[a] (nm)	CO uptake[b] Fresh	CO uptake[b] Spent	Surface metal sites[c]	Dispersion[d] (%)
SiO_2 blank	91	—	0	0	—	—
5.6% MoS_2/SiO_2	93	—	27[e]	—	—	5.2
17% MoS_2/SiO_2	—	—	7[e]	—	—	0.7
13% MoP/SiO_2	50	15[f]	50	26	110	4.9
20% WP/SiO_2	62	16[g]	19	6.5	94	2.0
MoP	8	18[f]	15	4.5	130	0.2
WP	10	23[g]	10	11	140	0.2

[a] Passivated catalysts.
[b] CO uptake at 298 K in μmol g^{-1}; sample pretreated at 723 K in H_2.
[c] Calculated in μmol g^{-1} from formula in text.
[d] CO uptake (fresh)/mol of metal.
[e] O_2 uptake at 78 K; sample presulfided at 678 K in 10% H_2S/H_2.
[f] Average of (100) and (101) directions.
[g] Average of (101) and (002) directions.

The chemisorption and surface area properties of the catalysts are summarized in Table 3. The incorporation of phosphides onto the silica reduced the surface areas of the samples in both cases. The surface area of the sulfide was unaffected, presumably because of its low metal loading and low preparation temperature. The experimental CO uptakes dropped during the catalytic test.

Crystallite sizes, theoretical CO uptakes, and dispersions were calculated for MoP and WP catalysts based on their crystallite size, density, and loading. These values are also reported in Table 3. The calculation of crystallite sizes (D_{hkl}) with the Scherrer equation was described earlier, in the experimental section. Table 3 also reports the theoretical number of surface metal sites (μmol g^{-1}), assuming that the samples are composed of uniform spherical particles. It was calculated from

$$\text{Surface sites} = S_g \cdot \bar{n} \cdot f, \qquad [1]$$

where S_g is the specific surface area ($m^2\ g^{-1}$) either measured (for the bulk samples) or calculated (for the supported samples) from the crystallite size and density by the equation

$$S_g = \frac{6}{D_{hkl} \cdot \rho}. \qquad [2]$$

The quantity $\bar{n}$ is the areal density, the number of metal atoms per unit surface, and f is the fractional weight loading (g of MoP/g of catalyst or g of WP/g of catalyst) of the sample. The areal density is taken here to be 16.1 μmol m^{-2} for MoP, as calculated from the value of the surface area per metal atom of 10.3 $Å^2$, as reported previously (2). The corresponding values for WP were derived from its crystal structure to be 14.5 μmol m^{-2} and 11.6 $Å^2$ $atom^{-1}$.The density, ρ, was taken to be 7.50 g cm^{-3} for MoP and 12.4 g cm^{-3} for WP (23). The crystallite sizes of the phosphides

supported on silica were smaller than the crystallite sizes of the bulk material.

Dispersions were calculated from the fresh chemisorption uptakes, assuming a stoichiometry of 1 CO per surface metal atom. These values are also reported in Table 3. The dispersions were generally low, indicating poor distribution of the components on the support. This is typical of the behavior of metallic compounds on silica supports.

Nuclear Magnetic Resonance Spectroscopy

Characterization of the catalysts by ^{31}P MAS–NMR was carried out on both fresh (*in situ*) and passivated (*ex situ*) samples. Figure 5 shows the NMR spectra of the bulk WP at different sample rotation (SR) speeds. The *in situ* spectra (Fig. 5a) displayed a complex pattern in which the positions of only two peaks, at 255 and −6 ppm (arrows), were invariant with rotation. The *ex situ* spectra (Fig. 5b) again showed a number of peaks, with the same ones remaining invariant, but with the intensity pattern changed considerably, and with the peak at low field becoming dominant and slightly shifted to −3 ppm. Figure 6 shows similar NMR results for the WP/SiO_2 sample. Again, the *in situ* sample (Fig. 6a) had two peaks that were invariant with rotation at 254 and −5 ppm (arrows), while the *ex situ* sample (Fig. 6b) had an altered pattern with the peak at low field becoming dominant and slightly shifted to −3 ppm. Table 4 gives a summary of the observed chemical shifts.

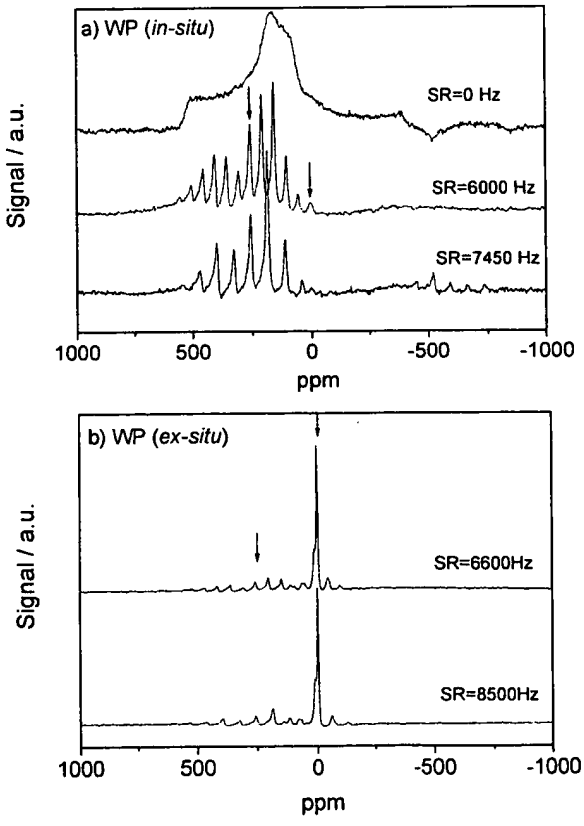

FIG. 5. ^{31}P MAS–NMR spectra: (a) WP *in situ*, (b) WP *ex situ*.

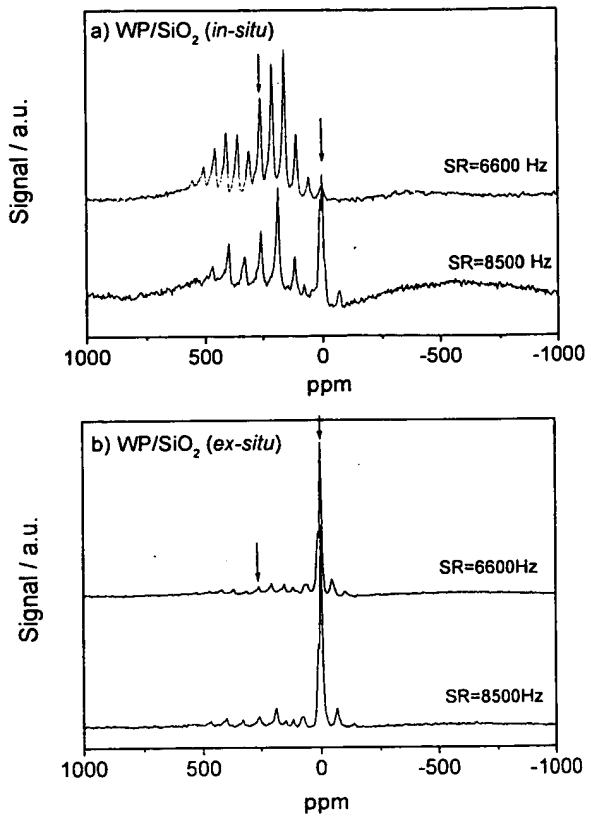

FIG. 6. ^{31}P MAS–NMR spectra: (a) WP/SiO_2 *in situ*, (b) WP/SiO_2 *ex situ*.

Figure 7 shows the NMR spectra of the unsupported MoP sample at *in situ* and *ex situ* conditions. The *in situ* spectrum (Fig. 7a) displayed a complex pattern that was completely different from that of the bulk WP sample, but which again had two peaks, at 214 and −5 ppm (arrows), that did not shift with sample rotation. The *ex situ* sample (Fig. 7b) showed a similar pattern but the signals were much noisier and were overlaid on a sinusoidal baseline. Again, two invariant peaks were observed, with the low-field peak enhanced and shifted to −3 ppm. Figure 8 shows the results for the MoP/SiO_2 sample. The *in situ* spectra (Fig. 8a) displayed considerable noise and an uneven baseline, with weak and unresolved features at 199 and −36 ppm (arrows). The *ex situ* spectra (Fig. 8b) were completely dominated by the low-field feature at −5 ppm, with the high-field peaks barely discernible.

Reactivity

The progress of the hydroprocessing reactions of dibenzothiophene and quinoline at 643 K and 3.1 MPa using MoP/SiO_2 and WP/SiO_2 are shown in Fig. 9. Both materials reached stable conversion levels after only 20 h of reaction.

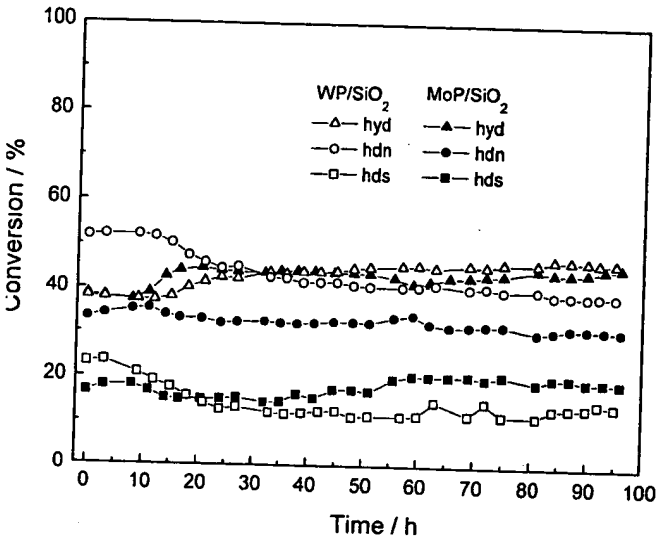

FIG. 9. Time dependence of the hydroprocessing activity of MoP/SiO_2 and WP/SiO_2 catalysts in the conversion of a model feed at 43 K and 3.1 MPa.

DISCUSSION

reparation and Characterization

The reduction profile obtained in the preparation of the oP/SiO_2 catalyst is presented in Fig. 1 and is compared the reduction profile of bulk MoP taken under similar nditions. The reduction trace of MoP/SiO_2 showed a fea- re at low temperature (370 K) and two peaks at high mperatures (680 and 820 K). The low-temperature fea- re was due to the dehydration of the sample, while the gh-temperature peaks were indicative of the reduction ıges of the phosphate. XRD analysis of the intermedi- : stage indicated that the first high-temperature peak, at) K, was due to the initial stages of reduction of Mo to a ver oxidation state, while the second peak, at 820 K, was ociated with the further reduction of both phosphorus d molybdenum to form MoP. These results will be pre- ıted in a separate, more detailed study of the preparation). It can be seen that the synthesis reaction was substan- ly over at 850 K and this was used as the final reduction ıperature for the preparation of the MoP/SiO_2 catalyst. ıolding time of 2 h was used at this temperature to ensure npletion of the reduction.

he bulk MoP reduction profile was obtained at the same ting rate of 0.0833 K s^{-1} (5 K min^{-1}) as the supported ıple and also showed two high-temperature reduction cesses. However, the first peak was unresolved and both ks were shifted to higher temperatures (770 and 920 K). ; was likely due to the presence of larger particles react- in a shell-to-core manner and inhibition of reaction by ;r formed by the reaction (25).

he TPR traces (Fig. 1) of the molybdenum phosphide ples can be analyzed to obtain the average rate of for- ion of the product phosphide, and hence the rate of

consumption of hydrogen. From the temperature program and duration of the main reduction peaks (full width at half maximum = 65 K) it is possible to extract the time of reaction (800 s). This information, combined with knowledge of the total amount of sample in the preparation, yields the average rate of hydrogen consumption. Assuming that the stoichiometry of the supported material is similar to that of the bulk, as determined gravimetrically, $MoPO_{5.5} + 5.5H_2 \rightarrow MoP + 5.5H_2O$, the rate of hydrogen consumption for the supported sample can be calculated to be 6.9 μmol g^{-1} s^{-1}. This compares to the flow rate of hydrogen of 650 μmol g^{-1} s^{-1}, which is a factor of 94 times larger. Therefore, the reaction is unlikely to be inhibited by the water produced by the reaction.

For the unsupported sample (full width at half maximum = 120 K, or 1500 s) the corresponding rate of hydrogen consumption is 28 μmol g^{-1} s^{-1}. The flow rate of hydrogen is now only 24 times larger, and the possibility of product inhibition by the water formed in the reaction is larger.

Another effect which is also likely to be contributing to the retardation of the reduction peaks in the bulk material is shell-to-core reduction. The average particle size of the bulk starting material can be calculated using the expression diameter = 6/surface area · density (where surface area = 1.3 m^2 g^{-1}, ρ = 3.54 cm^3 g^{-1}) to be 1.3 μm. This was likely to be much larger than the particle size of the supported phosphate precursor. Since the rate of reaction in the shrinking-core model depends on the square of the particle size (26, 27), this probably also contributed to the observed shift in the temperature of reaction between the bulk and silica-supported materials.

Assuming the stoichiometry of bulk reduction indicated above the final stoichiometry of the phosphides is MoP and WP. As is discussed below this is supported by the XRD and NMR results. These compounds have a metallic nature (28), so it is expected that the oxidation states of Mo and W will be close to zero. However, it is likely that some charge transfer will occur to the electronegative P atoms, so in fact the Mo and W should be slightly oxidized.

The XRD spectra of the bulk MoP and supported MoP samples prepared at 850 K, before and after the hydrotreating reactions, are shown in Fig. 2. The bulk MoP had a pattern which corresponded exactly to that reported in the literature (powder diffraction file 24-771). MoP has a hexagonal WC-type structure (strukturbericht designation, B_h) with space group $P_{\bar{6}m2}$ and lattice parameters a_0 = 322 pm and c_0 = 319 pm (29). The insert shows a schematic of the structure, which is based on a stacked arrangement of trigonal prisms. The supported MoP/SiO_2 showed a broad feature at ~22° 2θ produced by the amorphous silica support, and several distinct peaks which matched those of the bulk MoP phase.

The reduction profile for the preparation of WP/SiO_2 catalyst is presented in Fig. 3 and is compared to the reduction profile for bulk WP collected under similar conditions. The reduction trace of WP/SiO_2 showed a small feature at 370 K, a slight rise at 630 K, and a large peak at 890 K with a high-temperature shoulder at 970 K. The feature at 370 K was due to dehydration of the sample, while the high-temperature peaks were due to formation of phosphide. The slight rise at 630 K may have been due to small quantities of highly dispersed species, while the shoulder at high temperature may have arisen from larger particles which reduced more like the bulk WP. It is clear from the figure that the reduction process was essentially completed at 1000 K, which was used as the maximum temperature in the preparation of the WP catalyst. Again, a hold time of 2 h was used to ensure complete reduction of the sample.

The reduction profile of the bulk WP also showed the slight dehydration feature at 370 K and a high-temperature reduction peak at 1010 K. Similarly to the case of supported and unsupported MoP, the largest peak was shifted to higher temperature, likely as a result of the inhibitive action of water vapor and the presence of larger particles in the bulk material.

The XRD spectra of the bulk WP and supported WP samples prepared at 1000 K, before and after hydrotreating reactions, are shown in Fig. 4. The bulk WP had a pattern corresponding exactly to that reported in the literature (powder diffraction file 29-1364). WP adopts the orthorhombic MnP type structure (strukturbericht designation, B_{31}) with space group P_{nma} and lattice parameters a_0 = 571 pm, b_0 = 325 pm, and c_0 = 623 pm (30). The insert shows a schematic of the structure, which like MoP is based on a stacked arrangement of trigonal prisms. However, in WP the second row is displaced laterally half a lattice spacing and the phosphorus atoms are linked in chains. The supported WP/SiO_2 showed a broad feature at ~22° 2θ due to the silica support, and several distinct peaks which matched those of the WP phase.

The *ex situ* chemisorption characteristics and BET surface areas of catalyst samples are summarized in Table 3. The surface area of the MoS_2/SiO_2 catalyst (93 m^2 g^{-1}) precursor was close to that of the support (91 m^2 g^{-1}), as its loading was low. The surface areas of the MoP/SiO_2 (50 m^2 g^{-1}) and WP/SiO_2 (62 m^2 g^{-1}) samples were significantly decreased from that of the support. This is a common finding for phosphorus-promoted, supported catalysts (31, 32), and probably occurs as a result of solid state reactions or pore clogging promoted by phosphorus compounds. In the case of the phosphides studied here, the use of elevated temperatures during sample reduction, 850 K for MoP/SiO_2 and 1000 K for WP/SiO_2, may have contributed to the decrease in surface area by sintering of the silica support. Chemisorption quantities of O_2 and CO for the fresh catalysts were moderate and were found to decrease somewhat after reaction for the phosphides. Measurements taken after reaction were carried out on recovered samples washed in

hexane and re-reduced at 723 K for 2 h. The CO uptakes of MoP/SiO_2 and WP/SiO_2 and O_2 uptake of MoS_2/SiO_2 were used to calculate dispersions based on stoichiometries for adsorption of one CO molecule and one O atom per surface metal atom. The dispersions are reported in Table 3. They were low, 5.2% for 5.6% MoS_2/SiO_2, 0.7% for 17% MoS_2/SiO_2, 4.9% for MoP/SiO_2, and 2.0% for WP/SiO_2, consistent with the observation of crystalline phases for the phosphides.

The very low dispersion of the 17% MoS_2/SiO_2 was probably due to the formation of large domains exposing inactive basal planes. For this reason the low-loading 5.6% MoS_2/SiO_2 sample was used for the reactivity measurements.

The crystallite sizes of the phosphide samples were determined by Scherrer analysis and are reported in Table 3. As indicated in the table, the crystallite sizes were taken as averages over two principal directions. Although not shown, the crystallite dimensions in those directions were not substantially different (<5%), indicating that the particle morphology was globular.

The crystallite sizes can be used to calculate the theoretical number of surface metal sites (μmol g^{-1}) based on clean surfaces and spherical particles, and these are also reported in Table 3. For the unsupported materials the number of surface sites were considerably larger than the CO uptakes, indicating that a large proportion of the surface (89% for MoP, 93% for WP) was unable to chemisorb CO. This may have been due to site blockage by phosphorus or strongly held oxygen. For the supported samples the number of sites was closer to the actual uptakes, indicating that a smaller proportion of their surfaces was blocked (55% for MoP/SiO_2, 80% for WP/SiO_2).

Nuclear Magnetic Resonance

The ^{31}P MAS–NMR spectra (Figs. 5–8) are the first reported for supported metallic phosphides in the literature. The spectrum of the bulk WP (Fig. 5a) at zero rotation showed an asymmetric envelope characteristic of considerable electric-field anisotropy surrounding the phosphorus nucleus. This can be understood from the crystal structure (Fig. 4), which shows that the phosphorus atoms reside in sites which look different, when approached from the x, y, or z directions. When the samples were rotated, the anisotropy was folded over to the spinning side bands, resulting in a complex intensity pattern. Nevertheless, crystallographically all the phosphorus atoms were equivalent, and the position of only one major peak, at 255 ppm, was invariant with rotation. A smaller peak at −6 ppm was due to a small amount of phosphate impurity. Chemical shifts in this range are typical for phosphates (14). For the passivated WP sample (Fig. 5b) this peak shifted to −3 ppm and became the dominant feature of the spectrum. The passivation procedure for the NMR samples was less gentle (0.5% O_2/He followed by air exposure) than for the catalysts (gradual increase in O_2 concentration) and probably resulted in more oxidation. There is also the likelihood that the intensity of the insulator phosphate signal is intrinsically stronger than that of the metallic phosphide, where the phosphorus is surrounded by conduction electrons.

TABLE 4

Summary of Chemical Shifts for Phosphide Catalysts[a]

Sample	Phosphide (ppm)		Phosphate (ppm)	
	In situ	Passivated	*In situ*	Passivated
WP	255	254	−6	−3
WP/SiO_2	254	254	−5	−3
MoP	214	214	−5	−3
MoP/SiO_2	199	None	−36	−5

[a] Reference: 85% H_3PO_4.

The spectra of the supported WP/SiO_2 samples (Fig. 6) show features very similar to the bulk references (Fig. 5). The *in situ* pattern (Fig. 6a) indicated a larger amount of phosphate than in the bulk reference. This was likely due to the smaller crystallite size in the supported materials (Table 3), which resulted in easier oxidation. In passivated samples the phosphate peak dominated the pattern (Fig. 6b), but the phosphide signature was clearly present. XRD analysis of this sample (Fig. 4) indicated the presence of crystalline WP, supporting the contention that the phosphate NMR signal is intrinsically strong compared to the phosphide, and not a good indicator of the real amounts of each phase. All the chemical shifts are summarized in Table 4. There are small shifts in the lines, but all can be readily assigned to phosphate or phosphide compounds.

The spectrum of the bulk MoP at zero rotation (Fig. 7a) also showed an asymmetric envelope, but different from that of WP. This is because MoP has a different structure (Fig. 2) than WP, but still has considerable anisotropy surrounding the phosphorus atoms. Rotation of the sample again produced a complex pattern of spinning side bands caused by the anisotropy, but one main peak, at 214 ppm, remained invariant. A second smaller peak, at −5 ppm, was due to the presence of some phosphate contaminant. Again, as with WP it is expected that the intensity of this phosphate peak is much stronger than that of the metallic phosphide signal, so the relative size of the peaks is not indicative of the amounts of each substance. When the sample was exposed to air (Fig. 7b) the phosphate peak shifted slightly, to −3 ppm, and grew in intensity. The noise level also went up substantially. For the case of the supported MoP/SiO_2 at *in situ* conditions (Fig. 8a) the noise level was also large, and the peaks for the phosphide and phosphate were barely discernible. In the case of the passivated sample (Fig. 8b) the phosphate signal completely

dominated the spectrum. It is likely that the MoP/SiO_2 is more easily oxidizable than the WP/SiO_2. Again, a summary of chemical shifts is given in Table 4. In conclusion, for both WP and MoP the NMR spectra showed that supporting the materials on SiO_2 allowed retention of the phosphide phases. Passivation of the samples resulted in some oxidation, with a greater severity for the MoP system.

Reactivity

The activity of the catalysts in the hydrodesulfurization (HDS) of dibenzothiophene and the hydrodenitrogenation (HDN) of quinoline was evaluated in a three-phase flow reactor at 643 K and 3.1 MPa. Figure 9 shows the conversions as a function of time on the silica-supported MoP and WP in HDS and HDN. Both materials demonstrated good stability in their activity levels. It should be noted that those results were obtained with 58 μmol of sites of WP/SiO_2 and 70 μmol of sites of MoP/SiO_2 loaded in the reactor. The conversions were corrected to equal sites assuming a first-order kinetic expression. Denoting X_1 as the conversion corresponding to a quantity of sites S_1, and X_2 as the conversion corresponding to S_2 sites, then the quantities are related by

$$\ln(1 - X_2) = \left(\frac{S_2}{S_1}\right) \cdot \ln(1 - X_1).$$

The results, corrected to 70 μmol of sites, for the supported MoP/SiO_2, WP/SiO_2, and MoS_2/SiO_2 are summarized in Table 5, along with results from bulk MoP and WP and the silica support. The conversion levels of MoP/SiO_2 were similar to those of the bulk MoP (1). However, adjustment by the CO uptake made the bulk appear better. This was a consequence of the low CO uptakes of the bulk material compared to the supported sample. Because of the low surface area of the bulk MoP, a strong possibility exists that a large fraction of the active surface is underestimated. The WP/SiO_2 sample differed most substantially from its unsupported counterpart (4) by having lower HDS activity. Again, this was due to the low CO uptake of the bulk material. Compared to the MoS_2/SiO_2 both phosphides had significantly higher HDN, but lower HDS.

TABLE 5

Summary of Hydroprocessing of Model Feedstock at 643 K and 3.1 MPa

Sample[a]	HDN[b] (%)	HYD[c] (%)	HDS[d] (%)
SiO_2	2	32	1
5.6% MoS_2/SiO_2	11	45	31
13% MoP/SiO_2	31	45	20
20% WP/SiO_2[e]	46	46	16
MoP[e]	54	34	24
WP[e]	88	33	92

[a] Reactor catalyst loading was 70 μmol of sites except for WP/SiO_2 (58 μmol) and bulk samples (30 m^2).

[b] Hydrodenitrogenation of quinoline.

[c] Hydrogenation of quinoline to N-containing products.

[d] Hydrodesulfurization of dibenzothiophene.

[e] Percentage of HDN and HDS adjusted to 70 μmol of sites according to first-order equation given in text.

The low apparent activity of the supported phosphides compared to the bulk references was surprising. It may have been that passivation resulted in overoxidation of the catalysts, as shown by NMR. Re-reduction of the catalysts produced the phosphides again, but perhaps in a different, less-active form from the bulk phosphides. This form may have had phosphides that were phosphorus deficient because of segregation. Nevertheless, the samples were completely stable to reaction conditions, as clearly shown by the XRD patterns after reaction (Figs. 2, 4).

In recent work (3) the group of Prins studied the HDN on a series of bulk phosphides at conditions similar to those employed in this work (3.0 MPa and 643 K). In the presence of sulfur they found HDN conversions of 10% for MoP and 30% for WP, which are somewhat lower than those found in this study, 31 and 46%, respectively. The comparison is not exact because the previous work used *o*-propylaniline instead of quinoline, bulk catalysts instead of supported catalysts, and slightly different catalyst weights. Considering these differences the results are comparable.

An interesting conclusion of this study is that sample morphology is important, especially in the case of a weakly interacting support like silica. In the case of molybdenum sulfide the effect of loading showed that low concentrations were required to produce samples of sufficient active surface. This can be understood from the layered structure of MoS_2, which has inactive basal planes and active edge planes. As the size of the crystallites grow with loading, they do so at the expense of the desirable side planes. However, for molybdenum and tungsten phosphide, which do not have a layered structure, the smaller interaction with silica probably produces particles of a globular morphology whose site density is much higher. This represents a special opportunity for these new materials, which could be exploited by the use of better supports than the silica used in this study.

CONCLUSIONS

MoP and WP were prepared on a silica support. They were moderately active catalysts for the hydrodenitrogenation of quinoline and the hydrodesulfurization of dibenzothiophene in a complex mixture. The silica-supported catalysts had similar temperature-programmed reaction profiles as those of the bulk samples, while having reduced hydroprocessing activities compared to the bulk materials. The smaller activity was partly due to the inaccuracy of

counting sites by CO chemisorption on the low-surface-area bulk materials. It could also have been the result of oxidation of the small particles of the phosphide on the support on exposure to air. A low loading was required to generate a MoS_2/SiO_2 samples of sufficient O_2 uptake for catalytic testing.

The materials were characterized using ^{31}P magic-angle spinning–nuclear magnetic resonance spectroscopy. WP and MoP gave isotropic signals shifted 255 and 214 ppm from 85% H_3PO_4, respectively. The presence of oxide was indicated by signals between −3 and −6 ppm whose intensity increased substantially with passivation.

ACKNOWLEDGMENTS

We appreciate the United States Department of Energy for funding this project through Grant DE-FG02-96ER14669. We also appreciate the surface area measurements provided by Doohwan Lee, and the assistance of Geno Iannaccone and Thomas Glass with the NMR measurements.

REFERENCES

1. Li, W., Dhandapani, B., and Oyama, S. T., *Chem. Lett.* 207 (1998).
2. Stinner, C., Prins, R., and Weber, T., *J. Catal.* **191**, 438 (2000).
3. Stinner, C., Prins, R., and Weber, Th., *J. Catal.* **202**, 187 (2001).
4. Clark, P., Li, W., and Oyama, S. T., *J. Catal.* **200**, 140 (2001).
5. Robinson, W. R. A. M., van Gastel, J. N. M., Korányi, T. I., Eijsbouts, S., van Veen, J. A. R., and de Beer, V. H. J., *J. Catal.* **161**, 539 (1996).
6. Wang, X., Clark, P., and Oyama, S. T., *J. Catal.*, in press.
7. Oyama, S. T., Clark, P., Wang, X., Shido, T., Iwasawa, Y., Hayashi, S., Ramallo-López, J. M., and Requejo, F. G., *J. Phys. Chem. B* **106**, 1913 (2002).
8. Breysse, M., Portefaix, J. L., and Vrinat, M., *Catal. Today* **10**, 489 (1991).
9. Iler, R. K., "The Chemistry of Silica: Polymerization, Colloid and Surface Chemistry and Biochemistry." Wiley, New York, 1979.
10. van Veen, J. A. R., Hendriks, P. A. J. M., Andréa, R. R., Romers, E. J. G. M., and Wilson, A. E., *J. Phys. Chem.* **94**, 5282 (1990).
11. Bartholomew, C. H., and Farrauto, R. J., *J. Catal.* **45**, 41 (1976).
12. Scheffer, B., Heijeinga, J. J., and Moulijn, J. A., *J. Phys. Chem.* **91**, 4752 (1987).
13. Reinhoudt, H. R., Crezee, E., van Langeveld, A. D., Kooyman, P. J., van Veen, J. A. R., and Moulijn, J. A., *J. Catal.* **196**, 315 (2000).
14. Iwamoto, R., and Grimblot, J., *Adv. Catal.* **44**, 417 (1999).
15. Oyama, S. T., Clark, P., Teixeira da Silva, V. L. S., Lede, E. J., and Requejo, F. G., *J. Phys. Chem. B* **105**, 4961 (2000).
16. van Veen, J. A. R., Gerkema, E., van der Kraan, A. M., and Knoester, A., *J. Chem. Soc. Chem. Commun.* **22**, 1684 (1987).
17. Luck, F., *Bull. Soc. Chim. Belges* **100**(11–12), 781 (1991).
18. Marzari, J. A., Rajagopal, S., and Miranda, R., *J. Catal.* **156**, 255 (1995).
19. Kogan, V. M., and Parfenova, N. M., *Stud. Surf. Sci. Catal.* **106**, 449 (1997).
20. "Cab-o-sil® Untreated Fumed Silica Properties and Functions." Cabot Corporation, Tuscola, IL, 1993.
21. Cullity, B. D., "Elements of X-ray Diffraction," 2nd ed. Addison–Wesley, Menlo Park, CA, 1978.
22. Ramanathan, S., and Oyama, S. T., *J. Phys. Chem.* **99**(44), 16365 (1995).
23. Schönberg, N., *Acta Chem. Scand.* **8**, 226 (1954).
24. Clark, P., and Oyama, S. T., manuscript in preparation.
25. Oyama, S. T., Schlatter, J. C., Metcalf, J. E., III, and Lambert, J. M., Jr., *Ind. Eng. Chem. Res.* **27**, 1648 (1988).
26. Lemaitre, J. L., *in* "Characterization of Heterogeneous Catalysts" (F. Delany, Ed.), p. 21. Dekker, New York, 1984.
27. Bathia, S., Beltramini, J., and Do, D. D., *Catal. Today* **7**(3), 309 (1990).
28. Aronsson, B., Lundström, T., and Rundqvist, S., "Borides, Silicides, and Phosphides." Methuen, London/Wiley, New York, 1965.
29. Rundqvist, S., and Lundstrom, T., *Acta Chem. Scand.* **17**, 37 (1963).
30. Rundqvist, S., *Acta Chem. Scand.* **16**(2), 287 (1962).
31. Kraus, H., and Prins, R., *J. Catal.* **170**, 20 (1997).
32. Lopez Cordero, R., Esquivel, N., Lazaro, J., Fierro, J. L. G., and Lopez Agudo, A., *Appl. Catal.* **48**, 341 (1989).

ACADEMIC PRESS

Available online at www.sciencedirect.com
SCIENCE DIRECT®

Journal of Catalysis 218 (2003) 78–87

JOURNAL OF CATALYSIS

www.elsevier.com/locate/jcat

Alumina-supported molybdenum phosphide hydroprocessing catalysts

Paul A. Clark and S. Ted Oyama *

Environmental Catalysis and Materials Laboratory, Department of Chemical Engineering (0211), Virginia Polytechnic Institute and State University, Blacksburg, VA 24061, USA

Received 1 October 2002; revised 27 February 2003; accepted 27 February 2003

Abstract

Alumina-supported molybdenum phosphide hydroprocessing catalysts, MoP/γ-Al_2O_3, with weight loadings from 3.5 to 39 wt% were prepared by temperature-programmed reduction of alumina-supported molybdenum phosphate precursors. The precursors were obtained by incipient wetness impregnation of the support with aqueous molar solutions of ammonium paramolybdate and ammonium phosphate (Mo/P = 1/1). Effects of loading, reduction temperature, and heating rate on the catalysts were studied, and the samples were characterized by CO chemisorption, BET surface area, and X-ray diffraction (XRD) measurements. Compared to the bulk MoP and MoP/SiO_2 systems (which are similar to one another), the MoP/γ-Al_2O_3 material showed different behavior. Whereas calcined bulk and silica-supported molybdenum phosphates form Mo–P amorphous glasses which reduce directly to MoP, for the alumina-supported phosphates at high loadings (e.g., 13 wt% MoP/γ-Al_2O_3), a MoO_3 component is visible which reduces sequentially with temperature to MoO_2 and Mo metal, and then transforms to MoP. The difference in behavior between these systems is attributed to the formation of a strongly bound amorphous phosphate surface layer on the alumina support. Alumina has a strong affinity for phosphates, and appears to initially abstract a substantial amount of phosphorus from the stoichiometric molybdenum phosphate mixture. The alumina then releases the phosphorus at high temperature, allowing it to recombine with Mo metal to form MoP and generating active sites. The MoP/γ-Al_2O_3 catalysts performed well in hydroprocessing of a simulated distillate containing dibenzothiophene and quinoline at conditions representative of industrial hydroprocessing (643 K, 3.1 MPa). For the 13 wt% sample the hydrodesulfurization conversion was 57% and hydrodenitrogenation conversion was 62%. Catalytic activity, based on equal chemisorption sites loaded in the reactor (70 μmol), was generally independent of the amount of MoP deposited on the alumina surface, independent of the presence of X-ray visible molybdenum phases, and was associated with a relatively high temperature reduction peak found at all loading levels of MoP/Al_2O_3 but not in bulk MoP. We conclude that the high-temperature peak gives rise to highly dispersed MoP which is responsible for the bulk of the CO titration sites and the catalytic activity, and that the large MoP particles visible by XRD make smaller contributions.

Keywords: Molybdenum; Phosphide; Phosphorus; Alumina; Hydrodesulfurization; Hydrodenitrogenation; Dibenzothiophene; Quinoline

1. Introduction

Catalytic hydrotreating is an important refining process used to remove sulfur, nitrogen, and oxygen from hydrocarbon fuel liquids. Research in our laboratory has identified molybdenum phosphide, MoP, as an active and stable hydroprocessing catalyst [1–3]. Additional work by the group of Prins [4] has shown that MoP has six times higher activity in the HDN of orthopropylaniline than MoS_2/Al_2O_3. Studies in the group of Bussell have shown that MoP/SiO_2 has four times higher activity in the HDS of thiophene than MoS_2/Al_2O_3 [5]. In this paper we report the synthesis and catalytic properties of MoP deposited on a γ-alumina support.

MoP has a hexagonal WC-type structure, space group = $P_{6\bar{m}2}$, with lattice parameters a_o = 322 pm and c_o = 319 pm [6]. MoP is a metallic conductor with properties similar to ordinary intermetallic compounds [7]. Fig. 1 shows the WC structure type adopted by MoP. The WC structure type, along with the NiAs and WP structures, characterize the majority of transition metal monophosphides. The WP structure type is similar to NiAs, but distortions in the (001) plane form a rectangular net, resulting in an orthorhombic structure [8]. A recent review summarizes the structure, preparation, and catalytic activity of phosphides [9].

Removal of heteroatoms from fuel liquids is important because sulfur and nitrogen compounds corrode engine com-

* Corresponding author.
E-mail address: oyama@vt.edu (S.T. Oyama).

0021-9517/03/$ – see front matter
doi:10.1016/S0021-9517(03)00086-1

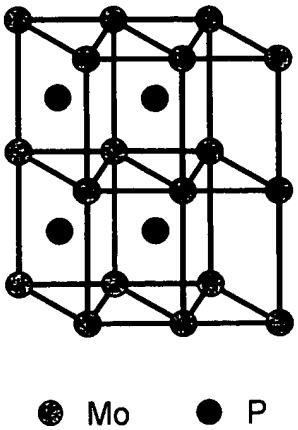

Fig. 1. Tungsten carbide (WC) structure type adopted by molybdenum phosphide, MoP.

ponents, pollute the air as SO_x and NO_x, cause gelling of untreated liquids, and foul downstream reforming catalysts. The problem is becoming increasingly important as government regulations become stricter [10] and the quality of petroleum feedstocks declines [11]. Although hydroprocessing catalysts have been widely studied, their basic compositions have changed little for many decades. They are typically alumina-supported molybdenum sulfides with nickel or cobalt promoters, $NiMoS/Al_2O_3$ or $CoMoS/Al_2O_3$ [12]. The catalysts described in this work are completely different, consisting of a compound of Mo and P with metallic rather than insulating or semiconducting properties.

In recent years, phosphorus has come to be used as a secondary promoter in commercial catalysts [13]. The use of phosphorus in hydroprocessing catalyst formulations was introduced in a series of patents dating back to the 1950s [14–16]. The phosphorus in these catalysts is dispersed on the catalyst surface in oxidized form, as shown by studies with X-ray photoelectron spectroscopy [17], nuclear magnetic resonance [18], and infrared spectroscopy [19]. The effect of phosphorus depends on its concentration and physical form, but in general it has a larger positive effect on the HDN performance of Ni–Mo sulfides than in the HDS performance of Co–Mo sulfide catalysts [20].

2. Experimental

Catalysts were prepared by impregnation and reduction. Desired quantities of ammonium paramolybdate tetrahydrate, $(NH_4)_6Mo_7O_{24}\cdot 4H_2O$ (Aldrich, 99%), and ammonium phosphate, $(NH_4)_2HPO_4$ (Aldrich, 99%), were dissolved in 1:1 stoichiometric proportions of metal to phosphorus to form clear solutions in distilled water. These solutions were used to fill the pores of a γ-alumina support (Degussa, Aluminumoxid C) by incipient wetness impregnation. The moist paste was calcined in air at 773 K for 6 h, ground with a mortar and pestle, pressed, broken, and sieved to particles between 650 and 1180 μm in diameter for use

Table 1
Compositional characteristics of MoP/Al_2O_3 samples

wt% MoP	mmol MoP g^{-1} Al_2O_3	Molecules MoP nm^{-2} Al_2O_3
3.5	0.29	1.9
6.8	0.58	3.8
13	1.16	7.7
23	2.3	15
39	3.8	25

(mesh size 14/20). Samples were prepared with loadings between 0 and 39 wt% MoP (0 and 3.8 mmol g^{-1} Al_2O_3). Specific compositional characteristics for the series of catalysts are reported in Table 1. The highest loading sample was prepared by double impregnation, due to solubility limitations of the metal and phosphate salts in distilled water. Much of this study used the 13 wt% (1.16 mmol MoP g^{-1} Al_2O_3) MoP/Al_2O_3 material. Reference samples containing only 1.16 mmol Mo g^{-1} Al_2O_3 (10.0 wt% Mo) or 1.16 mmol P g^{-1} Al_2O_3 (3.5 wt% P) were prepared in a similar manner to the catalysts, while aluminum phosphate, $AlPO_4$, was purchased from a commercial source (Alfa-Aesar Division of Johnson-Matthey, 99.999%).

Temperature-programmed reductions were carried out on pelletized catalyst samples (typically 0.3 g) placed in quartz u-tube reactors. The samples were heated with linear temperature ramps in flowing hydrogen (Airco, 99.999%) to reduce the metal phosphate to metal phosphide. Unless otherwise noted, the space velocity was set at 650 μmol H_2 s^{-1} g^{-1} of sample loaded (1000 cm^3 (NTP) min^{-1} g^{-1}), and the heating rate was 0.0833 K s^{-1} (5 K min^{-1}). The effluent was monitored continuously by a mass spectrometer (Ametek/Dycor, MA100). All samples were flushed in hydrogen flow for 2 h before starting the temperature program, to dry the sample and to provide a starting baseline in the mass spectrometer. After reduction, the product was cooled to room temperature (RT) under helium (Airco, 99.999%) flow, and passivated progressively with 0.1% O_2/He, 0.5% O_2/He (Airco), and slow diffusion of air to the sample for 24 h.

The total dynamic CO uptake (Air Products, 99.999%) was measured with a mass spectrometer by passing 5.6 μmol pulses over the sample in 65 μmol s^{-1} helium flow at RT until constant area peaks were obtained. Measurements made on freshly reduced samples are referred to here as in situ CO uptakes while measurements taken on passivated samples rereduced in H_2 for 2 h at 723 K are referred to here as ex situ CO uptakes. BET specific surface areas (S_g) of passivated samples were measured with a Micromeritics 2000 sorption unit.

X-ray diffraction (XRD) patterns were obtained at a scan rate of 0.035° 2θ s^{-1} using a Scintag XDS-2000 diffractometer with a Ni-filtered Cu-K_α ($\lambda = 0.1541$ nm) radiation source. Crystallite sizes were estimated using the equation of Scherrer, $D = K\lambda/\beta\cos\theta$. The constant K was taken here to be 0.9, λ is the wavelength of radiation, β is the peak width in radians, and θ is the angle of the reflection. The

average of the first three reflections in MoP was used to calculate an average particle diameter [21]. Activation energies for reduction reactions were estimated by the heating rate variation method of Redhead [22].

Hydrotreating activity was evaluated with a model distillate containing 2000 wppm N as quinoline (Aldrich, 99%), 500 wppm O as benzofuran (Aldrich, 99%), 3000 wppm S as dibenzothiophene (Aldrich, 99%), 20 wt% tetralin (Aldrich, 99%), and balance tetradecane (Fisher, 99%). The catalytic test was carried out in an upflow, three-phase, fixed-bed reactor as described earlier [23]. An amount of catalyst corresponding to 70 μmol of CO sites (measured ex situ) was loaded for each reaction. To start the reaction, catalysts were pretreated in flowing hydrogen (100 μmol s^{-1}) at 723 K and 1 atm pressure for 2 h. The pressure was then increased to 3.1 MPa (450 psig), the temperature was dropped to 643 K (370 °C), and a liquid feed rate of 5 cm^3 min^{-1} (delivering 9.7 μmol min^{-1} of quinoline and 6.3 μmol min^{-1} of dibenzothiophene) was initiated. Analysis of hydroprocessing liquids was performed with a gas chromatograph (Hewlett-Packard, 5890A) on samples collected at 2- to 3-h intervals for a time period of 60–80 h, until a stable steady state was reached. In this report, hydrodesulfurization (HDS) is defined as the percentage disappearance of dibenzothiophene (as no sulfur-containing intermediates were observed), hydrogenation (HYD) is defined as the percentage of original quinoline converted to hydrogenated quinolines, and hydrodenitrogenation (HDN) is defined as the percentage of nitrogen removed from the quinoline delivered to the catalyst.

3. Results and discussion

3.1. Synthesis of MoP/γ-Al_2O_3

Calcined catalyst precursors were reduced to MoP/Al_2O_3 catalysts by temperature-programmed reduction in hydrogen at 0.0833 K s^{-1} (5 K min^{-1}). Corresponding reduction profiles for 0–23 wt% MoP/Al_2O_3 samples are presented in Fig. 2. Five water peaks evolved through the reduction process, corresponding to reduction of different materials present in the precursor and to different stages in the reduction process. All of the samples, including the alumina support, exhibited a peak at 370 K (with a shoulder at 410–450 K) arising from physically adsorbed water. The alumina support alone exhibited no significant features above 500 K, while the molybdenum phosphate-loaded samples had features corresponding to reduction of the deposited species. These features were labeled α, β, γ, and δ in order of their appearance with temperature. The α peak occurred at the lowest temperatures, was relatively small, and was present in all of the samples. The δ peak was also present in all of the samples, occurred at the highest temperatures, and was generally large and diffuse. In the lowest loading materials, 3.5 and 6.8 wt%, the α and δ peaks constituted the majority of the reduction profile, and are attributed to well-dispersed

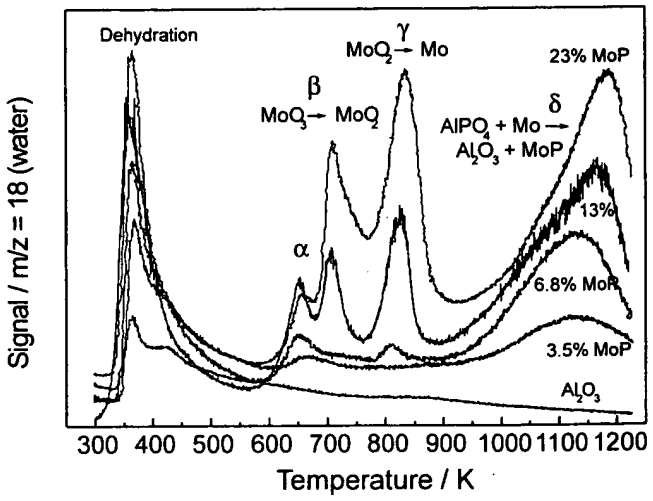

Fig. 2. Temperature programmed reduction profiles for various $MoPO_x/Al_2O_3$ samples reduced to 1223 K at 0.083 K s^{-1} (5 K min^{-1}).

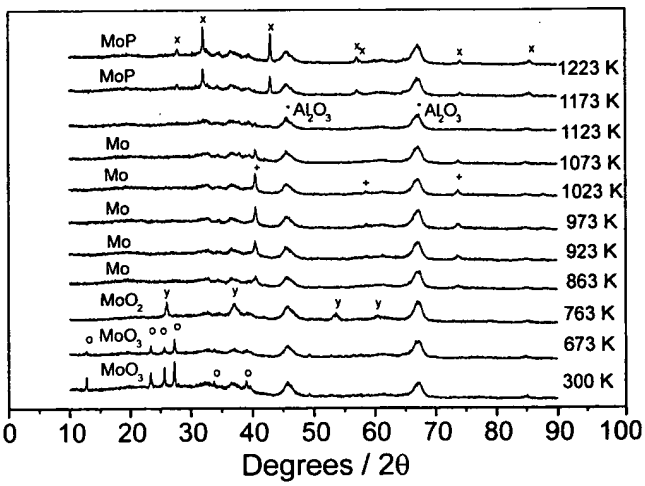

Fig. 3. Evolution of MoP during the reduction of $MoPO_x/Al_2O_3$ (13 wt% MoP). Samples were reduced to intermediate temperatures, quenched in helium, and characterized by in situ CO uptake before passivation. (o) MoO_3; (y) MoO_2; (+) Mo°; (×) MoP, and (*) Al_2O_3.

species on the alumina surface. The γ peak first appeared as a small feature in the 6.8 wt% material, and was prevalent at higher loadings along with the β peak. The β and γ features slightly overlapped the α and δ features. But the β and γ peak temperatures were in the range typically observed for the reduction of bulk molybdenum compounds, and will presently be shown to correspond to X-ray visible phase changes.

The reduction of the 13 wt% MoP/Al_2O_3 material was followed by XRD of quenched and passivated intermediates. These spectra are shown in Fig. 3. Comparison of Fig. 2 with Fig. 3 allows association of the reduction peaks α, β, γ, and δ with phase changes observed by X-ray diffraction. The alumina-supported MoP precursor differs from the X-ray amorphous precursors for unsupported MoP [1] or silica-supported MoP [3] because of the visibility of MoO_3. The formation of MoO_3 is attributed to abstraction of the

phosphate component by the alumina surface. The take up of phosphate by alumina in standard phosphorus-promoted catalysts is well established [24,25].

The α peak near 675 K resulted in no new features in the XRD spectrum, and was therefore attributed to dehydroxylation of well-dispersed molybdate species. The low temperature of this feature is thought to arise because the strength of the alumina–molybdate bonds weakens the remaining hydroxyl bonds, which are subsequently easier to remove.

The β peak and γ peaks correspond to the transformation of MoO_3 to Mo metal through the intermediate MoO_2. This behavior is typical of the reduction of bulk MoO_3 in hydrogen. This X-ray observable process must occur because the phosphorus species are unavailable to the free molybdenum species. This demonstrates that the alumina fully binds the phosphate at this concentration level (13 wt% MoP). At higher surface loadings, the phosphate groups saturated the alumina surface and become available to associate with the free MoO_3. Here, the β and γ peaks resulted in XRD changes similar to substoichiometric MoP_xO_y ($x < 1$) oxides, where the value of x depends on the relative amount of P and Mo. Fortunately for the context of this report, catalysts prepared at 1123 K contained only MoP in their X-ray patterns (regenerated in the δ peak at higher temperatures), and the catalytic activity was attributed to well-dispersed phases not observed by XRD. Therefore, detailed characterization of the phase behavior of the samples with loading 23 and 38 wt% at intermediate temperatures was unnecessary.

Fig. 3 shows that the δ peak is accompanied by the disappearance of molybdenum metal and the appearance of molybdenum phosphide above 1123 K. This demonstrates that the δ peak is associated with the freeing of phosphorus within the sample, and its return to the molybdenum species. Indirectly, this shows that the δ peak is associated with reduction of alumina-bound phosphate groups, and indicates that phosphorus has a relatively fast diffusivity in molybdenum—because the freed phosphorus can penetrate the molybdenum metal completely to form pure MoP.

Fig. 4 shows the development of the in situ CO uptake in intermediates from the reduction of 13 wt% MoP/Al_2O_3 superimposed on its reduction profile. The CO uptake correlates reasonably well with the degree of completion of the reduction process, in which the dip at the end is likely due to sintering/grain growth of particles of the active phase due to the high temperature at that stage.

Table 2 summarizes the CO uptakes obtained for the 13 wt% sample at the different stages of reduction marked by peaks α, β, γ, and δ. It can be seen that the majority of the uptake is generated following the δ peak. Since the δ peak is also the major reduction peak in the low loading sample which does not show an X-ray visible MoP phase, this result suggests that the measured CO uptake in all the samples is associated with well-dispersed molybdenum phosphide held tightly on the alumina surface, rather than the X-ray visible phases.

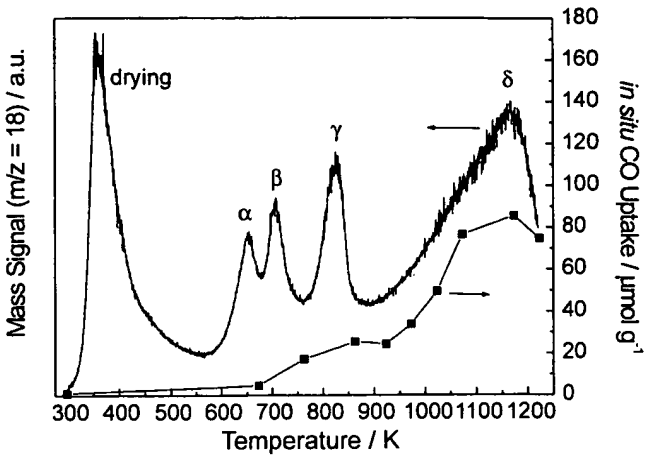

Fig. 4. Evolution of in situ CO uptake sites of quenched intermediates during the preparation of 13 wt% MoP/Al_2O_3.

Table 2
Evolution of CO uptake with the reduction peaks α, β, γ, and δ

Peak event	Temperature interval, K	CO uptake, μmol/g, %	X-ray visible phase change
α	298–673	4	None
β	673–763	15	$MoO_3 \rightarrow MoO_2$
γ	763–863	10	$MoO_2 \rightarrow$ Mo metal
δ	863–1173	71	Mo metal → MoP

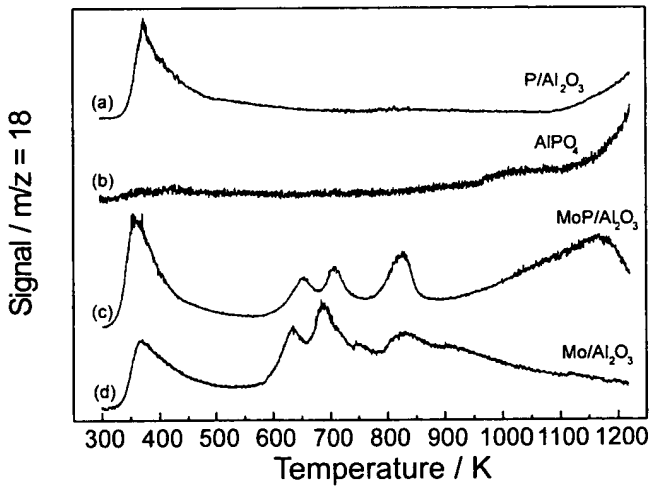

Fig. 5. Reduction profiles for "blank" alumina samples reduced to 1223 K at 0.083 $K\,s^{-1}$ (5 $K\,min^{-1}$). (a) 1.16 mmol g^{-1} PO_x/Al_2O_3; (b) $AlPO_4$; (c) 1.16 mmol g^{-1} $MoPO_x/Al_2O_3$; and (d) 1.16 mmol g^{-1} MoO_x/Al_2O_3.

Fig. 5 shows reduction profiles of reference materials including commercial $AlPO_4$, the Al_2O_3 support containing only ammonium phosphate, and the Al_2O_3 support containing only ammonium molybdate. The supported reference materials were prepared with procedures (impregnation, calcination, and pelletization) and molar loading (1.16 mmol g^{-1} Al_2O_3) identical to those used for generating the 13 wt% MoP/Al_2O_3 catalyst. Samples containing the alumina support exhibited a large dehydration peak near 373 K. This low temperature behavior is sim-

ilar to that of the alumina blank and the supported catalysts shown in Fig. 2, and is attributed to the release of physically adsorbed water condensed in fine pores. Reference samples consisting of only P and Al_2O_3 had smooth baselines between 600 and 900 K, and developed peaks above 1100 K. A yellow-brown deposit formed downstream on the interior walls of the quartz reactor tube during the high-temperature peaks of the P and Al_2O_3 samples. The deposit is probably elemental phosphorus transported as volatile reduced species such as P_2, P_4, or PH_3 [26,27], but could be oxidized phosphorus transported as volatile P_2O_5. Vapor-phase transport of phosphorus has been reported earlier for phosphorus-containing materials undergoing high-temperature TPR [19]. The molybdenum-containing materials, Mo/Al_2O_3 and MoP/Al_2O_3, both had identifiable α, β, and γ peaks. These peaks are respectively attributed to recombination of hydroxyl ligands from well-dispersed molybdates, MoO_3 to MoO_2 reduction, and MoO_2 to Mo metal reduction. The Mo/Al_2O_3 had a tail above 900 K, attributed to the reduction of strongly held molybdates. In contrast to the reference samples, the MoP/Al_2O_3 sample had a large feature, the δ peak, between 900 and 1200 K. This feature in this temperature range only occurred in the presence of both phosphorus and molybdenum. X-ray diffraction indicated a phase change from Mo to MoP accompanying the δ peak, demonstrating influx of phosphorus from a source outside the molybdenum grains. The δ peak in the MoP/Al_2O_3 samples included the reduction of aluminum phosphate above 1100 K, but with the reduction temperature of phosphorus decreased because of facilitation of the reduction process by molybdenum.

X-ray diffraction spectra showing the presence of MoP in samples of different loading reduced to 1223 K at 0.0833 K s^{-1} (5 K min^{-1}) are presented in Fig. 6. MoP was the only crystalline product observed, becoming visible at 6.8 wt%, and increasing in intensity with loading. The XRD spectra of the catalysts reduced to 1123 K at 0.0833 K s^{-1} (5 K min^{-1}) and held for 2 h were similar to those shown in Fig. 6. The lattice constants of the supported MoP catalysts are reported in Table 3. The lattice parameters of the MoP in the catalysts agree well with the literature values, indicating that supported MoP of good purity is formed.

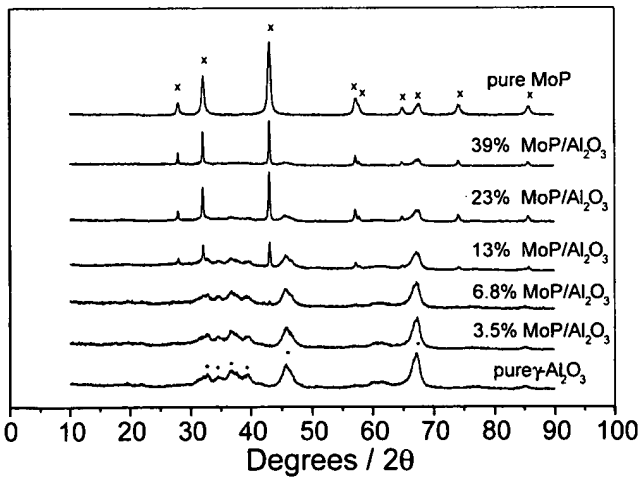

Fig. 6. X-ray diffraction results showing increased amounts of MoP with loading for samples reduced to 1223 K at 0.083 K s^{-1} (5 K min^{-1}). (×) MoP, and (*) Al_2O_3.

The effect of final reduction temperature (heating rate $\beta = 5$ K min^{-1}) on catalytic performance was evaluated for the 13 wt% MoP/Al_2O_3 material. Of four temperatures investigated, successful samples were produced only at 1023 and 1123 K. Here, the primary criterion for success was the presence of sufficient and stable CO uptake for catalytic testing. A sample reduced at 873 K for 2 h had insufficient ex situ CO uptake (= 12 μmol g^{-1}) to load 70 μmol of sites, and a sample reduced at 1223 K for 0.5 h exhibited significant daily decrease in its CO uptake (noticed because of the averaging procedure used for catalyst samples) and was therefore also not used. Although the sample prepared at 1023 K had adequate CO uptake, its XRD spectrum revealed the presence of both Mo metal and MoP, while the sample reduced at 1123 K contained only MoP. Because of this, most of the supported samples used for the characterization and reactivity studies were reduced at 1123 K.

Table 3 summarizes crystallite sizes of the molybdenum phosphide calculated using the Scherrer equation. These values correspond to an average over the low index (1000), (1010), and (0001) planes. The sizes of the alumina-supported MoP crystallites increased slightly with the loading amount. More dramatic, however, was their large size (about double) compared to the bulk material. This is attributed to grain growth (Ostwald ripening or sintering) of the crystallites at the 200 K higher temperature of 1123 K used in the preparation of the supported catalysts compared to the bulk material, which was prepared with a maximum temperature of 923 K.

Table 3 also reports site densities of surface metal atoms calculated from the crystallite sizes of the X-ray visible MoP and the wt% loading of the MoP in the sample. The calculations were performed assuming spherical or cubic particles having surface site densities equal to 9.71 atoms nm^{-2}. It is understood that the crystallite size as given by the Scherrer

Table 3
X-ray diffraction results for MoP/Al_2O_3 catalysts

Sample	Lattice parameter, a_0 (pm)	Lattice parameter, c_0 (pm)	Crystallite size,[a] nm	Total metal site density,[b] μmol g^{-1}
13% MoP/Al_2O_3	321	318	39	43
23% MoP/Al_2O_3	322	319	40	75
39% MoP/Al_2O_3	322	319	51	98
MoP	322	318	19	680
MoP reference[c]	322	319	–	–

[a] Average size calculated from line broadening in the ⟨1000⟩, ⟨1010⟩, and ⟨0001⟩ directions.

[b] Site density = surface metal atoms per gram of sample. Calculated using the surface metal areal density of MoP (9.7×10^{18} surface Mo m^{-2}), the MoP fractional weight loading, and the average MoP crystallite size.

[c] JCPDS-ICDD Powder Diffraction File 24-771.

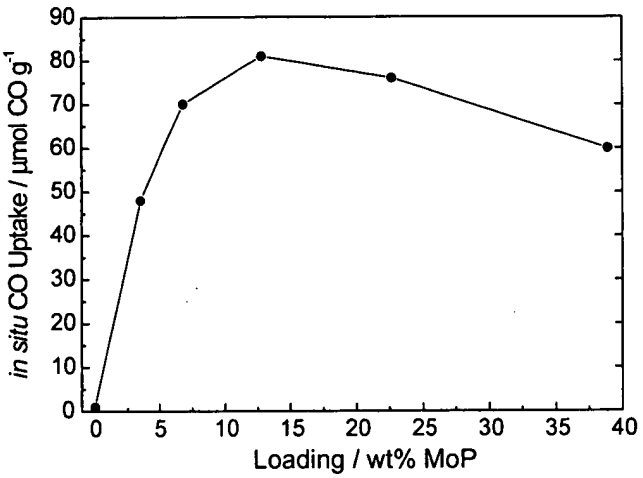

Fig. 7. Development of in situ CO uptake as a function of loading. The samples were reduced to 1223 K at 5 K min^{-1} in hydrogen flow at 670 μmol s^{-1} g^{-1} (1000 cm^3 min^{-1} g^{-1}).

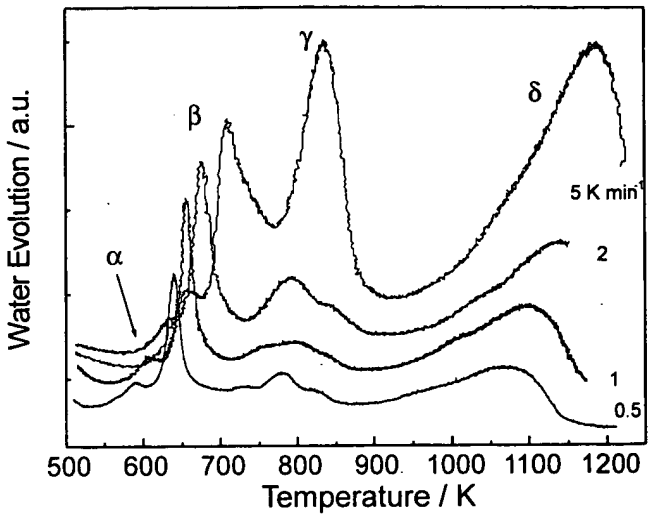

Fig. 8. Effect of heating rate on the temperature-programmed reduction forming 23 wt% MoP/Al_2O_3.

Table 4
Results of BET surface area and CO chemisorption measurements on MoP/Al_2O_3 samples

Sample	Surface area fresh,[c] m^2 g^{-1}	In situ[a] CO uptake, μmol g^{-1}	Ex situ[b] CO uptake fresh,[c] μmol g^{-1}	Ex situ[b] CO uptake spent,[d] μmol g^{-1}
γ-Al_2O_3	91[a]	1	0	–
6.8 wt% MoP	75	70	26	20
13 wt% MoP	71	81	36	31
23 wt% MoP	60	76	28	29
39 wt% MoP	49	60	36	26

[a] Samples reduced to 1223 K (β = 5 K min^{-1}, H_2 flow = 650 μmol g^{-1}) and then quenched.

[b] Pretreated in H_2 at 723 K for 2 h (β = 5 K min^{-1}, H_2 flow = 650 μmol g^{-1}).

[c] Catalysts prepared by reduction to 1123 K for 2 h (β = 5 K min^{-1}, H_2 flow = 650 μmol g^{-1}).

[d] Spent catalysts washed in hexane and dried in air.

Table 5
Apparent first-order activation energies of reduction events in the preparation of 23 wt% MoP/Al_2O_3

Peak	Activation energy, kJ mol^{-1}
α	152
β	157
γ	130*
δ	160

* Nonlinear. Estimated using heating rates of 2 K and 5 K min^{-1}. See text.

equation is only an approximation and ignores the presence of a distribution of sizes. The surface site density was calculated from the crystal structure of MoP [4] assuming exposure of equal numbers of low index planes. It is assumed in these calculations that the surface area to volume ratio of the MoP crystallites was proportional to 6/d (spherical or cube shaped particles), and that the particles had the density of bulk MoP [8] (7.50 g cm^{-3}). The site density of the unsupported MoP was much larger than the experimentally determined CO uptake of 18 μmol g^{-1} [1]. This reveals that the surface sites on bulk MoP are blocked in a ratio near 38:1, similar to results found for WP [28]. The calculated site densities were lower for the supported materials than the bulk due to a combination of larger MoP particles sizes and lower MoP weight fraction in the mixture.

Table 4 summarizes measurements of surface area, in situ CO uptake, and ex situ CO uptake for MoP/Al_2O_3 samples. The in situ CO uptakes were collected on the series of samples whose XRD spectra were presented in Fig. 6 and are plotted in Fig. 7. The in situ CO uptakes rose from 1 to 81 μmol per gram of sample as loading increased from 0 to 13 wt% MoP and then tapered off to 60 μmol per gram as loading was further increased to 39 wt%. The decrease at high loadings is likely due to blocking of pores by phosphide particles and consequent loss of surface area. Because the ex situ CO uptake of the fresh catalyst was used as the basis for loading the hydroprocessing reactor, these values were averaged over three measurements. The ex situ measurements on all of the catalyst samples were similar, regardless of loading, and the results on the fresh and spent catalysts show that the catalytic treatment led to only minor, if any, reductions in the ex situ CO uptake. Comparison of in situ and ex situ CO uptakes reveals that only a portion of the uptake sites are recovered after air exposure and subsequent rereduction.

Heating-rate variation between 0.5 and 5 K min^{-1} was investigated on the sample containing 2.3 mmol g^{-1} Al_2O_3 (23 wt% MoP/Al_2O_3). The reduction profiles are displayed in Fig. 8, and Table 5 reports the first-order activation energies calculated for each type of peak. As heating rate decreased, the relative intensity of the β peak increased, and the γ peak resolved into three smaller peaks. Furthermore, the γ peak maxima did not conform to a linear activation energy relationship. This behavior is consistent with satura-

tion of phosphorus on the alumina surface between 13 and 23 wt%, and the overlap of $MoO_2 \rightarrow Mo$ and $MoP_xO_y \rightarrow MoP_x$ processes in the γ peak. The origin of increased intensity of the β peak is not clear, but could be related to deeper reduction of the crystallites in the slower process.

3.2. Catalytic activity of $MoP/\gamma\text{-}Al_2O_3$ samples

The catalysts were evaluated for activity in hydrotreating of a simulated distillate containing quinoline (2000 wppm N) and dibenzothiophene (3000 wppm S) at 643 K and 3.1 MPa. Importantly, catalysts were loaded into the reactor using a constant 70 μmol ex situ CO uptake basis. The choice of ex situ CO uptake as the basis for comparison assumes catalytic activity to be due to surface sites generated through reduction at 723 K, and will be discussed later. The use of ex situ uptakes collected of air-exposed samples ensures that the sites are regenerated during catalytic pretreatment. Table 4 summarizes CO uptakes obtained after pretreatment in hydrogen at 723 K for 2 h.

Reference materials were also investigated for catalytic performance. These standards included the reduced support alone, a calcined phosphate blank containing 1.16 mmol PO_x g^{-1} Al_2O_3, and the phosphate blank exposed to the reduction procedure used for the majority of MoP/Al_2O_3 samples (1123 K for 2 h). An amount of 3.0 g of each blank was loaded, as their CO uptakes were negligible.

The hydrotreating performances of the samples are reported in Table 6. The blank reference materials had very low HDN and HDS conversions, as expected. For the MoP/Al_2O_3 samples there was only a minor effect of loading on the HDN and HDS performances, which averaged 56 and 52%, respectively. The amount of hydrogenated quinoline products was stable near 30% (except the phosphorus-containing blanks), consistent with equilibration between quinoline and 1,2,3,4-tetrahydroquinoline. Overall, the results indicate that a comparison of activity based on CO uptakes is reasonable. The single low HDS conversion of 44% for the 39 wt% sample is likely due to partial pore blockage for this high-loading sample. This would affect the larger dibenzothiophene more than the quinoline. The activity of the supported MoP/Al_2O_3 samples was moderately high, especially in HDN, and can be compared to that of a commercial $Ni\text{–}Mo\text{–}S/Al_2O_3$, which at the same hydroprocessing conditions had HDN conversion of 38% and HDS conversion of 79% [29].

Table 6
Hydroprocessing conversions of MoP/Al_2O_3 catalysts[a]

Sample	% HDN	% HYD	% HDS
Al_2O_3 blank	2.4	32	1.1
PO_x/Al_2O_3	3.3	18	4.7
P/Al_2O_3	3.8	19	1.0
6.8 wt% MoP	54	31	51
13 wt% MoP	52	33	57
13 wt% MoP[b]	62	29	57
23 wt% MoP	58	28	53
39 wt% MoP	54	33	44

[a] Reduced to 1123 K ($\beta = 5$ K min^{-1}, H_2 flow = 650 μmol g^{-1}) for 2 h.
[b] Reduced to 1023 K ($\beta = 5$ K min^{-1}, H_2 flow = 650 μmol g^{-1}) for 1.5 h.

Table 7 reports turnover frequencies (moles converted per CO uptake site per second) calculated for quinoline HDN and dibenzothiophene HDS for MoP supported on alumina compared with bulk MoP [1] and MoP on silica [3]. The silica-supported material shows somewhat lower activity when compared on this basis, and the alumina-supported material is similar to the bulk. This suggests that the MoP active sites formed on the alumina support are similar to the bulk material. Still the differences are small, and again indicate that CO uptakes are a reasonable method for comparing different samples.

Table 4 also reports the ex situ CO uptake values for the spent catalysts. For these measurements the samples were removed from the catalytic reactor, washed with hexane, and dried in air. Subsequently, they were reduced in hydrogen under the same conditions used for the fresh catalysts. The ex situ CO adsorption sites persisted following catalytic reaction conditions and exposure to air. This remarkable stability in CO uptake values before and after reaction is consistent with the stability in conversion levels noted for these catalysts.

X-ray diffraction traces for fresh and spent 13 wt% MoP/Al_2O_3 catalyst reduced to 1123 K are presented in Fig. 9. MoP and Al_2O_3 were the only crystalline phases observed, and the catalyst XRD signature was not significantly affected by the catalytic reaction. Similar results were found for catalysts of other loadings, whose XRD patterns were also stable toward the catalytic test, and which resembled the spectra shown in Fig. 6.

For the 13 wt% MoP/Al_2O_3 catalyst reduced at 1023 K (i.e., 100 K lower than the "standard" temperature of 1123 K), the X-ray diffraction patterns for the fresh and spent catalysts contained features of both Mo and MoP, as shown in Fig. 10. Nevertheless, this material was also active and stable toward the catalytic reaction conditions. This catalyst was prepared at 1023 K using a 1.5-h soak. Compared to the intermediate sample quenched at 1023 K, which contained only Mo metal in its XRD spectrum (Fig. 3), the diffraction trace of the catalyst sample reduced at 1023 K contained mostly MoP. Thus, the molybdenum phosphide in the catalyst sample appeared during the 1.5-h soak time en-

Table 7
Comparison of hydroprocessing turnover rates of 13% MoP/Al_2O_3 with 13% MoP/SiO_2 and bulk MoP

Sample	HDN, mol quinoline mol site^{-1} s^{-1}	HDS, mol dibenzothiophene mol site^{-1} s^{-1}
13 wt% MoP/Al_2O_3	1.2×10^{-3}	8.5×10^{-4}
13 wt% MoP/SiO_2	7.2×10^{-4}	3.0×10^{-4}
Bulk MoP	1.5×10^{-3}	5.2×10^{-4}

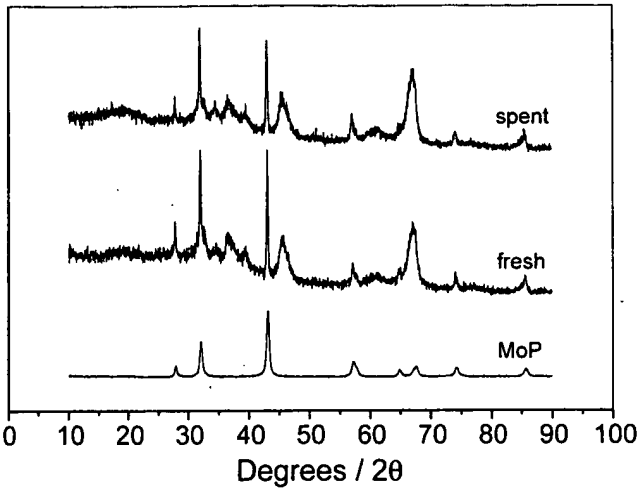

Fig. 9. X-ray diffraction of fresh and spent 13 wt% MoP/Al_2O_3 catalyst prepared at 1123 K.

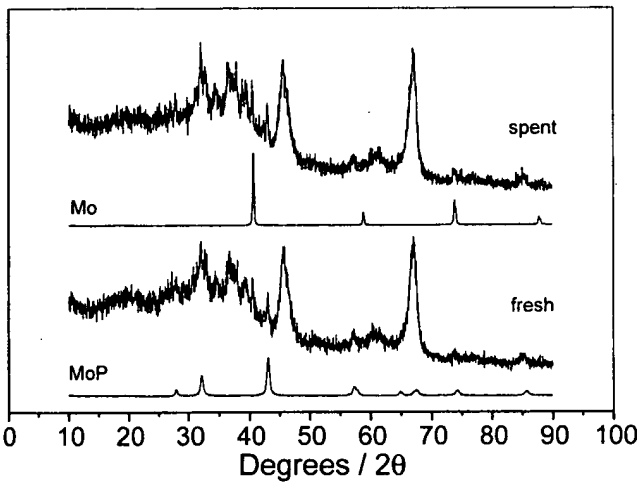

Fig. 10. X-ray diffraction of fresh and spent 13 wt% MoP/Al_2O_3 catalyst prepared at 1023 K.

tirely by the isothermal progress of the process giving the δ peak.

3.3. Nature of active sites

The choice of ex situ CO uptake as the basis of comparison of catalysts deserves commentary. Ordinarily for bulk materials, a surface area basis is chosen. However, in supported systems the surface area of the active phase and the support material combines and the relative surface of the active material is masked. By choosing a surface site titration technique (CO uptake) that is known to be roughly proportional to the total surface area [28], an estimate can be made of the amount of active surface available on a supported material. The CO uptake basis then allows comparisons of supported materials on the basis of equal active surface. While the correlation between CO uptake and catalytic performance is subject to experimental uncertainties, the relative correlation between CO uptake and catalytic activity (0.11 HDN, 0.25 HDS) in this study is substantially better than that found between catalytic activity and weight (0.32 HDN, 0.45 HDS), surface area (0.51 HDN, 0.33 HDS), or moles of molybdenum (1.33 HDN, 1.35 HDS). Here, the relative correlations represent variabilities, and are defined as the maximum span in values (maximum minus minimum) divided by the average value. For a previously undescribed catalyst system exhibiting a wide range of loadings and preparation conditions, we feel that the consistency of results based on CO uptakes is very good. Furthermore, the similarity of the turnover frequencies on CO uptake basis with bulk MoP is notable.

The majority of CO uptake in the MoP/Al_2O_3 system was generated by the δ reduction peak at much higher temperatures, about 200 K higher, than required for the formation of bulk MoP. The δ peak was observed in all of the MoP/Al_2O_3 samples, even at the lowest loading level of 3.2 wt%, and is attributed to highly dispersed molybdenum and phosphorus on the alumina surface. Our earlier EXAFS measurements [2] identified this dispersed phase in reduced 6.8 wt% MoP/Al_2O_3 to be clusters of MoP between 0.5 and 1.2 nm in size. The surface density (Table 1) of MoP on the 6.8 wt% sample is 3.8 MoP per nm^2, and appears to be slightly above the saturation limit of molybdenum on the alumina in this system (note the presence of traces of X-ray visible MoP in Fig. 6, and a slight gamma peak in Fig. 2). This saturation limit is slightly less than that of MoO_3, which forms a saturated monolayer on alumina at around 4.5 molecules/nm^2 [30]. Higher surface loadings of Mo and P up to 25 MoP/nm^2 (39 wt%) extend well beyond monolayer formation on the surface, and the excess molybdenum forms X-ray visible MoO_3 until phosphorus saturates as well, and substoichiometric molybdenum phosphate (MoP_xO_y, $x < 1$) species form at higher loadings. These X-ray visible excess molybdenum species undergo reduction in the temperature range of 650–850 K (at 5 K min^{-1}), as found in ordinary bulk Mo compounds, but the particles are generally very large. The relative sizes of the particles (Table 3) are much larger than bulk MoP produced at lower temperatures. The sizes of the particles and their dilution by alumina lead to much lower values of surface metallic densities than those found in bulk MoP. The relative similarity of turnover frequencies (Table 7) on the basis of CO uptake sites in alumina and bulk MoP materials indicates that the crystalline phases in the supported catalysts provide only a minimal contribution to the active surface in these materials.

Fig. 11 depicts a diagram of the proposed structure of the 6.8 wt% MoP/Al_2O_3 and 13 wt% MoP/Al_2O_3 materials. Here, the alumina particles and the associated oxide phases are highly simplified for the purpose of clarity. Nevertheless, the salient points of the process are clearly described. In the 6.8 wt% loading material, well-dispersed $MoPO_x$ reduces directly into MoP particles with diameters on the order of 1.2 nm. In the 13 wt% MoP material the precursor has distributed the molybdenum and phosphorus oxides as well dispersed $MoPO_x$, well dispersed aluminum phosphate,

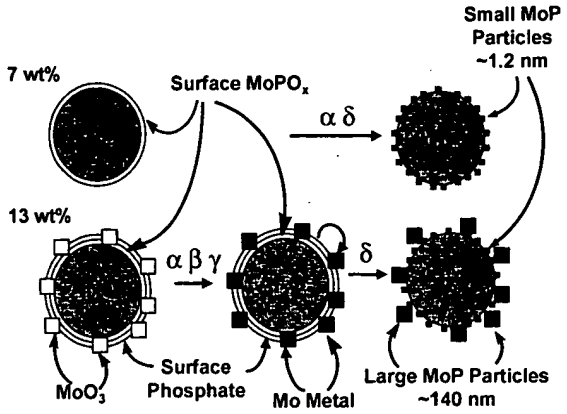

Fig. 11. Proposed structural model for 7 and 13 wt % MoP/Al_2O_3 catalysts.

and crystalline MoO_3. During the initial stages of reduction (i.e., the β and γ peaks), the crystalline MoO_3 reduces directly into metal, just as ordinary crystalline MoO_3 will do in the presence of hydrogen. During the latter stages of reduction (i.e., the δ peak), the dispersed aluminum phosphate is reduced to release phosphorus which is taken up by the molybdenum metal, and the well-dispersed $MoPO_x$ reduces directly into MoP particles with diameters on the order of 1.2 nm, as was found for the low loading sample.

3.4. Relationship to previous results in the literature

Although the nomenclature "MoP/Al_2O_3" has appeared before in the literature [31], the materials studied were in fact phosphate-promoted molybdenum sulfides. Such phosphate-promoted sulfidic hydrotreating catalysts have been widely investigated, as described in an extensive review by Iwamoto and Grimblot [13], but are not the same materials investigated in the present study. In our catalysts, the phosphorus is in a reduced state and the active molybdenum phosphide is metallic. Aside from the presence of Ni or Co promoters, comparison of the preparative conditions reveals that the relative amount of P to Mo in the promoted system is small, whereas in the present system it has exactly 1:1 molar proportions. For example, optimal activity for thiophene HDS in an alumina-supported sulfide catalyst containing 3.0 wt% NiO and 15 wt% MoO_3 was achieved with a phosphorus content of 1 wt% (0.24 mol P: mol Mo) [32]. Furthermore, the activation procedure for the promoted system typically involved low-temperature (ca. 723 K) reduction in a sulfidic atmosphere, whereas in the present study the reduction is at high temperature (1123 K) in pure hydrogen. No definitive evidence for phosphide formation has been given for the promoted system, whereas this study clearly demonstrates the presence of hexagonal MoP by XRD. Related work using EXAFS shows small crystallites containing Mo–P bonds [2].

There are also similarities between the phosphide and phosphorus-promoted sulfide systems. Both materials exhibit a strong interaction between phosphate and alumina [24,25]. Additionally, the presence of phosphate results in moderate reduction in the surface area of the catalysts. It has been found that the interaction of alumina and phosphate increases the dispersion of the metals in the Ni–Mo–S system [33]. Molybdena also interacts strongly with alumina, suggesting that the phosphate group alters the interaction of molybdenum with the surface [33].

Because the catalytic activity is roughly independent of loading from 6.8 to 39%, while the XRD of MoP increases dramatically in intensity, it is reasonable to conclude that the majority of active sites are associated with highly dispersed MoP clusters in close contact with Al_2O_3, as noted earlier [2]. The nature of phosphorus in MoP/Al_2O_3 catalysts reported here is quite different from its oxidized state in commercial phosphorus-promoted sulfides. The MoP/Al_2O_3 catalysts reported in this paper are reduced at substantially higher temperatures than those employed in standard sulfiding, and result in the reduction and transfer of phosphorus from alumina to the metallic phase. That the temperature of preparation is 200 K higher than for ordinary bulk MoP is also remarkable, because it reveals that the alumina support stabilizes very small MoP particles, protecting them from sintering and maintaining their surface sites.

4. Conclusions

A series of MoP catalysts supported on γ-Al_2O_3 was prepared and tested for hydroprocessing activity under simulated industrial conditions. MoP/Al_2O_3 catalysts were effective at HDN and HDS in our tests, averaging 57 and 52%, respectively. Interestingly, dispersion of the molybdenum phosphate precursor on alumina revealed substantially different phase behavior than found in bulk MoP and silica supported MoP. At loadings between 0 and ~ 6 wt%, both the molybdenum and phosphorus species were distributed on the alumina support with a strong interaction. At about 6 wt%, the molybdenum species saturated on the alumina support and increases in surface loading led to free MoO_3 in the oxidized system. Above 13 wt%, the phosphorus also saturates on the alumina surface and further increases in surface loading produced combinations of MoO_3 and substoichiometric MoP_xO_y ($x < 1$) species. Regardless of the X-ray visible phases, catalytic activity was independent of loading and was attributed to well-dispersed MoP formed from the reduction of the first 6 wt% of molybdenum phosphate deposited to the surface.

Higher loadings also resulted in strong interaction between alumina and phosphate. Evidence for this was found in the presence of MoO_3 in the oxidic precursor form of the 13 wt% MoP/Al_2O_3 catalyst, and by new peaks in the TPR profile. As reduction proceeded, MoO_2 occurred at 763 K, molybdenum metal was seen between 863 and 1073 K, and MoP was formed above 1173 K. The catalysts were active for hydroprocessing of both dibenzothiophene and quinoline, and were stable under hydroprocessing conditions. Analysis suggests that the active sites are associated

with small (~ 1.2 nm) phosphide crystallites on the alumina carrier surface.

Acknowledgments

This work was carried out with support from the United States Department of Energy, Office of Basic Energy Sciences, Grant DE-FG02-96ER14669. The authors thank Doo Hwan Lee for the surface area measurements.

References

[1] W. Li, B. Dhandapani, S.T. Oyama, Chem. Lett. (1998) 207.
[2] S.T. Oyama, P.A. Clark, V.L.S. Teixeira da Silva, E.J. Lede, F.G. Requejo, J. Phys. Chem. B 105 (2001) 4961.
[3] P.A. Clark, X. Wang, S.T. Oyama, J. Catal. 207 (2002) 256.
[4] C. Stinner, R. Prins, Th. Weber, J. Catal. 191 (2000) 438.
[5] D.C. Phillips, S.J. Sawhill, R. Self, M.E. Bussell, J. Catal. 208 (2002) 456.
[6] S. Rundqvist, T. Lundstrom, Acta Chem. Scand. 17 (1963) 37.
[7] S. Rundqvist, Colloq. Int. Centre Nat. Rech. Sci. 157 (1967) 85.
[8] N. Schönberg, Acta Chem. Scand. 8 (1954) 226.
[9] S.T. Oyama, J. Catal. (2003), in press.
[10] Chem. Eng. News May 22 (2000) 27.
[11] J.W.M. Sonnemans, Stud. Surf. Sci. Catal. 100 (1995) 99.
[12] H. Topsøe, B.S. Clausen, F.E. Massoth, Hydrotreating Catalysis-Science and Technology, Springer, Berlin, 1996.
[13] R. Iwamoto, J. Grimblot, Adv. Cat. 44 (1999) 417.
[14] J.N. Haresnape, J.E. Morris, British patent 701217, 1953.
[15] E.C. Housam, R. Lester, British patent 807583, 1959.
[16] G.A. Mickelson, US patents 3749663, 3755196, 3755150, 3755148, and 3749664, 1973.
[17] D. Chadwick, D.W. Aitchison, R. Badilla-Ohlbaum, L. Josefson, Stud. Surf. Sci. Catal. 16 (1983) 323.
[18] A.N. Startsev, O.V. Klimov, A.V. Kalinkin, V.M. Mastikhin, Kinet. Catal. 35 (1994) 552.
[19] P.J. Mangnus, J.A.R. van Veen, S. Eijsbouts, V.H.J. de Beer, J.A. Moulijn, Appl. Catal. 61 (1990) 99.
[20] P. Atanasova, T. Tabakova, Ch. Vladov, T. Halachov, A. Lopez Agudo, Appl. Catal. A 161 (1997) 105.
[21] B.D. Cullity, Elements of X-Ray Diffraction, 2nd ed., Addison–Wesley, Menlo Park, CA, 1978, p. 102.
[22] J.L. Falconer, J.A. Schwarz, Catal. Rev. Sci. Eng. 25 (1983) 141.
[23] S. Ramanathan, S.T. Oyama, J. Phys. Chem. 99 (1995) 16365.
[24] J.A.R. van Veen, P.A.J.M. Handriks, E.J.G.M. Romers, R.R. Andréa, J. Phys. Chem. 94 (1990) 5282.
[25] S.M.A.M. Beuwens, J.P.R. Vissers, V.H.J. de Beer, R. Prins, J. Catal. 112 (1988) 401.
[26] J.R. van Wazer, Phosphorus and Its Compounds, Interscience, New York, 1958, Vol. 1.
[27] K.A. Gingerich, J. Phys. Chem. 68 (1964) 2514.
[28] P. Clark, W. Li, S.T. Oyama, J. Catal. 200 (2001) 140.
[29] B. Dhandapani, S. Ramanathan, C.C. Yu, B. Fruhberger, J.G. Chen, S.T. Oyama, J. Catal. 176 (1998) 61.
[30] U.S. Ozkan, L. Zhang, S. Ni, E. Moctezuma, J. Catal. 148 (1994) 181.
[31] M. Jian, R. Prins, Bull. Soc. Chim. Belg. 104 (1995) 231.
[32] J.M. Lewis, R.A. Kydd, P.M. Boorman, P.H. van Rhyn, Appl. Catal. A 84 (1992) 103.
[33] P. Atanasova, R. López-Cordero, L. Mintchev, T. Halachev, A. López-Agudo, Appl. Catal. A 159 (1997) 269.